6-27-2016

Ventriculomegaly in Aging, Injury and Disease

Rebecca Acabchuk PhD
University of Connecticut, rebecca.acabchuk@uconn.edu

Ventriculomegaly In Aging, Injury And Disease

Rebecca Lynn Acabchuk, Ph.D.

University of Connecticut, 2016

The brain's ventricular system provides essential functions to the central nervous system, which include nutrient and signal delivery, waste clearance, and homeostatic regulation of critical factors, and waste clearance. It is therefore surprising that most studies neglect to consider the ventricular system and its ependymal lining in the etiology of neurodegenerative disease. Here, we investigate changes that occur to the brain in aging, injury and disease from the perspective of the ventricular system, its ependymal lining and surrounding periventricular structures. Using a combination of post-mortem human tissue, neuro-imaging and mouse models, our studies highlight the importance of maintaining a healthy ependymal lining in aging, and reveal periventricular areas of the brain that are likely vulnerable to acceleration and rotational forces in mild traumatic brain injury. Assessment of new protocols for three-dimensional visualization of whole tissue samples are included to promote future research of intact biological structures. Together, these studies emphasize the ventricular system as an important central nervous system feature that should be considered in the pursuit of understanding neurophysiological mechanisms underlying changes that occur to the brain in aging, head trauma and neurodegenerative disease.

Ventriculomegaly In Aging, Injury And Disease

Rebecca Lynn Acabchuk

B.A., Cornell University, 1998

A Dissertation Submitted in Partial Fulfillment

of the Requirement for the Degree of

Doctor of Philosophy

at the

University of Connecticut

2016

APPROVAL PAGE

Doctor of Philosophy Dissertation

Ventriculomegaly in Aging, Injury and Disease

Presented by Rebecca L. Acabchuk, B.A.

Major Advisor _____

Dr. Joanne Conover, Ph.D.

Associate Advisor _____

Dr. Joseph LoTurco, Ph.D.

Associate Advisor_____

Dr. Larry Renfro, Ph.D.

Associate Advisor_____

Dr. David Goldhamer, Ph.D.

Associate Advisor_____

Dr. Qian Wu, MD

University of Connecticut 2016

This work is dedicated to

those suffering from brain trauma,

whether directly, or through the suffering of a loved one.

I hope that someday there will be more treatment options available,

and until then, I wish you and your family peace.

Acknowledgements

First and foremost, I would like to express my sincere gratitude to Dr. Joanne Conover, for accepting me into your lab, for inspiring me with insightful guidance and allowing me to work on fascinating research projects. Joanne, you are an inspiration to me and to so many others for your commitment to excellence, your visionary ideas and your passion for striving to be at the forefront of research. I am so grateful for all of the opportunities you have helped to create for me, and I appreciate your commitment to promoting equality for females in the STEMs.

I would like to thank all of my fellow Conover Lab members, past and present, for making the lab like a family. Dr. Jessica Lennington, for helping me get started on an amazing project; Dr. Brett Shook, for answering all of my questions with fabulous explanations and astounding patience; Meredith Halling, for being the best bench partner anyone can ever wish for; Matt Eastman, for making me laugh; Alexandra Trausch and Amanda Coletti, for your enthusiasm and friendship; and Dr. Krysti Todd, for always being willing to help anyone with a smile. Krysti, your dedication is an inspiration.

Thank you to all of the undergraduate students who assisted me on my projects: Rich Wolferz, Lilly Talbot, Mai Stern, Mel Soloway, Andrew Trinh, Ye Sun, and Megan Powers (my fellow Cornellian), you were all so amazing to work with. I appreciate your commitment to the research, the care you took in processing tissue, and the positive attitudes you brought in each day. I loved all of the conversations we had at the bench, I know you will all go on to do amazing things!

A special thanks to our collaborators at Wayne State University, for providing us with the resources to make this project possible. Drs. Donald Kuhn, Denise Briggs and Mariana Perez, it was a pleasure working with each of you.

Thank you to my Committee Members, for your time, input and guidance. Dr. Goldhamer, I will never forget our first conversation in your office, I have followed your advice. Dr. Wu, thank you for allowing me to come into your Pathology Lab at UCHC and for providing us with precious donations that made this project possible. Dr. LoTurco, thank you for your guidance and insight on my project. Dr. Renfro, thank you so much for all of the professional and friendly advice you provided me anytime I stopped by.

I would also like to thank all of the members of the PNB department. Dr. Chen, Penny Dobbins and Chris Kimball, I appreciate all the work you put into the A&P program to make it an excellent learning experience for both the students and the instructors. A special thanks to Dr. Chris O'Connell for helping me take beautiful images. I loved working with you Chris, you are an amazing asset to our department.

I am grateful to Dr. Conover for taking me along with her when she began her directorship of WiMSE; David, Melissa, Jen, Kristen, Shawna, and all of the other LC staff, thank you all for your support and assistance. Dr. Kristen Govoni, I know I am leaving WiMSE in excellent hands. I have no doubt that the students of WiMSE will be our future innovators and leaders and I am honored to have had the opportunity to work with this amazing community.

I would like to thank all of the other professors at UConn I have had the opportunity to meet and learn from, including Drs. Salamone, Fein and Markus. Dr. Haim Bar, thank you for your assistance with statistical analysis. Janet Rochester, thank you for the opportunities to teach yoga at UConn. Dr. Blair Johnson, thank you for welcoming me into your universe. I am so excited for the work ahead of us.

I am grateful for the Café at the Benton Museum and the UConn Forest; my favorite places to work and run.

To all of my friends and family, thank you for your encouragement and support along the way. Mom and Dad, for inspiring me to dream big. Gram, for teaching me what is important in life, and reminding me not to hunch over. Dean, my dedicated partner, thank you for allowing me to pursue my goals and for your commitment to supporting our family. Amanda, Tori and Summer, my amazing daughters, your positive energy provides me with never-ending joy.

Abbreviations

3D	three dimensional
Aβ	amyloid beta
AB	antibody
AD	Alzheimer's Disease
ADHD	attention deficit hyperactivity disorder
ANOVA	analysis of variance
AQP4	aquaporin 4
CCI	controlled cortical impact
CNS	central nervous system
CSF	cerebral spinal fluid
CSP	cavum septum pellucidum
CT	computerized tomography
CTE	chronic traumatic encephalopathy
CUBIC	clear, unobstructed brain/body imaging cocktails and computational analysis
DBE	dibenzyl ether
DCX	doublecortin
DTI	diffusion tensor imaging
DTI	diffusion tensor imaging
FLAIR	fluid-attenuated inversion recovery
GFAP	glial fibrillary acidic protein
H	hemorrhage

H&E	hematoxylin and eosin
iDISCO	immunolabeling-enabled three-dimensional imaging of solvent-cleared organs
IHC	immunohistochemistry
ISF	interstitial fluid
IVP	intraventricular pressure
MBP	myelin basic protein
MRE	magnetic resonance elastography
MRI	magnetic resonance imaging
mTBI	mild traumatic brain injury
NA	neuraminidase
NFL	National Football League
NFT	neurofibrillary tangle
OASIS	Open Access Series of Imaging Studies
p-tau	phosphorylated tau
PACT	passive clarity technique
PBS	phosphate-buffered saline
PET	positron emission tomography
PET	positron emission tomography
PVH	periventricular flair
R/T	room temperature
RIMS	refractive index matching solution
RMS	rostral migratory stream
rmTBI	repeated mild traumatic brain injury

ROI	region of interest
SDS	sodium dodecyl sulfate
SF	skull fracture
SVZ	subventricular zone
SWITCH	system-wide control of interaction time and kinetics of chemicals
TBI	traumatic brain injury
TDE	thiodiethanol
TDP-43	transactive response DNA binding protein 43
TES	traumatic encephalopathy syndrome
THF	tetrahydrofuran
WMH	white matter hyperintensities

Table of Contents

Chapter 1: Introduction*

*** Excerpted in part from:**

Acabchuk RL, Sun Y, Wolferz Jr R., Eastman MB., Lennington JB, Shook BA, Conover JC, **3D Modeling of the Lateral Ventricles and Histological Characterization of Periventricular Tissue in Humans and Mouse**. J. Vis. Exp. (99), e52328, doi:10.3791/52328 2015.

Eastman MB, **Acabchuk RL**, Conover JC. Neural Stem Cell Behavior in the Subventricular Zone as a Function of Age. **Neural Stem Cells in Health and Disease.** World Scientific Press. 2015 October.

The Brain's Ventricular System

There are three main fluid systems in the brain: the ventricular system that contains and circulates cerebrospinal fluid (CSF), the interstitial fluid (ISF) of the parenchyma that surrounds neurons and glia, and the vasculature containing the blood supply. The ventricular system of the brain emerges during embryonic development from the neural tube, a fluid-filled cavity that becomes separated from the amnion. During embryonic development, CSF pressure within the ventricles, along with growth factors and morphogens within the CSF, act in coordination with the neuroepithelium as a main driving force of brain growth and morphogenesis (Gato, Desmond 2009). The fully formed ventricular system is comprised of four inter-connected cavities; the lateral ventricles are the two largest cavities located in the cerebrum. In humans, the anterior horns of the lateral ventricles are separated by the septum pellucidum, which is comprised of two thin vertical membranes that fuse together after birth. Separation of these leaflets in adulthood, known as cavum septum pellucidum (CSP), is a distinguishing feature of Chronic Traumatic Encephalopathy (CTE) (McKee, Stein et al. 2015). CSF flows from the lateral ventricles through the foramina of Monro into the third ventricle, then through the cerebral aqueduct into the fourth ventricle, where it then passes into the central canal of the spinal cord or into the cisterns of the subarachnoid space via the foramina of Luschka and Magendie. CSF is then re-absorbed into venous circulation through various routes including the arachnoid granulations and cervical lymphatics (Brinker, Stopa et al. 2014). The choroid plexus, located within the ventricles, assists in the production and filtration of CSF, forming the blood/CSF interface. In addition to CSF produced from the choroid plexus, a significant portion of CSF may be derived from ISF passing through the ependymal cells that line the ventricular system (McComb 1983). In this thesis I will focus on changes that occur in aging and injury to

the ventricular system and its ependymal cells, which form the site of fluid interchange between ISF and CSF.

Functions of the ventricular system and CSF include protection, delivery of signals and nutrients, fluid pressure control, removal of debris and brain homeostasis via regulation of neuroendocrine factors and other essential factors of the central nervous system (CNS). Disruption of CSF flow can contribute to CSF retention and stagnation with reduced ability to clear metabolites, which can contribute to toxic accumulations within the brain (Silverberg, Miller et al. 2010). More evidence is emerging to suggest alterations in ventricular flow dynamics may be linked to neurodegenerative diseases through either disturbed regulation of intracranial pressure, accumulation of toxic metabolites or a combination of both (Gupta, Soellinger et al. 2010).

Ventriculomegaly

Ventriculomegaly, or expansion of the lateral ventricles, is a common feature of many neurodegenerative diseases, including Alzheimer's Disease (AD) and CTE (Schott, Fox et al. 2003, McKee, Stein et al. 2015). Ventricle expansion in aged subjects with cognitive impairment is strongly correlated to increases in both cognitive decline and altered CSF metabolites that are known biomarkers for AD (Apostolova, Green et al. 2012, Chou, Leporé et al. 2009). Ventriculomegaly is also strongly correlated to normal aging (Resnick et al., 2003). However, the exact cause, progression and, importantly, the impact to normal brain function are currently not known. New automated segmentation tools that allow for less labor-intensive calculations of lateral ventricle volume from magnetic resonance image (MRI) scans may facilitate the clinical application of ventricle volume measurements as a predictive biomarker for

various disease states (Apostolova, Green et al. 2012).

Hydrocephalus is a term often used synonymously with ventriculomegaly. Due to the lack of a recognized definition of hydrocephalus, a definition was proposed by Rekate (2008) with the aim of achieving international consensus stating "Hydrocephalus is an active distension of the ventricular system of the brain resulting from inadequate passage of cerebrospinal fluid from its point of production within the cerebral ventricles to its point of absorption into the systemic circulation" (Rekate 2008). Thus, hydrocephalus is a *pathophysiological condition* thought to be caused by an imbalance between the production and resorption of CSF, which can take place at multiple sites within the ventricular system (Jiménez, Domínguez-Pinos et al. 2014). The resulting accumulation of CSF within the ventricle cavity leads to dilation of the lateral ventricles. In cases of adult-onset normal pressure hydrocephalus, it is likely that only a small increase in pressure is sufficient to generate ventricular expansion (Jiménez, Domínguez-Pinos et al. 2014). Depending on the rate of intraventricular pressure (IVP) changes, symptoms of hydrocephalus can vary from acute headache and vomiting to the more chronic triad of symptoms, which are gait disturbances, urinary incontinence, and dementia. “Normal pressure hydrocephalus” is a controversial diagnosis, as IVP is difficult to assess, and normal pressure hydrocephalus is often considered a misnomer, which can impede progress in both research and treatment. Case studies can be found throughout the literature of elderly patients presenting with deteriorating cognition and apparent normal CSF pressure that regain cognitive abilities following shunting (Chu, Zeidler et al. 2006, Shukla, Vinod et al. 2010, Kiefer, Unterberg 2012), suggesting changes in IVP, ICP and/or CSF flow are directly related to healthy brain functioning. However, shunting is not an ideal intervention, as it is often associated with infection and other complications (Del Bigio, Di Curzio 2016).

In humans, hydrocephalus is often associated with increased fluid accumulation in the surrounding periventricular tissue (Kim, Jeong et al. 2015). Periventricular fluid accumulation is best assessed using fluid-attenuated inversion recovery (FLAIR) MRI, which often reveals periventricular hyperintensities (PVH) in aged patients, indicative of edema (Fazekas et al. 1993; Sener 2002). Recently, symptomatic as opposed to asymptomatic hydrocephalus was found to be more highly associated with periventricular edema in dogs (Laubner, Ondreka et al. 2015). Other terms are also used to describe PVH, including periventricular lucency and white matter hyperintensities (WMH). While studies have found WMH are associated with increased risk of stroke, dementia, and death, these studies often do not distinguish between hyperintensities located throughout the brain and hyperintensities specific to the periventricular region (Debette, Markus 2010), which can have separate etiologies. While it is possible that increased fluid accumulation underlying WMH may be due to blood-brain barrier leakage indicating small vessel disease, periventricular edema may also be related to disruption of the CSF/ISF barrier. A recent computer-generated analysis using finite element modeling to test different trans-mantle pressure gradients found the degree of ventriculomegaly significantly influences the development of PVH, suggesting transependymal CSF absorption may be the cause of ventriculomegaly-related edema (Kim, Jeong et al. 2015). However, an intact ependymal lining was an underlying assumption of this model.

Ependymal Cells

Ependymal cells are postmitotic, cuboidal, epithelial cells that are highly polarized (Spassky, Merkle et al. 2005). Ependymal cells form a monolayer lining of the ventricle cavity separating the CSF from the parenchyma. The ependymal cell layer is joined together by tight junctions,

gap junctions and adherens junctions, and also contains the water channel protein aquaporin 4 (AQP4). Together, these junctions and water channels allow the ependyma to function as a bidirectional barrier and fluid transport system between the CSF and interstitial fluid (ISF) of the brain (Kuo, Mirzadeh et al. 2006). The majority of AQP4 channels are found along the basolateral membrane of the ependyma, which suggests that under normal conditions, the direction of bulk fluid movement flows from the parenchyma into the ventricle (Roales-Buján, Páez et al. 2012). Ependymal cells contain motile cilia on their apical surface that beat in coordination to facilitate CSF circulation, distribute signaling molecules, maintain fluid homeostasis and remove debris (Del Bigio 1995, Riquelme, Drapeau et al. 2008). Inhibition of ciliary beating in adult mice has been shown to cause hydrocephalus (Monkkonen, Hakumaki et al. 2007), highlighting the importance of maintaining healthy ependymal cilia for ventricular homeostasis.

A critical area of research is aimed at elucidating the mechanisms involved in clearing the brain of toxic accumulations that can contribute to age-related decline and neurodegenerative disease. In both aging and neurodegenerative diseases such as AD and CTE, there is a decrease in the brain's ability to eliminate toxins, placing the barriers of the brain as targets of age-related dysfunction (Marques, Sousa et al. 2013). AD and CTE are similarly marked by accumulations of amyloid beta (Aβ) and phosphorylated tau (p-tau), although they have distinct regional and temporal patterns. While specific transporters and receptors have not yet been clearly identified, new research suggests the ependyma is involved in both Aβ and p-tau clearance (Matsumoto, Chiba et al. 2015, Ueno, Chiba et al. 2016). Therefore, it is likely that damage to the ependymal lining may contribute to accumulation of Aβ and p-tau in diseases such as AD and CTE.

Alterations to the ependymal lining in aging

Alterations to the ependymal lining, including ependymal cell loss or destruction, are found in aging, injury and neurodegenerative disease. Our studies (Chapter 2, Shook et. al. 2014) along with others, have shown periventricular areas devoid of ependymal cells are typically marked by prominent gliosis along ventricle surface, displaying dense astrocytic processes marked by the intermediate filament glial fibrillary acidic protein (GFAP) (Del Bigio 2010) (**Figure 1B**). Reactive astrocytes that replace denuded ependymal cells are proposed to be an attempt to reestablish homeostasis at the CSF/ISF interface (Roales-Buján, Páez et al. 2012). However, while periventricular astrocytes partially resemble the ependymal lining by forming CSF-contacting microvilli and other similar features related to ependymal cell barrier functions, the astrocytes do not contain motile cilia nor do they display the same basolateral polarization of AQP4 water channels that is characteristic of ependymal cells (Jiménez, Domínguez-Pinos et al. 2014). Studies in our lab using mice have found modest 'ependymal repair' occurs in specific regions of the ventricle wall in aging, and that ependymal-like cells can be generated in response to injury (Luo et al. 2008). However, these studies were performed in mice, and it is important to consider that humans may not have the same regenerative capacity as rodents due to differences in the underlying neurogenic niche, the subventricular zone (SVZ). The changing composition of the rodent and human SVZ in aging is illustrated in **Figure 1**. In mice, an intact ependymal lining is maintained and SVZ neurogenesis persists throughout aging, albeit at reduced levels (Luo et al., 2006) (Capilla-Gonzalez, Cebrian-Silla et al. 2014) **(Figure 1A)**. In contrast, the adult human SVZ capacity is more limited, displaying a reduced number of neural stem cells with apical processes contacting the CSF and an absence of progenitor pools (Sanai et al., 2011;

Wang et al., 2011) (**Figure 1B**). The human SVZ structure differs further compared to rodents due to the presence of a hypocellular 'gap' region adjacent to the ependymal lining thought to be the remnant path of neuroblasts migrating during post-natal development (Capilla-Gonzalez, Cebrian-Silla et al. 2014). The 'gap' region is followed by a band of astrocytes, referred to as the 'astrocytic ribbon' (Sanai et al., 2004; Zecevic, 2004; Guerrero-Cazares et al., 2011). Why astrocytes remain clustered as an 'astrocytic ribbon' is not clear, especially since astrocytes in the brain parenchyma tend to 'tile' and do not typically cluster together, except in the cases of injury or lesion where a glial scar forms (Sofroniew, 2009).

Figure 1

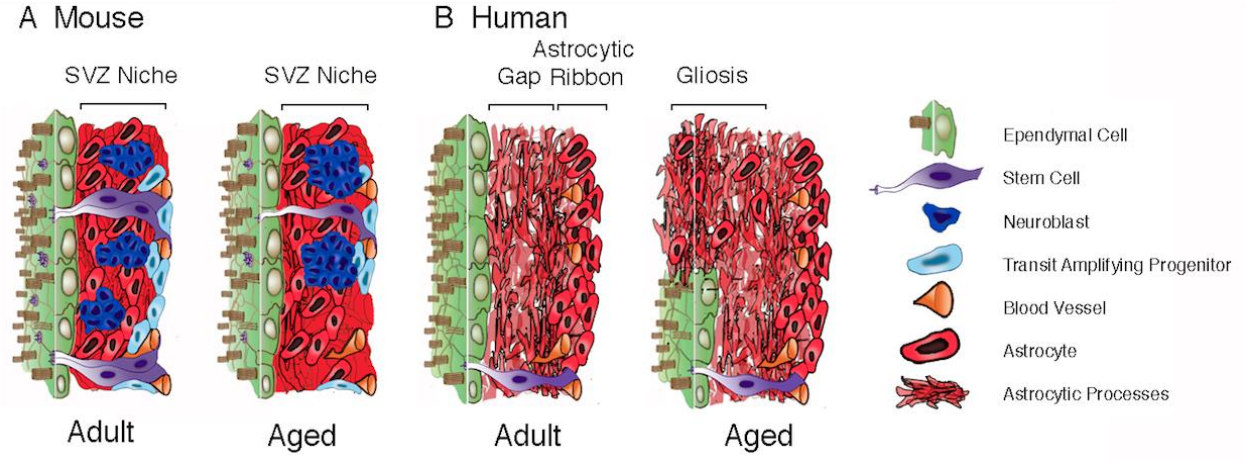

Figure 1. Schematic representations show the cytoarchitectural organization of the mouse (A) and human (B) SVZ stem cell niche in young adult and aged adult tissue.

Previous studies in our lab have demonstrated that along with an intact ependyma, ventricle volume remains constant throughout aging in mice (Shook et al., 2014). The studies I conducted show that humans, on the other hand, tend to have large regions of gliosis along the

ventricle lining in aging, and also have age-related ventricle expansion. The studies presented in Chapter 2 investigate the link between ependymal gliosis and ventricle expansion.

New discoveries highlight importance of ventricular system health

Recent advances using a combination of neuroimaging, molecular and cellular techniques have shown that ventricular system functions are much more complex than previously recognized (Brinker, Stopa et al. 2014). The traditional view of ventricular system flow dynamics suggests the majority of CSF is reabsorbed into venous circulation through arachnoid granulations into the superior sagittal sinus, with a small portion entering cervical lymphatics along the cranial nerves. This classical model of directed bulk flow movement of CSF is now being reconsidered, with new research questioning flow rate and primary locations of CSF formation and absorption. There is also new evidence that other important physiological functions, including the clearance of toxic metabolites and restoration of the brain during sleep, may depend on CSF circulation (Iliff, Wang et al. 2013, Kress, Iliff et al. 2014, Xie, Kang et al. 2013).

The importance of CSF as part of the functional waste clearance system of the brain and CNS is highlighted by the glymphatic system, which was recently identified by the Nedergaard Lab (University of Rochester Medical Center, Rochester, NY, USA) by observing the movement of fluorescent tracers into the brains of living mice. The glymphatic clearance pathway performs a similar function to the lymphatic pathway of the body, but relies on glial cells, hence the name glial + lymphatic. The glymphatic pathway allows CSF to wash over the brain parenchyma to help clear ISF and extracellular solutes from the interstitial spaces (Iliff, Wang et al. 2013). The pathway allows CSF to enter the brain along para-arterial spaces then exit along para-venous

spaces. The movement of fluid through the parenchyma is assisted by convective bulk flow of ISF and facilitated by AQP4 water channels along astrocytic endfeet that line the vasculature, guiding the flow of fluid along the outside of blood vessels.

The discovery of the glymphatic system should highlight the importance of the ventricular system as a whole, as well as the underlying elements, which include the ependyma. A well functioning glymphatic system is essential for healthy aging, as studies have shown that impairments of glymphatic clearance can contribute to toxic accumulations of interstitial solutes including A β and p-tau (Kress, Iliff et al. 2014).

Another recent advancement that has critical implications regarding the potential role of the ventricular system in neurodegenerative disease is the discovery of lymphatic vessels in the meninges of the brain (Louveau, Smirnov et al. 2015). The surprising discovery of lymphatic vessels around the brain was aided by a new technique in tissue preparation developed by Louveau and colleagues that allowed for whole sample visualization of intact tissue. While it was previously known that CSF flows into the cervical lymph node, it was not known how this occurs. Using injections of Evans blue, Louveau and colleagues demonstrated that the meningeal vessels are the primary route for CSF drainage to lymph nodes. The new discovery that lymphatic vessels exist in the brain meninges also implies that damage to the meningeal lymphatic vessels could have severe implications that are just beginning to be considered. Understanding the mechanisms of long-term damage from repeated mild traumatic injuries (rmTBI), commonly referred to as concussions, may have particular relevance. It is possible that damage to the brain's lymphatic vessels may cause inefficient drainage of CSF, contributing to

the development of neurodegenerative diseases such as AD and CTE through increased pressure, inefficient clearance of toxins, or a combination of both.

Together, recent discoveries highlighting the importance of the ventricular system and maintaining a healthy ependymal lining in aging may provide new insight into diseases marked by ventriculomegaly, which include schizophrenia, alcoholism, bipolar disorder, AD and CTE. CTE is believed to be caused by repetitive brain trauma and is of particular interest, because unlike the ventricular dilation found in AD that is attributed to ex-vacuo compensation, ventricular expansion precedes tissue atrophy in CTE (Kiernan, Montenigro et al. 2015).

Repeated mild traumatic brain injury (rmTBI)

Concussion: Definition, mechanisms of injury

Mild traumatic brain injury (mTBI) is used synonymously with concussion. The 2012 Consensus Statement on Concussion in Sport put forth the following updated definition: "Concussion is a brain injury and is defined as a complex pathophysiological process affecting the brain, induced by biomechanical forces" (McCrory, Meeuwisse et al. 2013). Biomechanical forces of mTBI include blunt impact, acceleration/deceleration, or rapid changes in pressure, such as in blast injury. Movement of the brain within the skull can be linear, rotational or a combination of both. Rotational force is considered to be the major component of concussion and is linked to symptom severity (Graham, Rivara et al. 2014). Acceleration and rotational forces cause shear force, which is the twisting that occurs when brain areas of different densities rotate at different speeds. Shear force is the cause of diffuse axonal injury, the main form of

structural injury following concussion that occurs from axonal stretching (Barkhoudarian, Hovda et al. 2011). The corpus callosum and midbrain structures are most affected by rotational forces (Ho et al. 2009, Giordano et al. 2014).

In addition to injury from mechanical forces, concussions generate a pathophysiologic cascade of events including neuronal depolarization, release of excitatory neurotransmitters, ionic shifts, changes in glucose metabolism, altered cerebral blood flow, and impaired axonal function (Giza, Hovda 2001). These alterations have been correlated with periods of post-concussion vulnerability and with neurobehavioral abnormalities.

Symptomatically, immediate neurological impairments following a concussion (i.e., dizziness, confusion, disorientation, blurred vision) generally resolve spontaneously. No abnormalities are generally found on routine imaging (CT or MRI), which increases the difficulty of diagnosis and assessment of severity. While concussion can result in loss of consciousness, the majority of cases do not. Symptoms of concussion vary widely and typically resolve within a few weeks (McCrory, Meeuwisse et al. 2013). However, history of prior concussion has been found to double the risk for prolonged symptoms in football players (Chrisman, Rivara et al. 2013). Prolonged symptoms following concussion fall under the diagnosis of post-concussive syndrome (Ryan, Warden 2003).

Chronic Traumatic Encephalopathy (CTE)

CTE is a progressive neurodegenerative disease mainly found in athletes with a history of repetitive concussive or subconcussive head injuries. Repeated brain trauma-related dementia

was characterized in boxers in 1928 by the term "Punch Drunk" (Martland 1928) then later named "Dementia Pugulistica" (Millspaugh 1937). The first published report of CTE in a professional American football player occurred in 2005 (Omalu, DeKosky et al. 2005). Recent neuropathological studies have identified CTE in athletes from various sports including soccer, baseball, ice hockey, rugby and most recently, BMX action sports. Currently, there have been approximately 250 confirmed cases of CTE based on post-mortem evaluation identifying the pathognomonic p-tau lesions required for conclusive diagnosis (McKee, Cairns et al. 2016). While the majority of cases thus far are in athletes exposed to repeated concussive or subconcussive hits to the head, cases have also been confirmed in non-athletes exposed to repeated head trauma and in military personnel exposed to blast injury (Stein, Alvarez et al. 2014). It may be important to note that the majority of military personal diagnosed with CTE also played contact sports. While repeated mild traumatic brain injury (rmTBI) is thought to be the main etiology behind CTE, symptoms often do not appear until years following injury (Galgano, Cantu et al. 2016). Symptoms associated with CTE include memory loss, confusion, impaired judgment, impulse control problems, aggression, depression, and, eventually, progressive dementia. Radiotracers are being developed that cross the blood brain barrier and bind to neurofibrillary and astroglial p-tau aggregates to allow visualization of p-tau in living patients using positron emission tomography (PET) (Barrio, Small et al. 2015). However, the results of these studies remain controversial due to lack of specificity (Zimmer, Leuzy et al. 2014), thus, CTE diagnosis can only be made upon post-mortem examination. Clinical guidelines for diagnosing probable, possible and unlikely cases of CTE-related syndrome in patients exposed to repeated head trauma have recently been put forth by clinicians under the term traumatic encephalopathy syndrome (TES) (Reams, Eckner et al. 2016). Recent combined

efforts have been made by groups of neurologists to improve clinical and pathological classifications for CTE.

Subtypes and stages of CTE

A consensus panel of neurologists recently described the defining pathological characteristic of CTE as follows: pathognomonic lesions marked by accumulation of abnormal p-tau in neurons, astrocytes and cell processes distributed around small blood vessels in an irregular pattern at the depths of the cortical sulci (McKee, Cairns et al. 2016). The report also listed several supportive characteristics of CTE that correspond to previously published definitions. While updates are being made on almost an annual basis, currently there are 4 stages of clinical development of CTE (McKee, Stein et al. 2015), and 4 corresponding stages of pathological development (Kiernan, Montenigro et al. 2015).

The 4 stages of clinical development of CTE are:

(i) headache, loss of attention and consciousness

(ii) depression, explosivity and short-term memory loss

(iii) loss of executive function and cognition

(iv) dementia

The stages of clinical development of CTE have been found to generally correspond to the stages of pathological development. The 4 stages of pathological development are marked by the following features upon post-mortem examination:

(i) isolated perivascular foci of p-tau positive neurofibrillary tangles (NFTs) and astrocytic tangles in the depths of the sulci and occasional mild ventricular dilation

(ii) increasing tauopathy in sulci, and also in deep structures (substantia nigra, dorsal and median raphe and thalamus), mild expansion of lateral ventricles and third ventricle, cavum septum pellucidum, Mild TDP-43 pathology but no A β plaques

(iii) mild frontal and temporal atrophy, enlargement of the lateral and third ventricles, septal abnormalities (50% of cases) including cavum septum pellucidum or fenestrations, extensive NFTs are found in the hippocampus, entorhinal cortex, amygdala and additional regions, increasing TDP-43 pathology in most cases

(iv) Severe atrophy in regions including cortex and hippocampus, thinning of corpus callosum, septal abnormalities (67% of cases) including cavum septum, fenestrations, or absence of the posterior septum. Widespread TDP-43 and P-tau are found throughout the brain as irregular clusters of glial tangles and NFTs

Relevant to our investigations, two important features to note that become more common or pronounced with advanced stages of pathological development of CTE are (1) increasing damage to the septal region and (2) ventricle expansion. Interestingly, ventricle expansion begins in the early stages (1 and 2) while atrophy does not occur until later stages (3 and 4). My research presented in Chapter 3 demonstrates that the septal region may be particularly vulnerable to injury following repeated brain trauma. Studies presented in chapter 3 also investigate ventriculomegaly and ependymal damage in an rmTBI mouse model.

Is damage to the ependymal lining a contributing factor to CTE?

Ependymal cell integrity may be an overlooked factor involved in the progression of CTE symptomology, possibly contributing to ventricular enlargement and p-tau accumulation. It is

possible that concussive injuries, whether by impact forces, rapid acceleration/deceleration, or rapid changes in pressure (such as in blast injury) cause a fluid wave that propagates through the CSF of the ventricle, creating structural damage to ependymal cells (Xiong, Elkind et al. 2014). Seismological predictions suggest mechanical pressure waves would cause more damage to large, unsupported objects, such as the motile cilia of ependymal cells that extend into the CSF (Toth, Hollrigel et al. 1997). As previously noted, inhibition of ciliary beating has been shown to contribute to the development of hydrocephalus in experimental mouse models (Monkkonen, Hakumaki et al. 2007). Regional tissue deformation generated by the shear force of tissues of varying densities moving across one another during concussive injury can cause stretching or tearing, also possibly contributing to periventricular gliosis, inflammation and ependymal cell damage. The rationale of our hypothesis that ependymal cell damage is a contributing factor in CTE is supported by the studies presented in Chapter 2 that demonstrate ependymal damage and subsequent gliosis leads to ventricular expansion in mouse models. The hypothesis is also consistent with the four progressive stages of CTE identified by Anne McKee's group that regularly demonstrate ventricular enlargement occurs at early stages of CTE, while mild brain atrophy begins to occur in later stages (McKee, Stein et al. 2015, Kiernan, Montenigro et al. 2015) implying that the pathogenesis of ventricular enlargement is due to factors other than brain atrophy.

Under normal conditions, waste molecules in the parenchyma diffuse transependymally into the ventricles, and are then either actively cleared by the choroid plexus or cleared by bulk flow through drainage into lymph or venous blood (Johanson et al, 2011). Damage to the ependymal cells can lead to replacement by astrocytic gliosis along the ventricle lining, creating an altered

CSF/ISF barrier. Alterations to the CSF/ISF interface may impair CSF flow, potentially disrupting the brain's ability to cleanse itself of waste molecules including p-tau. AQP4 localization along astrocytic endfeet that line blood vessels have been shown to facilitate glymphatic clearance, and TBI has been shown to disrupt AQP4 polarization (Ren, Iliff et al. 2013). Further studies by the same group used AQP4-/- mice to demonstrate that disruption to glymphatic system functioning can lead to increased accumulation of p-tau and activated microglia (Iliff, Chen et al. 2014). Therefore, it is possible that ependymal damage and associated changes in barrier function may contribute to ventricular enlargement and/or p-ta accumulation following repeated head injury.

While ventricle enlargement is a hallmark structural feature of CTE, no animal model has yet to recapitulate this phenotype. This may be because most rmTBI studies focus on cortical and hippocampal neuronal damage and gliosis, neglecting to investigate ventricle volume changes and the ependymal lining (see Chapter 5, Figure 1). TBI has been shown to cause reversible damage to motile cilia (Xiong, Elkind et al. 2014) but did not lead to ventricle enlargement as the cilia was repaired within 1 month and ependymal cells remained intact. A limitation of this study is that it only included a single brain injury, and it is possible that repeated injuries could have lead to more severe ependymal damage.

Repeated head injury is the main factor linked to CTE; however, the severity and the frequency of rmTBI required to cause CTE continues to be elusive (Galgano, Cantu et al. 2016). Thus, repeated head injuries are considered necessary to cause CTE, but not sufficient. In addition to the severity of injury and patient characteristics including history of prior concussions, the

mechanism of injury is thought to be an important factor in determining clinical outcome following concussion (Stemper, Shah et al. 2016). Animal models that recapitulate the acceleration and rotational forces of injury are required to improve our understanding of neuropathological sequelae of rmTBI.

Animal models of rmTBI/CTE

Repeated concussions have been linked to debilitating long-term consequences such as memory impairment and emotional instability (McKee 2009, Broglio 2012, Bailes 2013). Animal models of rmTBI that replicate forces of concussion (mTBI) and produce robust modeling of CTE disease pathology do not currently exist (Dewitt et al, 2013); however, animal models of rmTBI are necessary to help elucidate the pathological mechanisms of CTE, as human tissue studies provide end-point analysis only, and neuroimaging studies are still limited. Ideally, such a model would generate the neuropathological features matching human post-mortem tissue with CTE, which include p-tau accumulations, neurofibrillary and astrocytic tangles, ventricular enlargement, chronic inflammation, and TDP-43 accumulations. Many studies using animal models of rmTBI have been recently published using a variety of impact methods, various numbers of hits and different inter-injury intervals (see Chapter 5, Table 1 for list of studies with experimental paradigms including hit numbers and intervals). The majority of these studies use C57/BL/J male mice age 2-3months. The histological findings of the studies vary, and it is clear that further improvements need to be made in order to create improved reliable models that better replicate human exposure (Turner, Lucke-Wold et al. 2015).

Tissue clearing and three dimensional (3D) imaging

Technological advances in 3D imaging and new tissue clearing protocols are paving the way to

enhance histological investigations in intact tissue specimens, which is of great benefit to researchers as biological specimens are inherently 3D. CLARITY, iDISCO, TDE and CUBIC are among the many newly published tissue clearing protocols that are designed to allow deep penetration of high quality imaging, which is ideal for investigations assessing regional brain injury and periventricular structures. The studies presented in Chapter 4 demonstrate that 3D imaging can be performed consistently to a depth of 120μm on 500μm thick sections using a modified whole mount protocol without tissue clearing for certain antibodies of interest. These results pave the way for future studies by enabling researchers to use the baseline images provided to evaluate the added value of tissue clearing, which is often difficult because results often vary by antibody and sample size. Different clearing methods are evaluated, as each comes with its own benefits and drawbacks, and the iDISCO protocol is tested resulting successful clearing but unsuccessful labeling. Applications of advanced imaging and clearing techniques will be particularly useful for visualizing structures that span beyond single imaging planes such as investigating below the surface of periventricular gliosis and visualizing septal and hippocampal changes following rmTBI. 3D imaging of cleared, immunolabeled tissue can be applied to injury models to investigate the astrocytic and microglial reaction in scar formation within the brain in response to injury.

Organization of thesis

My work has focused on histological and structural changes that occur in periventricular regions of the brain during aging and following repetitive mild brain injury

In **Chapter 2**, by directly linking postmortem human MRI sequences with histological features of periventricular tissue, we show that substantial areas of lateral ventricle surface gliosis are

associated with ventriculomegaly. To examine whether loss of ependymal cell coverage resulting in ventricle surface glial scarring can lead directly to ventricle enlargement independent of any other injury or degenerative loss, we modeled in mice the glial scarring found along the lateral ventricle surface in aged humans. Together, these studies demonstrated a direct link between lateral ventricle surface gliosis and ventricle enlargement, highlighting the importance of maintaining an intact ependymal cell lining throughout aging.

In **Chapter 3**, to advance our understanding of regional and temporal cellular responses to repeated mild traumatic brain injury (rmTBI), we used a mouse model of rmTBI that allowed for free head and neck movement and incorporated acceleration, deceleration and rotational forces. We investigated two protocols, rmTBI-short (5 hits delivered over 3 days) and rmTBI-long (5 hits delivered over 15 days). The rmTBI-short protocol generated an immediate, localized microglial and astroglial response in the dorsolateral septum and hippocampus, with the astroglial response persisting in the dorsolateral septum. The rmTBI-long protocol showed only a transitory astroglial response in the dorsolateral septum. Our results demonstrate that the inter-injury interval is a critical factor in determining the magnitude of response, and that the lateral septum and hippocampus are particularly vulnerable regions in rmTBI, possibly contributing to memory and emotional impairments associated with repeated concussions.

Chapter 4 explores new methods for obtaining 3D images of intact biological tissue structures by creating an optimized whole mount preparation strategy and using advanced imaging techniques. Various tissue clearing protocols are considered, and results from the iDISCO tissue clearing protocol are presented. While these studies were performed in the context of young wild-type mice, the procedures discussed were devised to enhance histological investigations to

better define and visualize the scope of regional injury in rmTBI mouse models, as well as other applications.

In **Chapter 5**, I summarize the importance of maintaining a healthy ependymal lining and discuss implications of gliosis and ventriculomegaly. I provide a review of current rmTBI literature, including limitations, significance and implications. This discussion will highlight difficulties of modeling CTE in rodents, implications for concussions, future perspective for concussion research and applications of 3D imaging.

Chapter 2: Ventriculomegaly Associated With Ependymal Gliosis And Declines In Barrier Integrity In The Aging Human And Mouse Brain*

* **Excerpted from**: Shook BA[1], Lennington JB[1], **Acabchuk RL**[1], Halling M, Sun Y, Peters J, Wu Q, Mahajan A, Fellows DW, Conover JC. **Ventriculomegaly associated with ependymal gliosis and declines in barrier integrity in the aging human and mouse brain**. Aging Cell. 2014 Apr;13(2):340-50. doi: 10.1111/acel.12184. ([1] Co-first authors)

Note: This chapter is comprised of work that was performed in a team effort. My main contribution to this work included the processing and analysis of human tissue, creating and compiling figures and assisting with the writing of the publication. I also assisted with processing of MRI scans and mouse tissue. Sections of the publication to which I did not contribute have been removed. Credit to other graduate students is provided after the legends for each figure.

INTRODUCTION

Throughout adulthood and following injury, most epithelial linings of the body display remarkable plasticity and show considerable regenerative ability due to their associated stem cell niche (Fuchs et al., 2004; Blanpain et al., 2007; Snippert et al., 2010). A proliferative stem cell niche, the subventricular zone (SVZ), is also maintained along the lateral wall of the lateral ventricles in the adult mouse brain (Doetsch et al., 1997; Tropepe et al., 1997; Jin et al., 2003; Enwere et al., 2004; Maslov et al., 2004; Conover & Shook, 2011; Shook et al., 2012), and SVZ stem cells can contribute to repair of the lateral ventricle epithelial lining, the ependyma, throughout aging (Luo et al., 2006, 2008; Conover & Shook, 2011). However, we found that while regenerative stem cell-mediated repair can address the modest ependymal cell loss found in aged mice, extensive damage to the ependyma instead results in dense surface gliosis or 'scarring' (Del Carmen Gomez-Roldan et al., 2008; Luo et al., 2008).

The ependyma provides a bi-directional barrier and transport system for cerebral spinal fluid (CSF) and interstitial fluid (ISF) exchange (Del Bigio 2010; Johanson *et al.* 2011; Roales-Bujan *et al.* 2012), helping to keep the brain toxicant-free and in physiologic balance (Johanson *et al.* 2011; Roales-Bujan *et al.* 2012). The repercussions of periventricular gliosis instead of regenerative ependymal cell repair would be significant due to the loss of the bi-directional transport system provided by the ependymal cells lining the ventricles (Roales-Bujan *et al.* 2012).

Fluid-attenuated inversion recovery-MRI (FLAIR-MRI) scans of aged humans typically show ventriculomegaly and periventricular hyperintensities indicative of edema (Fazekas *et al.* 1993;

Sener 2002). While the demise of the ependymal lining has been linked to hydrocephaly/ventriculomegaly, and many neurological/psychiatric illnesses (e.g., autism, ADHD, schizophrenia) display comorbid ventriculomegaly [(Palha *et al.* 2012) and references therein], the molecular and cellular mechanisms underlying ependymal cell loss and its involvement in the initiation or progression of ventriculomegaly or other disease mechanisms remain largely enigmatic. It is important to note that the human SVZ stem cell niche, while highly active in infancy, dramatically declines by 18 months of age (Sanai *et al.* 2011; Wang *et al.* 2011; Bergmann *et al.* 2012), but individual variations are likely to exist. Through aging insults such as infectious agents, toxic substances and trauma may result in ependymal cell loss (Del Bigio 2010; Johanson *et al.* 2011), suggesting that stem cell-mediated regenerative replacement of lost or damaged ependymal cells is likely not an option in aged humans. As a result, loss of ependymal cell coverage and functionality would affect periventricular interstitial fluid homeostasis and transependymal bulk flow mechanisms. Since the human brain is larger than the mouse, Cserr postulated that there would be a greater dependence on efficient clearance of interstitial solutes, particularly larger molecules in humans (Cserr 1971), suggesting that loss of a functional ependyma would be of greater consequence to humans (Del Bigio 2010; Johanson *et al.* 2011).

Through an extensive comparison of mouse and human periventricular tissue, we reveal striking species-specific differences in the integrity and general maintenance of the lateral ventricle lining through aging. In addition, we present the first comprehensive documentation of the aged human lateral ventricle apical surface based on whole mount preparations of portions or the entire lateral ventricle wall. Findings from human tissue analysis then informed our generation of appropriate

models in mice. We show that following extensive insult to the ependymal lining in mice similar repair mechanisms do exist between mouse and human, allowing further investigation into the association between ventricle surface gliosis and ventriculomegaly.

MATERIALS AND METHODS

Animals

Male CD-1 mice (Charles River, Wilmington MA, USA) were aged in our vivarium; 3-month and 20-24-month mice were designated as young adult and aged, respectively. Animal procedures were approved by the University of Connecticut IACUC and conformed to NIH guidelines.

Mouse Brain Tissue Immunohistochemistry

Mice were perfused transcardially with 0.9% saline followed by 4% paraformaldehyde and coronal sections (50µm) immunostained, as described (Luo *et al.* 2008). Goat anti-GFAP (1:250, Santa Cruz Biotechnology, Santa Cruz CA, USA); mouse anti-GFAP (1:500, EMD Millipore, Billerica MA, USA) and rabbit anti-S100β (1:500, Dako, Glostrup, Denmark) antibodies and Alexa Fluor dye-conjugated secondary antibodies (Molecular Probes Life Technologies, Grand Island NY, USA) were used. Immunostained sections were imaged on a Zeiss Axio Imager M2 microscope with ApoTome (Carl Zeiss MicroImaging, Inc., Thornwood NY, USA), with a HAMAMATSU ORCA-R^2 digital camera C10600 or on a Leica TCS SP2 confocal laserscan microscope (Leica Microsystems, Buffalo Grove IL, USA). Secondary antibodies alone were used for controls.

Lateral ventricle wall wholemounts were prepared as described (Mirzadeh *et al.* 2008) and imaging protocols of whole mount tissue preparations are as previously detailed (Shook *et al.*

2012). Wholemounts were immunostained with the following antibody combinations: mouse anti-□-catenin (1:250, BD Biosciences, San Jose CA, USA); rabbit anti-□-catenin (1:100, Cell Signaling Technology, Danvers MA, USA); mouse or rabbit anti-γ-tubulin (1:500, Sigma-Aldrich, St. Louis MO, USA); mouse anti-GFAP (1:400, EMD Millipore, Billerica MA, USA); goat anti-GFAP (1:250, Santa Cruz Biotechnology, Santa Cruz CA, USA); rabbit anti-AQP4 (1:400, Sigma-Aldrich, St. Louis, MO, USA) and imaged. The imaging focal plane was set at the ventricle surface as determined by the use of β-catenin (marks apical adherens junction proteins) and □-tubulin (marks basal bodies of cilia) as indicators of surface depth.

Neuraminidase Injections

Mice were anesthetized using isoflourane and then positioned in a stereotaxic apparatus (Stoelting, Wood Dale, IL). Body temperature was maintained using heating pads. A sterile syringe loaded with neuraminidase (*Clostridium perfringens*, Roche Diagnostics, Indianapolis IN, USA) diluted in saline (0.9% NaCl) was delivered unilaterally to the right lateral ventricle using the following coordinates relative to bregma (lateral: 0.65mm, ventral: 2.65mm). Neuramindase (1□l) was injected at a rate of 0.5μL/min for 2 minutes. Control mice were injected with an equal volume of saline.

Lateral Ventricle Volume Measurements: Mouse

To determine age-related changes in lateral ventricle volume every fourth section (10-12 coronal sections total, n=3 per age, coordinates $^{+}$1.78-$^{-}$1.2mm relative to Bregma) was stained for S100β □ependymal cells) and imaged. Contour tracings of the ventricle walls and resulting 3D models were constructed using StereoInvestigator and Neurolucida Explorer (MBF Bioscience,

Williston VT, USA). To evaluate expansion, the same procedure was used on all sections from most anterior to the point when the 3rd ventricle became visible.

Human Brain Tissue Histology/Immunohistochemistry

Postmortem human brain tissue (hemispheres and slices) was obtained from the Harvard Brain Tissue Resource Center (McLean Hospital) and from the UCHC Department of Anatomic Pathology and Laboratory Medicine. Tissue was fixed in 10% formalin (minimum 2 weeks, maximum 6 weeks), rinsed thoroughly in 0.1M PBS and wholemounts of the lateral ventricle lateral wall were processed for antigen retrieval and immunohistochemistry, as described above. Wholemounts of all regions of the lateral ventricle (Subject 1: 36 15mm x 8mm sections and Subject 2: 18 15mm x 8mm sections) were prepared as described above. Coronal sections were taken from the superior-most region of the anterior lateral ventricle to investigate the integrity of the ependymal lining and SVZ.

For immunoperoxidase labeling, 8□m paraffin sections were processed using a Bond Max autostainer (Leica Microsytems, Buffalo Grove IL, USA). Hematoxylin and eosin staining was performed as described (Luo *et al.* 2008).

Lateral Ventricle Volume Measurements: Human

For evaluation of lateral ventricle volumes across age, high-resolution MRI sets were obtained from the Open Access Series of Imaging Studies (OASIS) database (www.oasis-brains.org) (Marcus *et al.* 2007; Marcus *et al.* 2010). Only male and female subjects remaining non-demented (clinical dementia rating < 0.5) throughout the length of the study were analyzed (Marcus *et al.* 2007). MRIs of younger individuals (non-demented subjects age 20 to 34-years) were obtained from Yale Medical School. In total, 70 individuals were analyzed in six different

age groups: 19-39 (n=23), 40-69 (n=6), 60-69 (n=10), 70-79 (n=13), 80-89 (n=13), and >90 (n=5). The lateral ventricles were defined on high-resolution MRI T1-weighted images using a semi-automated 3D segmentation tool, ITK-SNAP (www.itksnap.org)(Snippert *et al.* 2010). Pre-processing of the images was performed prior to automatic isolation of the lateral ventricle, including setting an upper threshold for image intensity at 30%. For automatic segmentation, lateral ventricle expanding balloon force was set to 3.0, detailed curvature force set to 0.20, and 125 iterations at step size 1 was sufficient to isolate the lateral ventricle. Volumes were rendered using Slicer3D [www.slicer.org]. Longitudinal MRI sets (OASIS) were used from healthy subjects that underwent MRI scanning in three or more sessions spanning multiple years(Marcus *et al.* 2010).

Post-Mortem MRI: Human

Post-mortem MRI was performed using a 1.5 Tesla MR unit (Siemens Avanto, Siemens Medical Solutions, Malvern PA, USA). A contiguous thin section (1.3mm), 3-D T1-weighted MP RAGE sequence was performed on formalin-fixed brains of two individual subjects. Subject 1 (female, 82 years) was diagnosed with Alzheimer's disease and died of pneumonia and Subject 2 (male, 86 years) died of cardiac arrest. Lateral ventricle volumes were processed and rendered, as described above.

Statistical Analysis

Results are reported as mean ± SEM. Statistical analysis across multiple ages was assessed using 1-way ANOVA with Bonferroni's multiple comparisons post-test. Statistical analysis between ages was assessed using a two-tailed unpaired Student's *t*-test. Statistical analysis between neuraminidase injected and controls was performed using a two-tailed Student's *t*-test. Statistical

analyses were performed in Prism (GraphPad) software or Excel. Significance was set at $p < 0.05$.

RESULTS

Humans exhibit age-related lateral ventricle expansion and periventricular gliosis

Using data from the 'Open Access Series of Imaging Studies' (OASIS) database (Marcus et al., 2007) that included cross-sectional MRI data from young, middle-aged, and older non-demented adults, we examined changes to the lateral ventricles. Semi-automated segmentation using ITK-SNAP (Snippert et al., 2010), followed by 3D reconstruction of the lateral ventricles using Slicer3D (www.slicer.org), revealed age-related increases in total volume (**Fig. 1A,B**). Based on longitudinal data from the OASIS collection, which included 150 subjects aged 60–95 years (Marcus et al., 2010), we observed sequential age-associated lateral ventricle volume increases in both males and females (**Fig. 1C,D**), similar to other previously reported studies (Scahill et al., 2002; Resnick et al., 2003). These data illustrate that ventricle expansion occurs in aging even in the absence of dementia.

To evaluate the integrity of the ependymal lining through aging, we examined aged lateral ventricle tissue samples collected by the Harvard Brain Tissue Resource Center and the University of Connecticut Health Center, Department of Anatomical Pathology (see Experimental Procedures, Table 1, Supporting information). Both coronal sections and whole-mount preparations of the lateral walls of the lateral ventricles were evaluated based on 12 mm 9 12 mm tissue samples. Tissue was categorized as having (i) intact ependymal cell coverage; (ii) dense areas of surface gliosis; or (iii) an intermediate phenotype consisting of a disorganized and compromised ventricle lining showing absence of cuboidal ependymal cells as indicated by diffuse or absent b-catenin staining (marker of adherens junctions) and the presence of several

surface astrocytic processes (see **Table 1**). Typically, in subjects > 55 years old, a combination of both small and large expanses of intact ependymal cell coverage (**Fig. 1E,F**) and large areas devoid of ependymal cells were detected. Staining for glial fibrillary acidic protein (GFAP) indicated surface gliosis in regions where an intact ependymal lining was absent (**Fig. 1G–I**), and a dense array of astrocytic processes occupied an enlarged hypocellular region that typically defined the narrow subependymal zone (Quinones-Hinojosa et al., 2006), often creating a gliotic bulge at the ventricle surface (**Fig. 1G–I**).

Whole-mount preparations of the lateral ventricle provide a unique ability to examine the apical surface of the ventricle wall and have been used to observe the organization of ependymal cells and surface- projecting neural stem cells in mice (Mirzadeh et al., 2008). Here, we used whole-mount preparations to characterize alterations that occur to the surface ependymal cell layer (Doetsch & Alvarez-Buylla, 1996; Conover et al., 2000) in aged human tissue samples. Our analysis revealed both zones of contiguous ependymal cell coverage and regions of extensive gliosis (**Fig. 1J–M).** While these studies indicate that surface gliosis occurs in regions where ependymal cell coverage has been lost and this phenotype is prominent in tissue from aged humans, these studies provided only limited information because accompanying measurements of ventricle volumes were not available.

Pairing Postmortem MRI with Histological Analysis of Periventricular Tissue Reveals Association Between Gliosis and Ventriculomegaly

To examine directly the relationship between ventriculomegaly and glial scarring at the ventricle surface in human tissue, we paired postmortem MRI scans with histological processing of periventricular tissue. Two age-matched subjects were selected based on dramatic differences in

lateral ventricle volumes. A contiguous thin section (1.3mm), 3D T1-weighted MP RAGE sequence was performed on the formalin-fixed brains of the two subjects. Automatic segmentation of the lateral ventricles defined on high-resolution MRI was performed using ITK-SNAP (Snippert *et al.* 2010) and volumes rendered using Slicer3D. 3D reconstructions showed that Subject 1 (82-years) had an age-appropriate lateral ventricle volume (59241.4mm^3) (Subject 1 volume indicated in red on graph in **Fig. 1B**, see also **Fig. 2A**). Local microscopic features of periventricular tissue were then mapped using corresponding lateral ventricle tissue processed for histology (**Fig. 2B-D**). Both coronal sections (**Fig. 2B**) and 15mm x 8mm *en face* whole mount samples (**Fig. 2C**) were analyzed, effectively covering the entire lateral ventricle lateral wall. Tissue samples from Subject 1 contained regions showing an attenuated ependymal cell lining (**Fig. 2B**) and immunohistochemical analysis of whole mount preparations of the lateral ventricle wall revealed that while the inferior portion of the anterior and middle wall consisted mainly of intact ependymal cell coverage (**Fig. 2C, D**, green), 'islands' of dense gliosis were found scattered throughout (**Fig. 2C, D**, red). In the superior/anterior region, large areas of 'mixed' composition were detected. These regions were comprised of areas of surface gliosis (red); isolated areas containing intact ependyma (classic cobblestone appearance, green); and regions lacking an intact ependyma as marked by absence of clear □-catenin$^+$ surface adherens junctions, surface astrocytic processes, but no overt gliosis (compromised, yellow) (**Fig. 2D**). Along the superior (mid and posterior) and entire posterior lateral ventricle wall, large GFAP$^+$ gliotic expanses predominated (**Fig. 2C, D**, red).

In contrast, MRI scans from Subject 2 (86-years) showed a ventricle volume (11279.5mm^3) more typical of a 20-40 year old (Subject 2 volume indicated in red on graph in **Fig. 1B**, see also **Fig.**

3A). Hematoxylin and eosin staining of coronal sections of the anterior wall revealed a monolayer of cuboidal ependymal cells, indicative of a healthy ependymal lining **(Fig. 3B).** Whole mount preparations of the entire lateral ventricle from Subject 2 revealed intact ependymal cell coverage along the complete lateral wall of the lateral ventricle (**Fig. 3C**, green); we did not detect any gliosis along the lateral wall.

To examine whether the two Subjects showed differences in dividing cells within the SVZ, we labeled fixed tissue samples with Ki67 to mark cycling cells. We found only a few $Ki67^{+}$ endothelial cells; no other SVZ cells were labeled in either Subject 1 or 2. As with all end-state fixed tissue samples, it is impossible to determine if any differences in cycling cells may have existed at earlier time points for the two subjects.

The thickness and density of the astrocytic ribbon layer and hypocellular gap region of the two Subjects were also compared. No significant differences were observed in regions containing an intact ependymal cell lining (data not shown). However in regions lacking ependymal cell coverage (Subject 1), large masses of ventricle-contacting astrocytic processes formed increasing the thickness of astrocyte coverage from the glial ribbon to the ventricle surface. Whole mount preparations allowed us to observe clearly areas of intact ependymal cell coverage, regions with some superficial glial processes and other regions with extensive surface glial scarring with no ependymal cell coverage.

Generation of a Mouse Model of Periventricular Gliosis

The directionality of the relationship between ventricle surface gliosis and ventricle expansion cannot be easily deduced from MRI scans and endpoint human tissue histology. To investigate

this relationship we needed to replicate in mice the phenotype of periventricular glial scarring found in aged humans. Under normal conditions we never observed periventricular gliosis in mice of any age. Whole mount preparations of the entire lateral ventricle lateral wall consistently revealed an intact ependymal cell lining with no gliosis. However, damage to the ependymal cell monolayer by intraventricular injection of high concentrations of neuraminidase (100-500ng/□l) caused large stretches of ependymal denudation, resulting in extensive gliosis along the ventricle surface (Del Carmen Gomez-Roldan *et al.* 2008; Luo *et al.* 2008). Neuraminidase, found in a range of organisms including bacteria and viruses, cleaves sialoglycoproteins involved in cell recognition and adhesion (Rutishauser & Jessell 1988; Kuchler *et al.* 1994; Figarella-Branger *et al.* 1995) and can thereby mimic ependymal loss due to infection [(Johanson *et al.* 2011) and references therein]. By titering the neuraminidase concentration, varying degrees of ependymal cell denudation can be generated to yield differing levels of ventricle surface gliosis (Luo *et al.* 2008). We found that 10-50mU resulted in ventricle surface scarring similar to that typically found in aged humans (**Fig. 1**). Immunohistological analysis of the lateral ventricle wall showed an increase in astrocytic process density at the lateral ventricle surface in the form of scars (**Fig. 4A**, arrows), similar to that found along the surface of the lateral ventricles in aged humans (**Fig. 1J & M, Fig. 2C, Fig. 4B**). No scarring or damage was detected in the 3rd or other ventricles, indicating a direct and local effect of the intraventricular injections. In addition, loss of the ependymal lining resulted in loss of the associated SVZ stem cell niche [(Luo et al. 2008; Jimenez et al. 2009; Rodriguez et al. 2012) and references therein]. With this mouse model we could then investigate the connection between periventricular gliosis and ventriculomegaly and begin to dissect the cellular mechanisms that lead to ventricle surface gliosis.

Aquaporin-4 is Upregulated in Sites of Lateral Ventricle Gliosis in Mouse and Human

Along with ventricle enlargement, FLAIR-MRI of elderly human brains consistently reveals age-associated periventricular edema (Leys *et al.* 1990), suggesting that transependymal bulk flow is compromised. To assess periventricular scarring and compromised CSF-interstitial fluid homeostasis in aged human tissue, we analyzed aquaporin-4 (AQP4) expression patterns. Aquaporins are water channels and AQP4 is expressed throughout the brain on perivascular astrocytic endfeet and on the basal surface of ependymal cells (Haj-Yasein *et al.* 2011; Iliff *et al.* 2012). AQP4 expression has been found to increase during gliosis (Sofroniew 2009). Deletion of AQP4 has been shown to reduce the effects of cytotoxic edema and improve outcome after stroke (Sofroniew 2009; Zador *et al.* 2009). Therefore, changing expression patterns would suggest alterations to CSF-interstitial fluid regulation (Papadopoulos & Verkman 2007; Haj-Yasein *et al.* 2011; Iliff *et al.* 2012). We found high levels of AQP4 in aged human tissue at sites of glial scarring, but not where there were intact ependymal cells (**Fig. 4B**). Similarly, following neuraminidase treatment, we found substantially enhanced expression of AQP4 in regions of periventricular scarring in mouse tissue (**Fig. 4A**, left of dotted line), but no increase in AQP4 expression in the uninjured tissue (**Fig. 4A**, * area of intact ependymal cells). By demonstrating that increased AQP4 expression occurs in periventricular scarring in both mouse and humans, our studies indicate the bi-directional fluid transport of CSF/ISF may be altered in aged humans, which may contribute to periventricular edema.

Extensive Ventricle Surface Gliosis Results in Ventricle Expansion

We next examined the possibility that loss of ependymal cells lining the ventricle can initiate ventricle expansion, independent of neurodegeneration or other injury to the brain. Neuraminidase (50mU, 1□l at 500ng/□l) or saline vehicle (1□l) was injected unilaterally into the lateral ventricle of young adult mice (3-4 months). After a two-month period the brains were

collected and sectioned. Upon visual inspection, the lateral ventricles of mice injected with neuraminidase appeared dilated compared to the lateral ventricles of mice injected with the same volume of saline vehicle (**Fig. 5A**). Contours were traced around the lateral ventricles and then uploaded into Neurolucida Explorer software for compilation into 3D reconstructions (**Fig. 5B**). Lateral ventricle volume measurements determined from the 3D models revealed that mice injected with a dose of neuraminidase sufficient to denude regions of ependymal cells similar to that found in aged humans were significantly larger than both saline-injected ($p=0.025$) and non-injected littermates ($p=0.024$) (**Fig. 5C**). Ventricle surface gliosis was verified using immunohistochemistry two months after introduction of neuraminidase into the lateral ventricles (**Fig. 5D**, bracket).

DISCUSSION

The ventricular system of the brain is a network of communicating cavities that encloses and circulates the CSF. Together with the blood-brain barrier the ventricles are responsible for solute clearance from the brain. Interstitial solutes are thought to be cleared to the CSF via convective bulk flow of ISF, and a recently described 'glymphatic' pathway has been identified for the para-aterial influx of sub-arachnoid CSF into the ISF for further clearance along large-caliber draining veins that function together with and support other clearance routes (Iliff *et al.* 2012). Biochemical changes in the brain are thereby reflected in the CSF and any alterations to the ependymal monolayer would affect efficient bi-directional transport and clearance mechanisms.

The functional units of the ventricles are the ependymal cells, which are organized as a monolayer of ciliated epithelial cells that provide both barrier and filtration functions, and generate laminar flow of CSF at the ventricle surface. We examined the relationship between

partial loss of the ependymal cell lining of the lateral ventricle to surface gliosis and ventricle expansion, and found that significant ventricle surface gliosis can be linked directly to lateral ventricle expansion, independent of any injury or degenerative loss of brain tissue. Increased expression of the water channel AQP4 was detected in sites of glial scarring, suggesting abnormalities in CSF/ISF homeostasis and interstitial solute clearance. Our work and the work of others suggests that the effects of replacing functional ependymal cells with a glial scar would be cumulative over time, supporting in part the progressive nature of ventriculomegaly (Sival *et al.* 2011). While we show that destruction of the ependymal lining alone is sufficient to initiate lateral ventricle expansion, it is likely that a combination of factors, such as neurodegeneration, vascular defects and the inappropriate accumulation of soluble proteins work in concert to generate ventriculomegaly found in humans.

Lateral Ventricle Ventriculomegaly and Periventricular Gliosis in Aging Humans

In aging humans there is a strong correlation between lateral ventricle ventriculomegaly, not involving dementia or obstruction of CSF flow, and aging (Scahill *et al.* 2002; Resnick *et al.* 2003). However, the exact cause, progression and importantly the impact to normal brain function are currently not known. Along with ventricle enlargement, FLAIR-MRI consistently reveals age-related periventricular edema, suggesting that transependymal flow is compromised. Through lateral ventricle volume measurements and 3D modeling using MRI scans from the OASIS database of non-demented humans (Marcus *et al.* 2007; Marcus *et al.* 2010), we demonstrated age-associated lateral ventricle enlargement, with longitudinal data typically showing progressive increases in lateral ventricle size. Based on histological analysis of postmortem forebrain tissue samples from a population of aged subjects, we found that

widespread gliosis along the lateral ventricle walls is typically found. However, these initial studies were incomplete, since access to both longitudinal MRI sequence data and tissue samples for histological analysis of the entire lateral ventricle wall were not available.

In two contrasting case studies involving brain samples from elderly subjects, we were able to analyze post-mortem MRIs paired with histological tissue samples of the entire lateral ventricle. This pairing was unique since the two subjects showed significant differences in ventricle volume, which gave us the rare opportunity to examine tissue quality along the entire surface of the lateral ventricles. Our findings of regional glial scarring at the ventricle surface in the expanded ventricle sample and the complete absence of scarring and presence of an intact ependymal lining in the small ventricle sample supported our hypothesis that gliosis is associated with ventriculomegaly and not solely age. However, the sequence of events that led to gliosis at the ventricle surface and ventriculomegaly could not be deduced from this single endpoint analysis of lateral ventricle volume and surface histology. Ultimately, reconstruction of medical histories, together with a multi-modal imaging paradigm including longitudinal FLAIR-MRI to show areas of edema and volume changes, and diffusion tensor imaging (DTI), to show changes in major fiber tracts, would provide the level of criteria over the lifetime of the subject necessary to validate histological findings and map directionality in a correlation. So while there is no clear way to prove causality in the human cases we investigated, the information we obtained informed and guided our mouse model strategies.

Periventricular Tissue Comparisons: Mouse Versus Human

Due to limited availability of longitudinal, multi-modal human subject data and complete histological samples of the ventricle linings, we were reliant on animal models to examine the

relationship between ventricle enlargement and periventricular gliosis. Our comparison of mouse and human periventricular tissue through aging revealed some striking species-specific differences. In adult mice, the lack of significant age-associated change in lateral ventricle volume, only limited levels of ependymal cell stretching (measured as increased apical surface area) and the capacity for modest ependymal repair through SVZ stem cell-mediated regenerative replacement of ependymal cells supports our finding of an intact ependymal cell lining with no surface gliosis or scarring throughout aging (Luo *et al.* 2006; Luo *et al.* 2008; Bouab *et al.* 2011). It should be noted that caged mice do not experience infection or trauma that may result in denudation of the ependymal lining. Periventricular gliosis occurred only in situations when we deliberately created extensive injury to the ependymal lining.

Humans, in contrast, do not appear to possess an active stem cell niche in adulthood (Sanai *et al.* 2011; Wang *et al.* 2011; Bergmann *et al.* 2012) and endothelial cells were the only proliferative cells we found within the SVZ of aged human tissue that we surveyed, regardless of ventricle size. These studies are in agreement with the work of others describing few proliferating cells in the adult human SVZ (Sanai *et al.* 2004; Sanai *et al.* 2011); however, the existence and quantity of quiescent SVZ stem cells in the adult human remains a point of controversy (Curtis *et al.* 2007; Sanai *et al.* 2007). Interestingly, aged, non-demented humans (>60 years), in contrast to mice, typically show age-associated ventriculomegaly and accompanying ventricle surface gliosis (Scahill *et al.* 2002; Resnick *et al.* 2003). However, some level of variability may exist between humans, as we report no periventricular gliosis along the lateral wall of the lateral ventricles in an 86 year old who also did not show enlarged lateral ventricles. This subject died of a cardiac arrest and did not show any cortical brain atrophy. So, it is possible that this subject

did not experience the one or several inciting events that typically result in ventricle surface gliosis in the human population. We did not find any overt difference in cycling cells or cytoarchitecture in the subependymal layer in regions containing an intact ependyma between Subject 1 and 2. However, this was based on a snapshot view at the end of life; it is possible that at an earlier (maybe even mid-life) stage there were differences in stem cell number or capacity for repair between the two Subjects. The repercussions of periventricular gliosis instead of regenerative repair would seem significant, since loss of a bi-directional transependymal transport system appears to be inextricably linked to periventricular edema, loss of ISF homeostasis and proper solute clearance (Roales-Bujan *et al.* 2012).

Generating Mouse Models of Periventricular Scarring

Mouse studies help us to interrogate the human condition variable by variable. Here we isolated one variable, ependymal cell denudation resulting in glial scarring at the ventricle surface, to examine whether this alone could result in ventricle enlargement in the adult lateral ventricles. Bacterial and viral infections are known to cause destruction of the ependymal lining (Johanson *et al.* 2011). Neuraminidase, a surface enzyme associated with bacteria and viruses, can result in ependymal cell denudation following severe infection. Previous studies have shown that ependymal cell denudation via injection of high concentrations of neuraminidase into the lateral ventricle resulted in glial scarring at the ventricle surface and in some instances SVZ cells (neuroblasts) formed clusters where there were breaks in the ependymal lining (Del Carmen Gomez-Roldan *et al.* 2008). By titering the concentration of neuraminidase injected into the lateral ventricles, we could control the degree of ependymal cell denudation (Luo *et al.* 2008) and generate levels of ventricle surface gliosis to mimic what we detected in human tissue. At the concentration and volume used in this study, we only observed glial scars at the surface and

never detected any damage to the ependymal lining in the 3rd ventricle and ventricle system communication was maintained. Thus we developed an effective and clinically relevant mouse model to examine the mechanics and consequences of scar formation. Indeed studies have identified abnormal or mis-expression of adherent junction proteins as a cause for ependymal denudation in human fetuses [(Sival *et al.* 2011; Rodriguez *et al.* 2012) and references therein].

We found that the ventricle surface scars generated in mice were very similar to those observed in human tissue and showed upregulation of AQP4 expression patterns at sites of ventricle surface gliosis. This is of particular significance as AQP4 is implicated in water uptake into brain tissue during the development of cytotoxic edema, as well as in water clearance after vasogenic edema (Papadopoulos & Verkman 2007; Verkman 2008; Haj-Yasein *et al.* 2011). In glial scars the expression and localization of AQP4 constitutes a neuropathological condition resulting in disturbed interstitial bulk flow and failure to clear neurotoxic solutes (e.g., Aβ, tau) [(Verkman 2008) and references therein]. Reduced brain swelling and improved clinical outcome occurred in $AQP4^{-/-}$ mice in a model of bacterial meningitis (Papadopoulos & Verkman 2007); demonstrating that altered AQP4 expression may be a maladaptive response that exacerbates periventricular water accumulation. The water-transporting function of aquaporins has also been implicated in the initial formation of glial scars, affecting both the migration to the site of injury and the rate of glial scar formation [(Verkman 2008) and references therein]. This feature may be critical and in its absence result in the inability to properly seal the ventricle lining following denudation of ependymal cells. Ultimately, $AQP4^{-/-}$ mice in combination with our neuraminidase model should provide further mechanistic insight into the phenomenon of age-related ventricular enlargement.

Conclusion

Mice possess an active subventricular zone stem cell niche that is capable of modest ependymal repair throughout aging. Ependymal cell integrity and barrier function appear to be maintained and age-related changes in lateral ventricle volume are not detected in mice. In contrast, aged humans appear to lack a functional SVZ stem cell niche and typically develop ventriculomegaly during the course of aging. Unlike other epithelial linings of the body, the regenerative replacement of the human lateral ventricle ependymal lining would appear to be very limited. Since many diseases or injuries (Alzheimer's disease, schizophrenia, traumatic brain injury, etc.) can result in ventricle enlargement, we aimed to establish some of the underlying characteristics of ventriculomegaly and found that damage to the ependymal lining resulting in lateral ventricle surface gliosis is one potential initiator of ventriculomegaly.

Future studies incorporating non-invasive imaging for assessing ventricle lining integrity and interstitial solute movement following perturbations to the ventricle lining will be necessary to establish the time course for decline of ventricle lining health and the progression of ventricle enlargement. Since we observed regional differences in the integrity of the ventricle lining in humans, it will be of particular value to determine whether there is regional vulnerability along the ventricle surface. Together our studies highlight the importance of ventricular system health in maintaining critical barrier and filtration functions within the brain – a surprisingly understudied area in brain barrier biology.

FIGURES AND LEGENDS

Table 1

Table 1. Summary of tissue analysis: ependymal coverage versus scarring

Age	Gender	Cause of death	Regional Tissue Analysis		
51	Male	myocardial infarction	SA	SM	SP
			A	M	P
			IA	IM	IP
54	Female	N/A	SA	SM	SP
			A	M	P
			IA	IM	IP
58	Male	pancreatic cancer, no metastasis	SA	SM	SP
			A	M	P
			IA	IM	IP
59	Male	N/A	SA	SM	SP
			A	M	P
			IA	IM	IP
61	Female	pneumonia*	SA	SM	SP
			A	M	P
			IA	IM	IP
62	Male	myocardial infarction	SA	SM	SP
			A	M	P
			IA	IM	IP
76	Male	cardiac arrest	SA	SM	SP
			A	M	P
			IA	IM	IP
77	Female	cardiac arrest	SA	SM	SP
			A	M	P
			IA	IM	IP
82	Female	N/A*	SA	SM	SP
			A	M	P
			IA	IM	IP
83	Male	myocardial infarction	SA	SM	SP
			A	M	P
			IA	IM	IP
85	Male	N/A	SA	SM	SP
			A	M	P
			IA	IM	IP
86	Male	myocardial infarction	SA	SM	SP
			A	M	P
			IA	IM	IP
89	Female	N/A*	SA	SM	SP
			A	M	P
			IA	IM	IP
91	Female	congestive heart failure	SA	SM	SP
			A	M	P
			IA	IM	IP

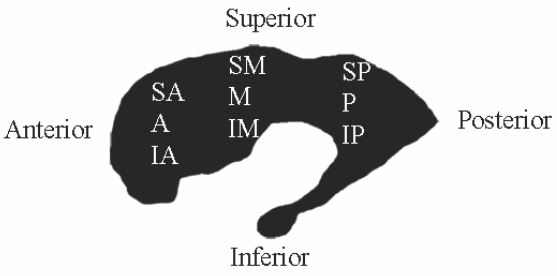

Region Key

SA	Superior portion of anterior region
A	Central anterior region
IA	Inferior portion of anterior region
SM	Superior portion of middle region
M	Central middle region
IM	Inferior portion of middle region
SP	Superior portion of posterior region
P	Central posterior region
IP	Inferior portion of posterior region

Color Key

- Intact ependyma throughout region
- Limited surface astrocytic processes
- Contains areas of dense astrocytic scarring on surface
- Not available

* indicates Alzheimer's Diagnosis

Post mortem intervals range from 11-28 hours

Figure credits: RA

Figure 1

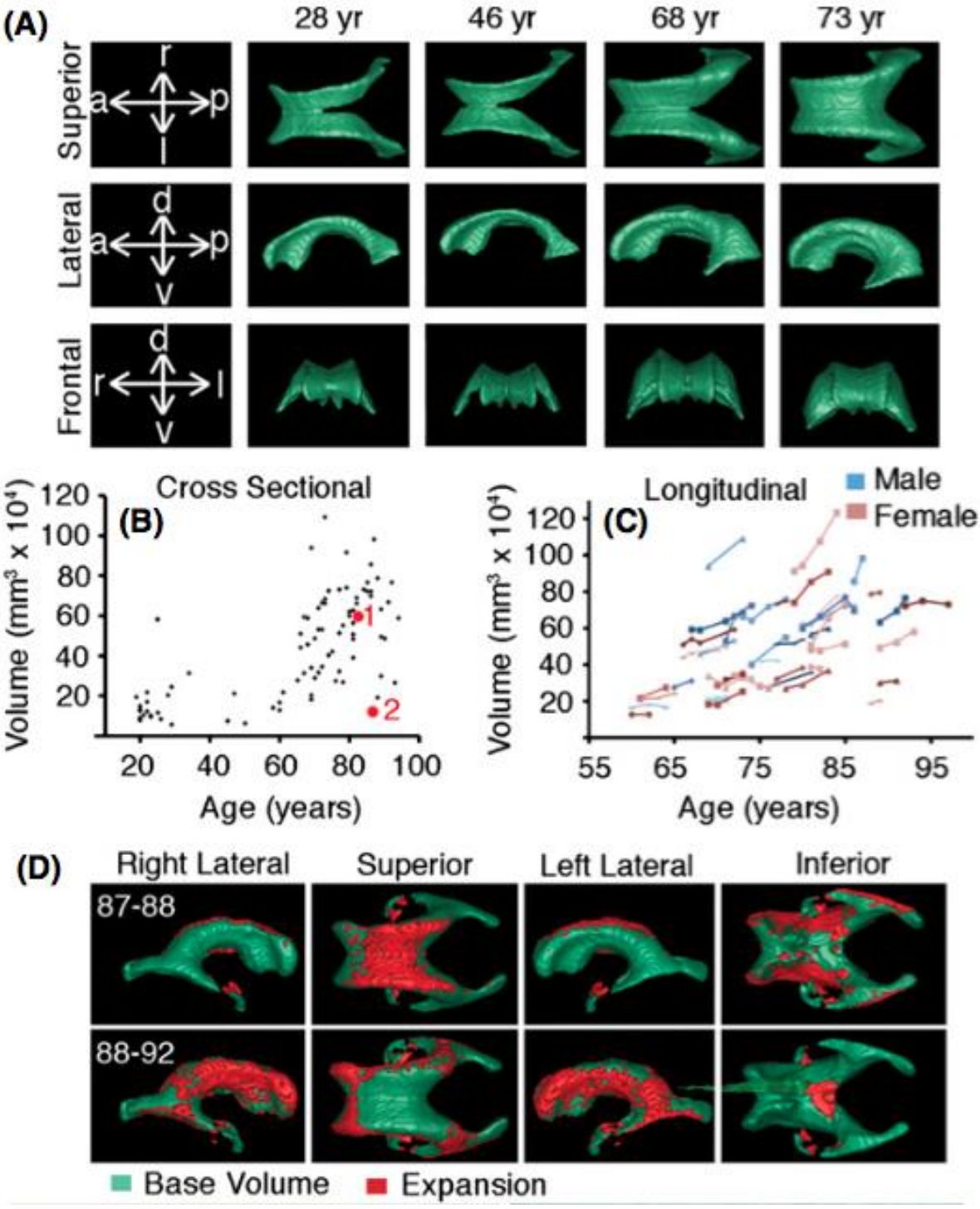
(A)
28 yr
46 yr
68 yr
73 yr
Superior
Lateral
Frontal
r
a
p
l
d
v
(B)
Cross Sectional
Volume (mm³ x 10⁴)
Age (years)
(C)
Longitudinal
Male
Female
(D)
Right Lateral
Superior
Left Lateral
Inferior
87-88
88-92
Base Volume
Expansion

Figure 1 Continued.

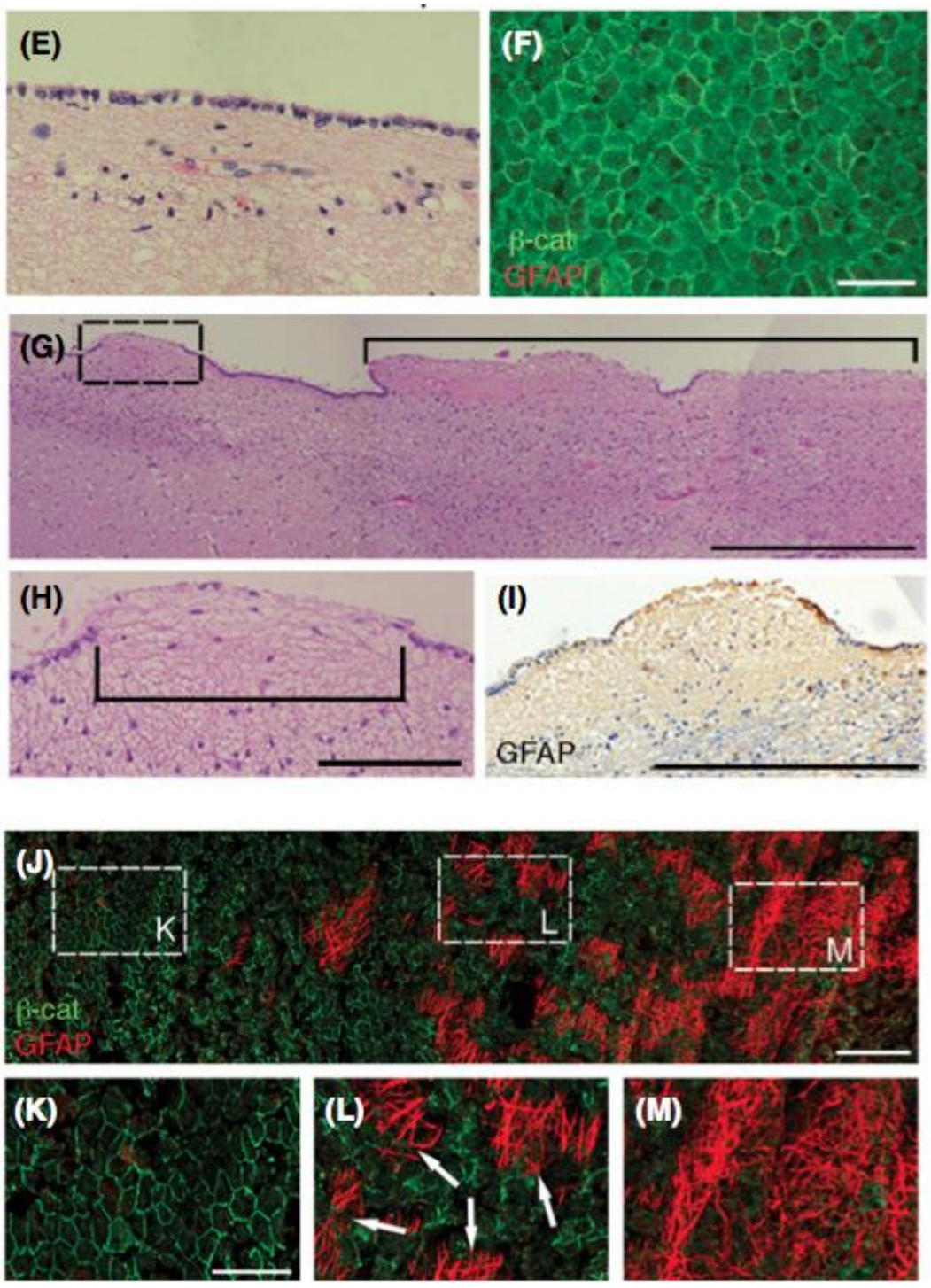

Figure 1. Increased ventricle volume and periventricular gliosis are typically associated with age in humans. (**A**) Representative MRI-based 3D reconstructions of the lateral ventricle from humans of different age groups. (**B**) A cross sectional sampling of MRI scans from the OASIS dataset (non-demented) demonstrates increased lateral ventricle volume is associated with age. (Subject 1 and 2 volumes are denoted with red dots). (**C**) Longitudinal data shows expansion typically occurs over time in both males and females. (**D**) MRI-based lateral ventricle reconstructions show example of regional expansion (red) over time. (**E,F**) From aged tissue, periventricular, coronal section stained with H&E and whole mounts preparations of the lateral wall of the lateral ventricle show regions of intact ependyma. (**G**) H&E staining of representative coronal sections of aged tissue (77 yrs old) clearly show areas devoid of an intact ependymal layer (bracket). (**H**) Enlarged region denoted in (**G**) shows regions lacking ependymal cells and (**I**) immunohistochemical analysis reveals that areas without an ependymal monolayer have $GFAP^+$ processes at the ventricle surface. (**J**) Whole mount preparation (tissue from 62 year old) revealed areas of intact ependyma (**K**) and large expanses of $GFAP^+$ processes (**L, M**) – magnification of contiguous sheets of ependymal cells (**K**), ependymal cells with small $GFAP^+$ clusters (**L**), and regions of extensive gliosis (**M**). Scale bars, 25μm (**F**), 500μm (**G, I**) and 100μm (**H, K**); and 200μm (**J**). Figure credits: BS, JL, RA, YS.

Figure 2

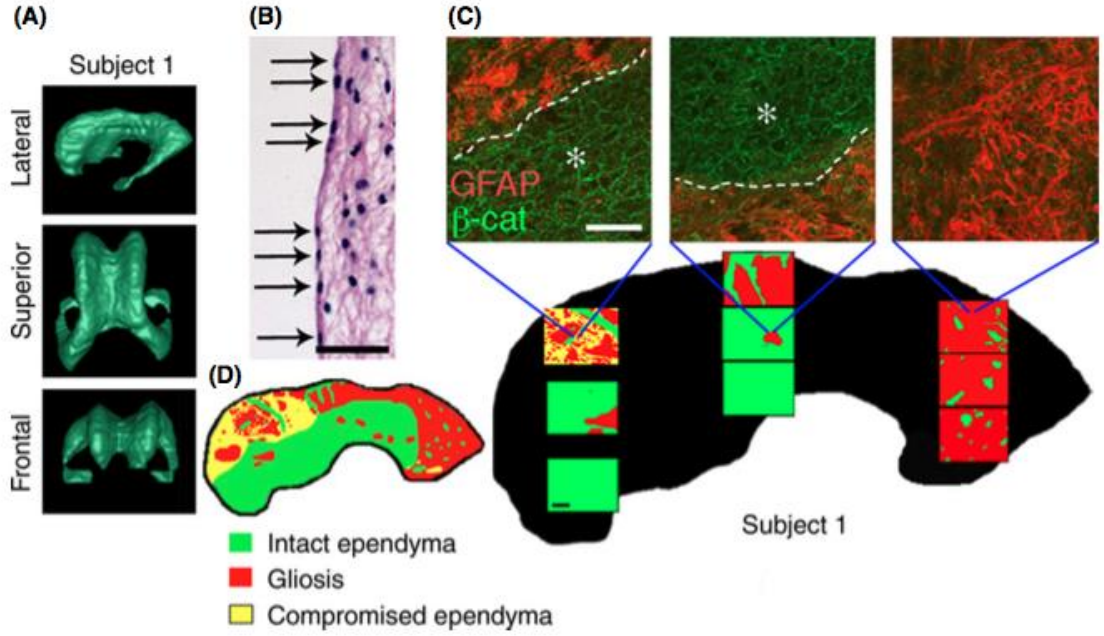

Figure 2. Large ventricular volume is associated with widespread gliosis at the ventricle surface in humans. (A) MRI-based 3D reconstructions of the lateral ventricle for Subject 1. (**B**) H&E staining of periventricular tissue revealed a compromised ependymal cell lining of mixed cell composition, including areas devoid of ependymal coverage (arrows indicate separation between nuclei of ependymal cells). (**C**) Representative regional images from extensive immunohistochemical analysis of the ventricle surface revealed that while some areas with normal ependymal cell coverage were present (green* in IHC image, green in schematic), large expanses of gliotic scarring at the ventricle surface (schematic: red) predominated. (**D**) Coded schematic of entire lateral wall of the lateral ventricle, with red indicating areas of astrocytic gliosis, yellow indicating a compromised ependymal lacking a distinct layer of cuboid ependymal cells, and green indicating intact ependyma. Scale bars, 100μm (**B**); 40μm, confocal image (**C**); 1mm, schematic (**C**). Figure Credits: RA, MH, BS.

Figure 3

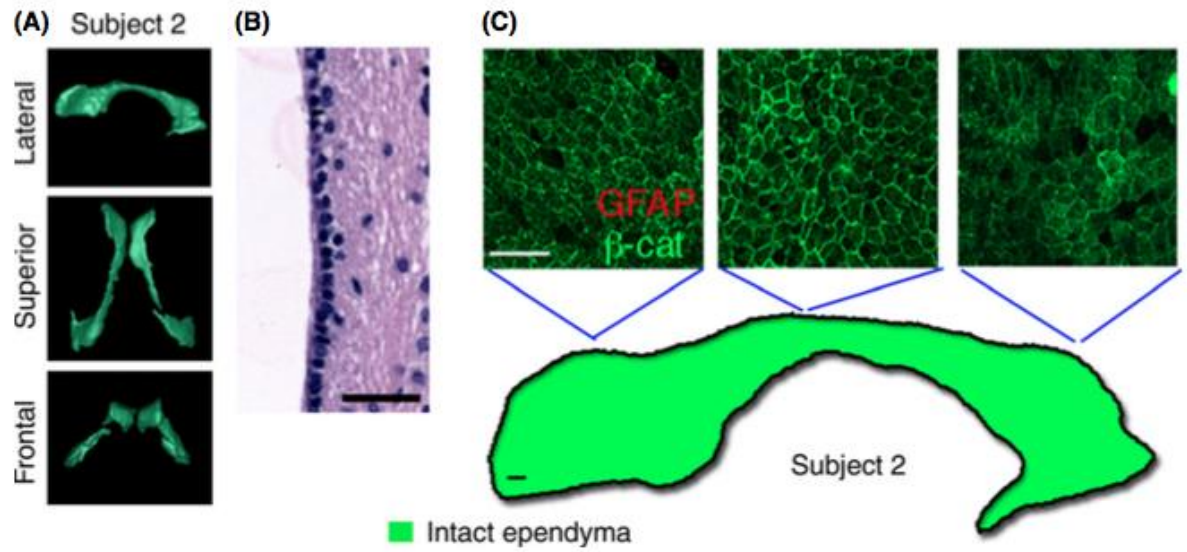

Figure 3. An intact ependyma is found along the entire ventricle surface in the elderly subject with a small volume ventricle. (**A**) MRI-based 3D reconstructions of the lateral ventricle for Subject 2. (**B**) H&E staining revealed a robust ependymal monolayer and (**C**) immunohistochemistry of whole mount preparations showed uninterrupted ependymal cell coverage with no surface gliosis. Scale bars, 100μm (**B**); 40μm, confocal image (**C**); 1mm, schematic (**C**). Figure Credits: RA, MH, BS.

Figure 4

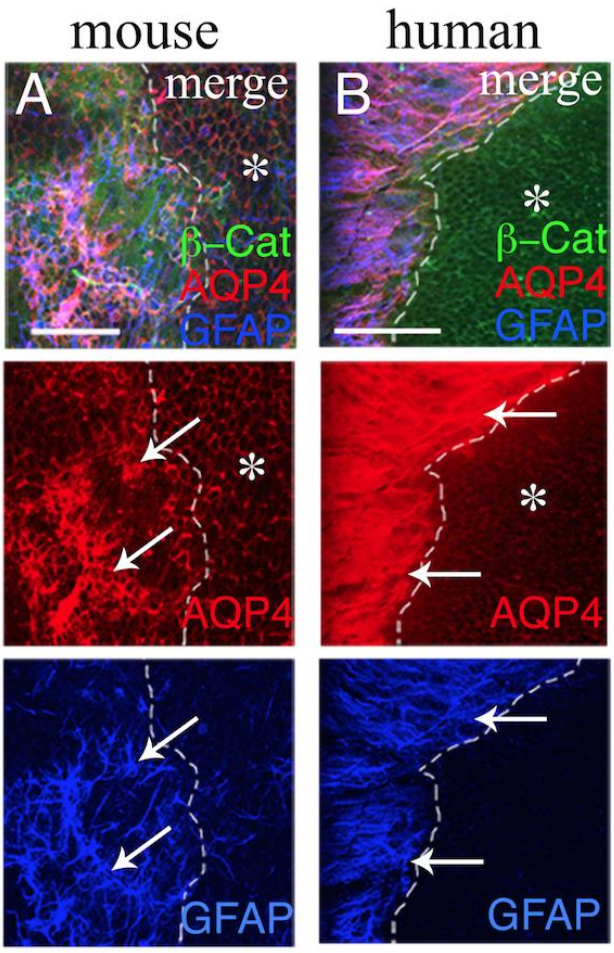

Figure 4. In mice, neuraminidase-induced ependymal cell denudation leads to gliosis at the ventricle surface and upregulation of AQP4, similar to AQP4 labeling in glial scars found along ventricle wall in aged humans. (**A**) Following intraventricular injection of neuraminidase, areas of gliosis ($GFAP^+$, denoted by arrows and demarcated by the dotted line) show increased expression of AQP4. Ependymal cells (*) show low levels of AQP4 staining in non-scarred regions. (**B**) Similarly, in human tissue, areas of surface gliosis (arrows, demarcated by the dotted line) in human tissue show increased expression of AQP4, whereas areas of ependymal cell coverage (*) are marked by □-catenin and low levels of AQP4. Scale bars, 100μm (**A**); 50□m (**B**). Figure Credits: RA, MH.

Figure 5

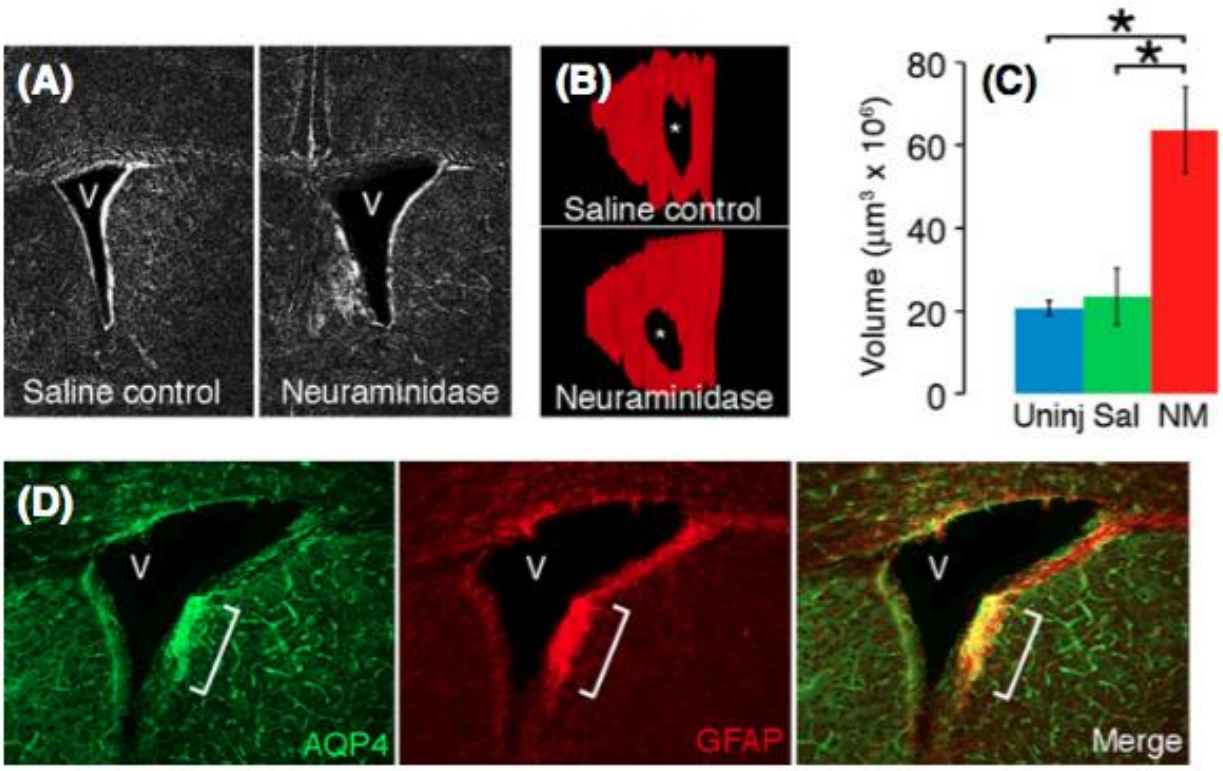

Figure 5. Extensive ventricle surface gliosis results in lateral ventricle enlargement in mice. (**A**) Two months after intraventricular injection of neuraminidase lateral ventricles are significantly larger (V, ventricle). (**B**) Contours traced around the ventricles were complied to create 3D reconstructions to determine lateral ventricle volumes (* denotes adhesion between lateral and medial walls). (**C**) Ventricle volumes at two months post-injection were larger in mice that received neuraminidase compared to mice injected with saline or the uninjected littermates (n=5 for neuraminidase (NA) group, n=3 for saline and uninjected controls, * $p<0.03$) Student's t-test). (**D**) Immunohistochemistry confirmed gliosis at the ventricle surface (bracket) and showed that it persisted two months after neuraminidase injection. Data are means, error bars are SEM. Figure Credits: MH, RA.

Chapter 3: Repeated Mild Traumatic Brain Injury Causes Focal Response in Lateral Septum and Hippocampus*

***From publication:** **Acabchuk RL**, Briggs D, Angoa-Pérez M, Powers M, Wolferz Jr. R, Soloway M, Stern M, Talbot LR, Kuhn DM, Conover JC, **Repeated Mild Traumatic Brain Injury Causes Focal Response in Lateral Septum and Hippocampus,** In Press, *Concussion*

INTRODUCTION:

Mild traumatic brain injury (mTBI), frequently referred to as "concussion", is a major public health concern due its prevalence, especially in youth sports. Estimates based on emerging data suggest that the likelihood of a concussion in a single season of youth, high school or collegiate football is 1 in 30, 1 in 14 and 1 in 20 players respectively [1]. A growing body of evidence suggests repeated incidents of concussive and sub-concussive blows, described as repeated mTBI (rmTBI), cause more significant neurological damage than a single mTBI, including longer recovery time and a higher likelihood of subsequent brain injury [2-5]. rmTBI has also been linked to debilitating long-term consequences such as memory impairment, emotional instability and the progressive neurodegenerative disease chronic traumatic encephalopathy (CTE) [6-8].

In animal models of rmTBI the hippocampus, corpus callosum, amygdala and cortex are the regions most commonly examined for histological changes [9-12]; however, histological analysis has not been exhaustive, so this list may be incomplete and possibly should include other regions. Computer-generated modeling of human concussion demonstrates 'hot-spots' of impact strain just below the sulci at interfaces of gray and white matter [13] and finite element modeling of 58 reconstructions of concussive impacts in the National Football League (NFL) predicts the largest strain in the corpus callosum [14]. Based on acceleration-deceleration and rotational forces causing tissues of varying densities and compositions to move at different speeds (shear force) and from finite element modeling data [13, 14], we predicted that areas associated with gray and white matter interfaces would be most vulnerable and at highest risk for acute/primary injury. In order to determine which regions of the brain are most adversely affected by rmTBI,

we performed a comprehensive multi-region investigation of the brain following injury using a rotational model of rmTBI.

In order to replicate accurately the rapid acceleration/deceleration and rotational forces common in sport concussions, we selected a mouse model that employs an unrestrained closed-skull modified weigh drop method that results in 180° free rotation [15]. To enhance clinical relevance, we compared two protocols that varied in the time intervals between injuries. We investigated regional and temporal histological alterations following rmTBI including astrogliosis, microglial activation, phosphorylated tau accumulation and axonal injury. We also examined changes in ventricle volume and integrity of the ependymal cell lining, as ventricular expansion is a common feature of CTE. We found that the dorsal lateral septum, immediately below the corpus callosum and adjacent to the lateral ventricles, is the most dramatically affected region. The hippocampus displayed similar cellular changes, but to a lesser degree. Our results support the inclusion of the lateral septum as a region of particular interest in rmTBI research and highlight the dangers of repetitive head injury occurring in rapid succession.

MATERIALS AND METHODS:

Animals. All animal procedures were approved by the Wayne State University IACUC and conformed to NIH guidelines. Male CD-1 mice (Charles River, Wilmington, MA, USA) were 8 weeks of age at the beginning of experiments and weighed between 30-35 grams. Strain selection was based on previous documentation of consistent ventricle volumes in CD-1 mice [16]. To adhere to the investigation of "mild" TBI, mice demonstrating signs of skull fracture or hemorrhage were excluded from all experiments. Skull fractures and hemorrhage were assessed upon sacrifice following perfusion by manually inspecting skull integrity and by visually

inspecting for blood accumulation on the surface or within the brain during sectioning. Mice presenting signs of skull fracture (SF) and/or hemorrhage (H) were discarded from all experiments. Rates of SF and/or H for the rmTBI-short protocol were 11% SF, 3% H and 22% SF+H. No skull fractures or hemorrhage were observed with the rmTBI-long protocol.

rmTBI Protocols. A closed-skull rmTBI was administered as previously described [12] with the following improvements: the tin foil platform was replaced with a transversable 'trap door' platform magnetically bound and calibrated to the animal's weight to reduce resistance to acceleration following impact. Briefly, mice were anesthetized using isoflurane then placed on the 'trap door' platform. To ensure accuracy and reproducibility of impact, a 1-meter vertical guide tube was aligned over the mouse's head with the weight initially lowered to ensure the cap (diameter: 10mm) of 95-gram weight was centered directly on the midline between the ears. The weight was then raised and released, causing an impact to the top of the mouse's cranium. Laser guides ensured precise alignment with the skull and video analysis ensured reproducible movement upon impact. After impact, the mouse was propelled through the trap door and underwent an 180° free rotation before landing supine on the collecting sponge cushion (10 cm) below. The mice were then moved to a carrying container and placed in a supine position to evaluate righting reflex response.

The experiments consisted of two protocols for hit delivery: short inter-injury interval and long inter-injury interval. The 'rmTBI-short' protocol consisted of five rounds of weight drop impact to the top of the skull over a three-day period. Hits were delivered as follows: Day 1: am hit, 6 hr recovery, pm hit. Day 2: am hit, 6 hr recovery, pm hit. Day 3: am hit. For the 'rmTBI-long' protocol hits were delivered once every 3 days for a 15-day period, for a total of 5 hits with a 3-4

day inter-injury interval. The overall mortality rate for the rmTBI-short and rmTBI-long protocols was 37.5% and 0% respectively. Early termination (within 1 hr) due to motor impairments (i.e. paralysis) accounted for 20% of the mortality. The remaining mice died within 4 minutes of impact (with death occurring in equal proportions across impacts 1-5). Of the mice that did not survive the procedure, 25% had skull fracture and meningeal bleeding, 25%, had meningeal bleed without skull fracture, and the remaining 50% had no observable bleed or fracture [17].

Separate groups of control mice were treated with time-matched doses of isoflurane anesthesia for each experimental protocol. Following treatment, hit and control mice were either sacrificed immediately or kept in normal living conditions until time of sacrifice (2-weeks or 6-weeks post-rmTBI).

Immunohistochemistry (IHC).

Mice were sacrificed by pentobarbital overdose and perfused with PBS followed by 4% paraformaldehyde. Brains were removed, photographed and inspected for gross morphological injury including cortical deformation and subdural or subarachnoid hemorrhage. Perfused brains were stored in 4% PFA at 4° C for 72 hours then shipped overnight in PBS from Wayne State University to the University of Connecticut. Brains were embedded in agarose and sectioned coronally on a vibratome (VT-1000S; Leica) generating 50µm thick serial slices. Coronal tissue sections from 2mm anterior to 2.5mm posterior of Bregma were blocked in 10% horse serum (Invitrogen Life Technologies, Grand Island, NY, USA) in PBS/0.1% Triton X-100 for one hr. Tissue sections were immunostained overnight with the following primary antibodies in blocking

solution: rat anti-glial fibrillary acidic protein (GFAP, 1:250; Life Technologies, Grand Island, NY, USA), rabbit anti-aquaporin 4 (AQP4, 1:400; Sigma-Aldrich, St. Louis, MO, USA), mouse anti- S100β (1:500; Sigma), rabbit anti-IBA1 (1:500; Wako Chemicals, Richmond, VA, USA), rabbit anti-Myelin Basic Protein (MBP, 1:200, EMD Millipore, Billerica, MA, USA), mouse anti-SMI-32 (1:1000, BioLegend, San Diego, CA, USA), mouse anti-AT8 (1:200; Pierce Biotechnology, Waltham, MA). AT8 phosphorylated tau specificity was validated with mouse anti-PHF-1 (1:200) and mouse anti-CP13 (1:200), which were generous gifts from Dr. Peter Davies (Albert Einstein College of Medicine, Bronx, NY). After three washes in PBS, sections were incubated for 2 hr at room temperature with Alexa Fluor dye-conjugated secondary antibodies (1:500, Life Technologies) diluted in blocking solution. Tissue sections were then treated with DAPI nuclear stain for 5 min followed by three final PBS rinses. Tissue sections were mounted sequentially from anterior to posterior and coverslipped with aquapoly mount (Polysciences, Inc.; Warrington, PA).

Image Analysis and Acquisition. All images were acquired on a Zeiss Axio Imager M2 microscope with ApoTome (Carl Zeiss MicroImaging, Inc., Thornwood, NY, USA), with a HAMAMATSU ORCA-R2 digital camera C10600. Age matched controls for each time point of sacrifice and each hit protocol were processed and analyzed in tandem with treatment groups using IHC. The number of mice used for analysis in each protocol group and for each time point were as follows: rmTBI-short protocol - immediate 3 hit/8 control; 2week 6 hit/6 control; 6week 8 hit/5 control, and rmTBI-long protocol - immediate 4 hit/3 control; 2week 5 hit/4 control; 6week 4 hit/4 control. Full tissue section image montages (generated every 300μm from the anterior forebrain through the entire hippocampus) were used to inspect for alterations in GFAP,

IBA-1, AQP4, S100β or AT8. SMI-32 and MBP were assessed with the same procedure in the 2-week time point only. Upon scanning all brain regions for IHC alterations, observations of overt changes in GFAP and IBA-1 led to the lateral septum, corpus callosum and hippocampus being identified as regions of interest (ROI) for further analysis. High magnification images, taken from three consecutive brain slices (50μm), were then collected for both ROIs using the same exposure settings for all hit and control brains for each group (time-point and protocol) for unbiased evaluation of histopathology. Septal montages were taken at 0.5 mm and hippocampus montages at -1.5 mm relative to Bregma. Evaluation of microglial activation was performed in the lateral septum, corpus callosum, hippocampus, amygdala and cortex by examining morphological changes in microglia using the microglial marker IBA-1. An increase in the number of IBA-1^{+} cells with retracted processes and enlarged cell bodies were taken as an indication of microglial activation. Images were acquired of all consecutive slices that demonstrated microglial activation, further validating a defined ROI. Comparison of mice across each group within a ROI was used for representative images.

GFAP Quantification. Immunoreactivity for GFAP was quantified using the mean pixel intensity in a given ROI using FIJI/ImageJ software (NIH, Bethesda, MD, USA). To ensure unbiased quantification and account for possible variability across groups, a uniform threshold value was obtained by averaging the automated threshold values of all control montages for each group (time-point and protocol). The group specific uniform threshold value was applied to all hit and control brains of a given group to obtain quantification values based on the average pixel density values across three consecutive tissue slices. Data acquisition was replicated under blinded conditions to ensure reproducibility and objective measurement technique. To determine

the extent and pattern of gliosis in the septal region, the dorsal lateral septum was quantified in three locations (mid lateral, peri-mid lateral septum, lateral septum), using the average values of the right and left hemisphere for the areas defined as 'peri-mid' and 'lateral'. GFAP quantification in the corpus callosum was derived from the average values of three locations within the corpus callosum: center, left and right hemispheres directly above the mid and lateral septal areas (starting at 0.5mm anterior to Bregma). Hippocampal GFAP expression was measured using a single area directly adjacent to the midline at the beginning of the dentate gyrus, averaging the left and right hemispheres. In the cortex, GFAP quantification was performed in a single box. Quantifications were performed using a 200x200px/μm area in all regions of the septum, corpus callosum and cortex and a 1350x600px/μm area in the hippocampus.

Lateral Ventricle Volume Analysis and Ependymal Lining Evaluation. Lateral ventricle volumes were calculated based on the tracing protocol we developed and described previously [18]. Briefly, volumes were generated from serial coronal sections of the lateral ventricles, marked by S100β^{+} ependymal cells that line the ventricles, traced in StereoInvestigator and then compiled in Neurolucida Explorer, generating 3-D volumetric renderings. Volume analysis was performed for all three time-points of both hit and control brains. The ependymal lining of the lateral ventricles was examined for ependymal denudation (S100β□ and astrogliosis (AQP4 and GFAP) in all experimental groups.

Statistical Analysis. To determine which factors significantly influenced changes in GFAP expression in each region of the septum, hippocampus and corpus callosum following rmTBI, 2-

way full factorial ANOVAs were performed (group X protocol) for each region and for each post-injury time period using GraphPad Prism software (**Table 1**). Post-hoc (t-test) analysis was performed to test for differences between levels within each factor (testing for differences between hit and control for each region, protocol and time point). The p-values were adjusted using Bonferonni correction, to account for multiple testing **(Table 2)**. All data are presented as the mean ± standard error of the mean (SEM). Statistical significance was determined by adjusted p values of <0.05.

RESULTS:

We employed a modified weight-drop method to deliver an impact to the top of the head that caused rapid acceleration and unrestrained 180° rotation of the mouse (**Figure 1A-B**). Mice showed no evidence of seizures, paralysis or behavioral abnormalities. Our studies compared two protocols with differing inter-injury intervals, 'rmTBI-short' delivering 5 hits in 3 days, and 'rmTBI-long' delivering 5 hits in 15 days (see timeline in **Figure 1C**). Average righting times following were 2-3 min following rmTBI-short, 1-2 min following rmTBI-long, with <1 min for both sets of control mice (details of righting times, see **Table 3**). Following rmTBI, mice were perfused at three post-injury time points, immediate, 2-weeks and 6-weeks, and the brains were sectioned from 2mm anterior to 2.5mm posterior to Bregma.

Following exclusion of mice presenting signs of skull fracture and/or hemorrhage, gross examination revealed the brains from both protocols to be indistinguishable from control mice at all time-points following injury. No sign of morphological deformities, hemorrhaging, focal damage or contusion was observed on the surface of the brain (**Figure 1D-E).** The absence of

injury to the cortical region directly below the site of impact indicates the mild nature of this protocol. In addition, there were no signs of diffuse axonal injury (SMI-32) or changes in myelin integrity (MBP) at the 2-week time point of both protocols (**Figure 5**).

rmTBI causes acute microglial activation in the lateral septum and hippocampus.

Neuroinflammation in response to brain injury can be acute and/or chronic [19]. To perform a regional analysis inspecting for areas of microglial activation, we examined changes in IBA-1 expression throughout all brain regions. These studies revealed activated microglia, as indicated by an increase in the number of IBA-1-positive cells with retracted processes and enlarged cell bodies, accumulated in the dorsal lateral septum **(Figure 2A)** and hippocampus (**Figure 2B**) immediately following the rmTBI-short protocol. No other brain regions showed increased IBA-1-positive cells. High magnification images of the lateral septum and hippocampus from the immediate time-point clearly illustrate morphological changes indicative of reactive microglia **(Figure 2**). IBA-1 expression was restored to baseline levels in both regions at the 2-week time-point. With the rmTBI-long protocol, we did not observe microglial activation at any time-point. Since changes in activated microglial expression were restricted to the septal and hippocampal regions, with the cortex, amygdala and corpus callosum exhibiting only baseline IBA-1 levels following both protocols *(data not shown),* we concluded that the lateral septum and hippocampus are particularly vulnerable in rmTBI.

Astroglial response is observed in the lateral septum, corpus callosum and hippocampus.

Astrocytes help maintain homeostatic conditions in the central nervous system and display a complex and graded response to injury [20]. To perform a regional analysis inspecting for areas

of astrocytic response, we examined changes in GFAP expression throughout all brain regions. Similar to the microglial analysis, qualitative analysis revealed an astrocytic response in the septal and hippocampal regions. No changes in GFAP expression were observed in the cortex or amygdala at any time point *(data not shown).* In order to perform a quantitative analysis to compare GFAP intensity levels across experimental groups and protocols within each region, GFAP intensity was quantified in the hippocampus, corpus callosum and lateral septum, which was further sub-divided to provide a more comprehensive analysis of GFAP alterations in the septal region (**Figure 3A**). To compare GFAP expression across the protocols (short, long) at each given time point (immediate, 2-week, 6-week) within each region, we used 2-way full factorial ANOVAs on treatment (hit, control) X protocol (short, long) for each time point and region. This was followed by post-hoc (t-test) analysis with Bonferonni correction testing for differences between levels within each factor, allowing for comparison of hit and control groups processed in tandem with identical protocols and post-injury time points. The full list of F and P values for the ANOVAs are listed in **Table 1** and the full list of adjusted t and P values are listed in **Table 2**.

Immediately following the rmTBI-short protocol, there was a highly significant increase in GFAP expression in all septal regions (Mid LS t=20.7, Peri Mid LS t=14.78, Lat LS t=4.71) (**Figure 3B, C**), with both treatment and protocol acting as highly significant factors (significant factors are not displayed on graph, see **Table 1)**. The increase in GFAP staining remained significant in the septal region 2- and 6-weeks post-injury. In contrast to the rmTBI-short protocol, the rmTBI-long protocol caused only an immediate increase in two of the septal regions (Mid LS t=4.452, Peri Mid LS t=3.505) with no persisting changes in the septal region

GFAP expression relative to control levels at 6-weeks post-injury. ANOVA results yielded a significant interaction between treatment and protocol in the mid LS (F=291.2) and peri-mid LS (F=51.53) at the immediate time point.

The corpus callosum showed mixed results following rmTBI-short (**Figure 3B, C**), with a significant increase in GFAP expression at the immediate and 6-week time-point. When the source of variation is taken into account, it appears the increase in GFAP at 6-weeks in the corpus callosum is specific to the short protocol. No changes were observed in the corpus callosum following the rmTBI-long protocol at any time point. High magnification images (**Figure 3D, E**) show changes in GFAP expression in the lateral septum and corpus callosum with increased $GFAP^+$ processes appearing thicker and more numerous in the treatment conditions.

In the hippocampus, we found an immediate astroglial response similar to that seen in the septal region (**Figure 4B, C, left panel).** Specifically, in the rmTBI-short protocol, GFAP immunoreactivity was significantly increased over control levels at the immediate time-point (t=3.069) and also after 2-weeks (t=4.218), but GFAP levels were no longer significantly different at 6-weeks. Following the rmTBI-long protocol, there was no significant increase in GFAP intensity in the hippocampus at any time-point (**Figure 4B, C, right panel**). While an interaction between treatment and protocol was found in the hippocampus at 2-weeks, this was likely related to variability in control levels of GFAP expression. High magnification images of the dentate gyrus of the hippocampus (**Figure 4 D**) show changes in GFAP expression similar to what is found in the septal region following the rmTBI-short protocol.

To examine further the extent of the astrocytic reaction in the septum, hippocampus and corpus callosum, we investigated the calcium binding protein S100β and water channel protein AQP4. Astrocytes have been shown to increase expression levels of S100β and AQP4 during reactive gliosis [21-23]. No changes were observed in either S100β or AQP4 expression in any region examined, including the amygdala and cortex (**Figure 5**), suggesting that the astrocytic response observed in our studies was localized and mild in nature.

Overall, results of GFAP quantification suggest that a shorter inter-injury interval causes a more significant astrocytic response in the lateral septum than a longer inter-injury interval with the same total number of hits. The hippocampus shows a similar pattern initially, displaying an immediate astrocytic response following the short protocol only. However in the hippocampus, GFAP levels return to baseline levels by 6-weeks. The corpus callosum appears to have a slight astrocytic response following the rmTBI-short protocol only.

No significant changes in phosphorylated tau in rmTBI protocol.

We also examined changes in phosphorylated tau marker AT8. Accumulation of hyper-phosphorylated tau is considered to be a hallmark feature of CTE [6, 24]. Using the AT8 antibody that detects tau phosphorylation at Ser202/Thr205, our studies did not reveal significant changes in phosphorylated tau accumulation in any of the brain regions investigated (cortex, hippocampus, corpus callosum, lateral septum and amygdala) at any time point, following either protocol. AT8 was observed in the cortex at 6-weeks following rmTBI-short (**Figure 5**), which allowed for confirmation of positive antibody staining using additional phosphorylated tau

markers, but the level was not significantly different from controls.

Ependymal lining and lateral ventricle volumes remain unchanged following rmTBI.

As dilation of the lateral ventricles is a morphological feature of CTE and ependymal damage may contribute to ventricle expansion and/or impaired clearance of phosphorylated tau, we sought to determine if our rmTBI model resulted in lateral ventricle expansion. To evaluate the integrity of the ependymal lining, we used S100β, a marker for ependymal cells, and AQP4, an indicator of astrogliosis at the ventricle surface [25]. Our analysis confirmed the presence of an intact ependymal lining throughout the lateral ventricles following both the 'short' and 'long' protocols. GFAP expression was slightly elevated in selected regions of the ependymal lining, there was no overt indication of astrogliosis in the ventricle lining (**Figure 5**). In addition, when the volumes of the lateral ventricles were evaluated we did not detect any changes in volume at all 3 time-points compared to experimentally matched controls *(data not shown).*

DISCUSSION:

The objective of these studies was to perform an extensive regional investigation of forebrain and midbrain histological alterations in a biomechanically relevant model of rmTBI. The model we employed generated an impact that caused a very rapid and rotational acceleration of the head, which is fundamentally very similar to human concussive injury [15]. The absence of cortical damage and the observation of normal microglial and astroglial expression throughout the cortex confirmed the mild nature of the model. rmTBI delivered in short inter-injury intervals (rmTBI-short) led to an immediate increase in IBA-1 and GFAP expression signifying acute microglial activation and astrocytic response in the dorsolateral septum and hippocampus.

The microglial response was resolved throughout the brain by 2-weeks post-injury. Six-weeks post-injury, the astrocytic response persisted in the lateral septum, but was resolved in the hippocampus. The corpus callosum appeared to have a mild astrocytic response present initially and six-weeks post-injury. When the inter-injury interval was lengthened (rmTBI-long protocol), the effect was diminished. We found an immediate astrocytic response in the lateral septum only, but no microglial activation was found in any brain region examined. Six weeks following the rmTBI-long protocol, GFAP expression in the septum returned to baseline levels (**Figure 6**).

The purpose of comparing two rmTBI protocols with different inter-injury intervals was to provide insight into repetitive injury scenarios where repeated concussive and/or subconcussive injuries occur at different frequencies. The protocol comparison of 5 hits over 3 days versus 5 hits over 15 days demonstrates that the inter-interval periods (time between hits) are a critical factor in the extent of histological response. Currently, there are no clinical tests capable of confirming the presence or absence of cellular changes following mTBI in humans, increasing the difficulty of making concussion diagnosis or developing a treatment regimen [8]. Our results demonstrate that a shorter inter-injury interval can lead to a more significant cellular response in the form of acute microglial activation and prolonged astrogliosis in select regions of the brain. These results are in accordance with other studies that found that the brain is subject to exponential damage when hits are delivered in quick succession, within 24 hours [26]. The finding of microglial activation immediately following the rmTBI-short protocol, but not following the rmTBI-long protocol indicates microglial priming may play a role in the exaggerated microglial response found following the rmTBI-short protocol. Whereas the longer 48-72 hour inter-injury interval in the rmTBI-long protocol may be sufficient time to return to

homeostatic neuroimmune conditions prior to a subsequent hit, at least in mice. It is also possible that other factors contributed to the amplified microglial activation found with the rmTBI-short protocol, such as increased intracranial pressure or microbleeds that were too small to identify. While further investigation of the M1/M2 phenotype would help elucidate the nature of the microglial reaction, the changes observed in our model were temporary (resolved by 2-weeks) and region specific, suggesting the reaction is not replicating the long-term neuroinflammatory response found in human CTE [27, 28].

The increase in GFAP expression levels found in the dorsolateral septum and hippocampus in our studies is indicative of an astrocytic response, but would not be considered a glial scar. GFAP is known to impart mechanical strength in astrocytes, and astrocytes increase the intermediate filament GFAP in response to mechanical stress [29]. Our results suggest the astrocytic response observed in our studies is a reaction to impact and rotational forces imparting higher levels of mechanical stress in these two regions.

To determine the degree to which the current protocols generated a CTE-like phenotype, we tested for phosphorylated tau accumulation and ventricular dilation, neither of which were found in our studies. Activation of a chronic immune response has been linked to progressive neurodegeneration and phosphorylated tau accumulation [30, 31]. In our studies, we did not see signs of diffuse axonal injury and the microglial response was resolved within 2-weeks even under the more severe condition (rmTBI-short), which suggests the current protocols are unlikely to generate phosphorylated tau accumulation. We also did not observe changes in ventricle size in our studies; however, this may also be due to a variety of factors (i.e., the disparity of brain volume to ventricle volume ratio between humans and mice, the location of the impact, lack of

damage to ependymal lining). Our selection of CD1 mice for the current study was based on their consistent ventricle volume; C57 mice can spontaneously develop hydrocephalus and therefore were not appropriate for our studies. While mortality, attributed to central respiratory depression [32], skull fractures and hemorrhaging necessitated the exclusion of several subjects from the rmTBI-short protocol, our findings of a focal response in the septum and hippocampus were consistent in the experimental group of mice that showed no signs of bleeding, skull fracture or cortical damage. Our analysis did not reveal signs of diffuse axonal injury or myelin damage in the corpus callosum at the 2-week post-injury time point.

Behavioral and functional testing in mice exposed to similar mTBI models has revealed impaired cognitive skills (Morris water maze), impaired motor skills (wire grip and rotarod), anxiety-like behavior (open field test), acute sleep disturbances and disturbances to species-specific behaviors, such as nesting [15, 33-35], and changes in hippocampal synaptic plasticity [9, 28]. The current study may generate similar behavioral and functional deficits due to the patterns of cellular damage identified in the current model. However, it is also possible that the impact of persistent, but subtle, astroglial responses in the lateral septum and hippocampus may necessitate sensitive physiological recordings in order to detect functional changes within the brain.

Importantly, our results show that both the lateral septum and hippocampus have a heightened cellular response in the form of microglial and astroglial activation following rmTBI. Similar neuroinflammatory response has been identified in the hippocampus of retired NFL players with a new non-invasive, *in vivo* radiolabeling technique using PET and MRI imaging [36]. Both structures are similarly located along the neuraxis directly below the corpus callosum and between the lateral ventricles. An underlying feature of the two regions is that they are found

where different tissue types and densities interface (corpus callosum-dorsolateral septum, corpus callosum-hippocampus). These regions may be more susceptible to injury due to anisotropic shear force generated by mechanically induced tissue deformation. Our results show the most prominent cellular response is in the lateral septum and hippocampus, directly below the corpus callosum, which is consistent with results from computer generated modeling that predict the highest rate of strain to occur in the corpus callosum [14]. It is important to note that structural damage to the septal region may be linked to fenestrated and/or cavum septum pellucidum, which is a common feature of CTE [4]. A recent MRI study shows the prevalence, grade and length of cavum septum pellucidum are higher in retired American pro-football players compared to memory clinic controls [37]. Functionally, the lateral septum is part of the septo-hippocampal axis and limbic system, which modulates memory and emotions, and the lateral septum has been implicated in the neuronal circuitry of anxiety and fear [38, 39]. Therefore, it is possible that the microglial and astroglial responses found in the current studies may impact these networks.

CONCLUSION:

Our studies used two mouse models of rmTBI that incorporated acceleration, deceleration and rotational forces to investigate regional vulnerability. We found that the inter-injury interval plays a significant role in determining the extent of damage, whereby an immediate activation of microglia and a prolonged astrocytic response arose only when the hits occurred within a 16-hour timeframe (rmTBI-short). Our results highlight the lateral septum, corpus callosum and hippocampus as regions of particular interest following rmTBI. Damage to the septo-hippocampal axis from rmTBI may contribute to clinical rmTBI symptomology, including

anxiety and memory problems, and fenestrated septum pellucidum, which is a notable feature of CTE.

FIGURES AND LEGENDS

Figure 1

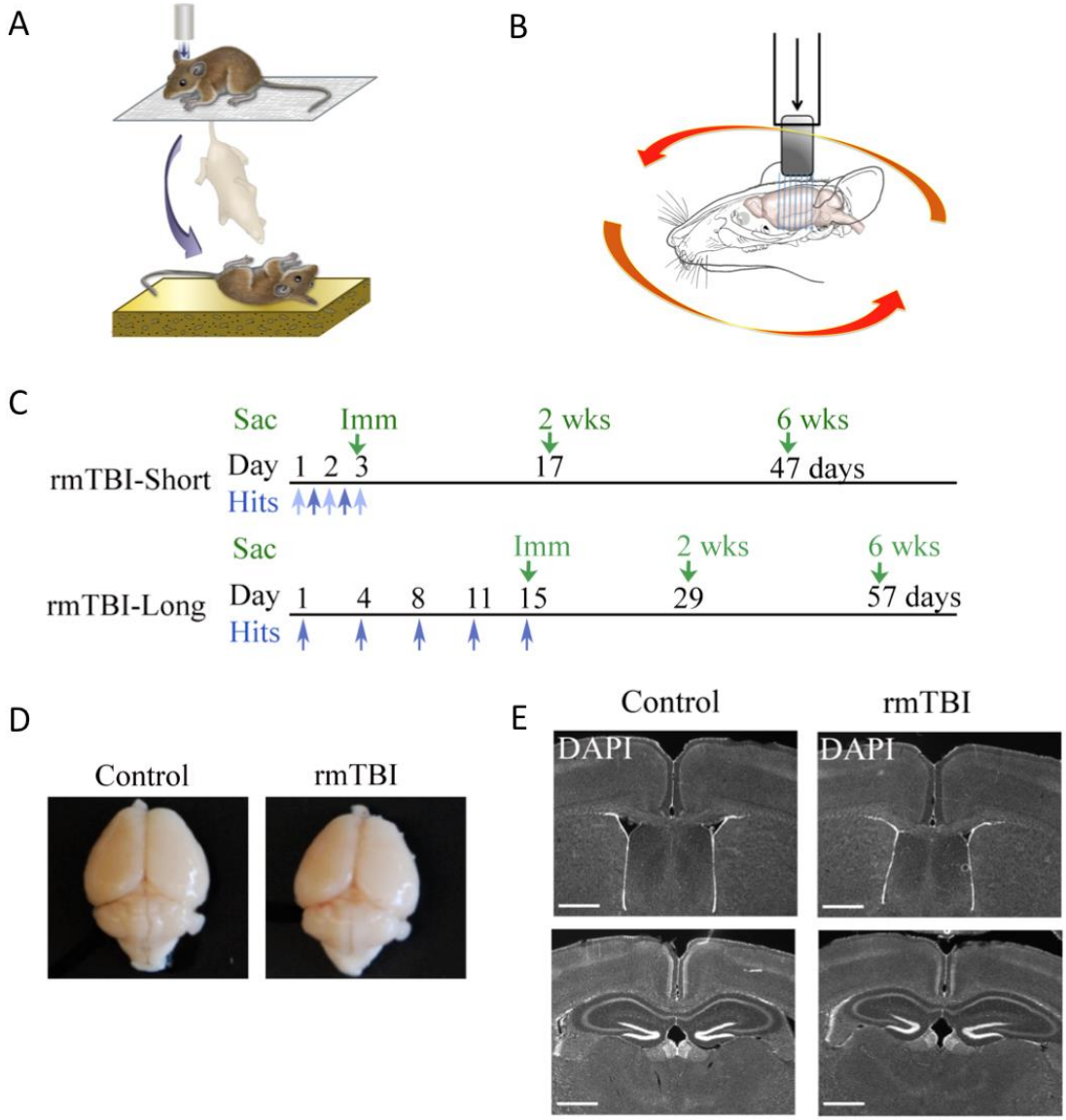

Figure 1: Experimental Overview (A) A modified weight drop method delivers impact to the top of the head, propelling the mouse through a trap door stage onto a collecting sponge, modeling rapid acceleration and rotational forces found in concussion. (B) Illustration showing location of hits, direction of rotation (red arrows) and regions of the brain investigated (blue lines). (C) Timeline of experimental procedures that vary in their inter-injury interval: 5 hits in 3

days (rmTBI-short), 5 hits in 15 days (rmTBI-long). Sacrifice and collection of brain tissue samples occurred at immediate, 2-week and 6-week post-injury time-points. (D) No significant gross damage is observed following impact procedures. (E) Immunohistochemical analysis of DAPI nuclear staining at the immediate time point for rmTBI-short and control brains demonstrates rmTBI brains are indistinguishable from controls in cortical regions, including regions directly below impact (E), thus modeling rmTBI. (Scale bars, 1000μm)

Figure 2

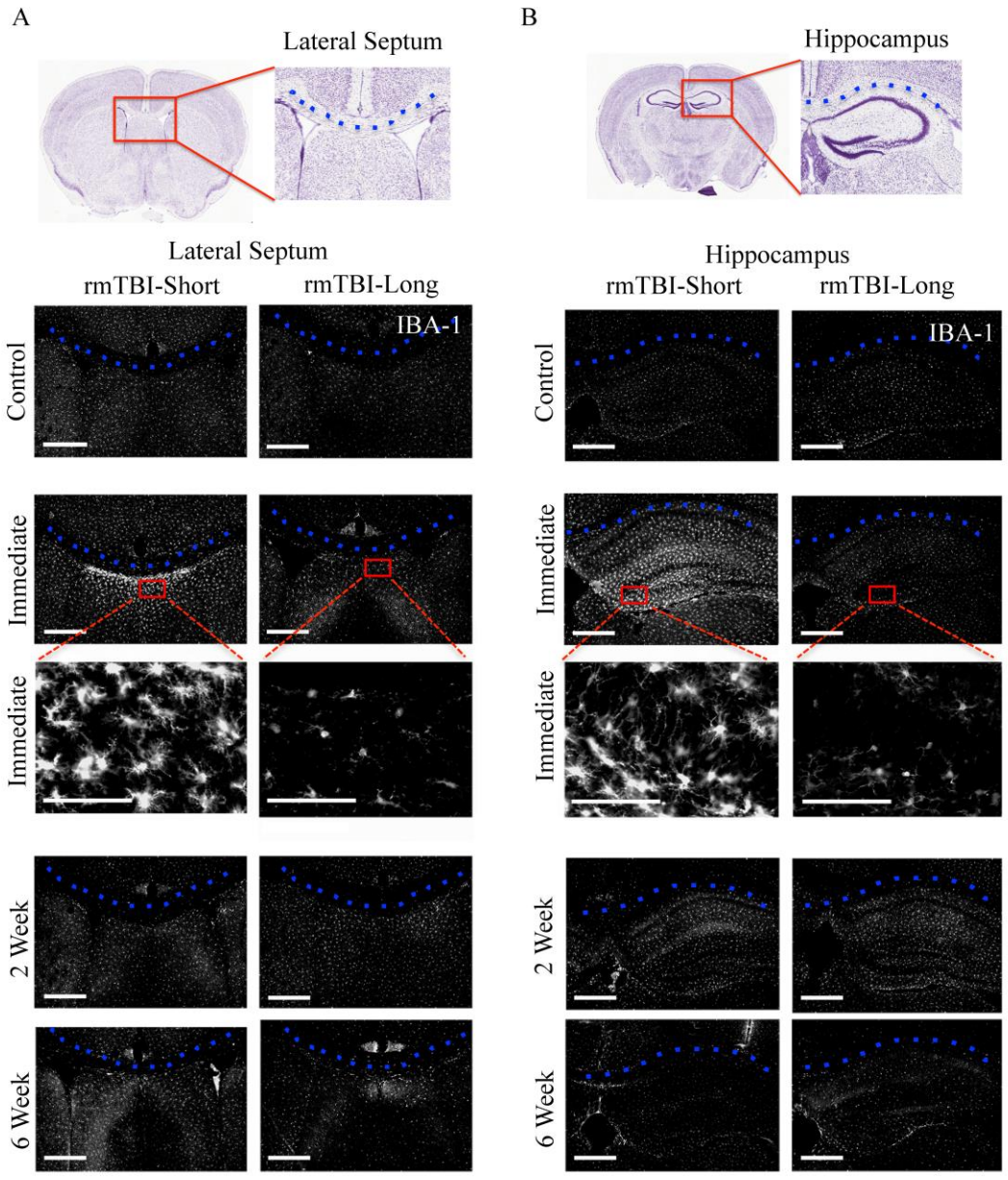

Figure 2: Isolated microglial activation (IBA-1) is present in lateral septum and hippocampus immediately following rmTBI-short. (A-B) For orientation, a blue dotted line was drawn through the center of the corpus callosum. Left panels show increased IBA-1 expression localized to the dorsal lateral septum and hippocampus immediately following the

rmTBI-short protocol. Higher magnification images of the septum and hippocampus show morphological changes indicative of reactive microglia immediately following rmTBI-short, but not rmTBI-long. No changes in microglial activation were observed at the 2-week and 6-week time-point of either protocol. (Small scale bars, 500μm; large scale bars (magnified images), 100μm).

Figure 3

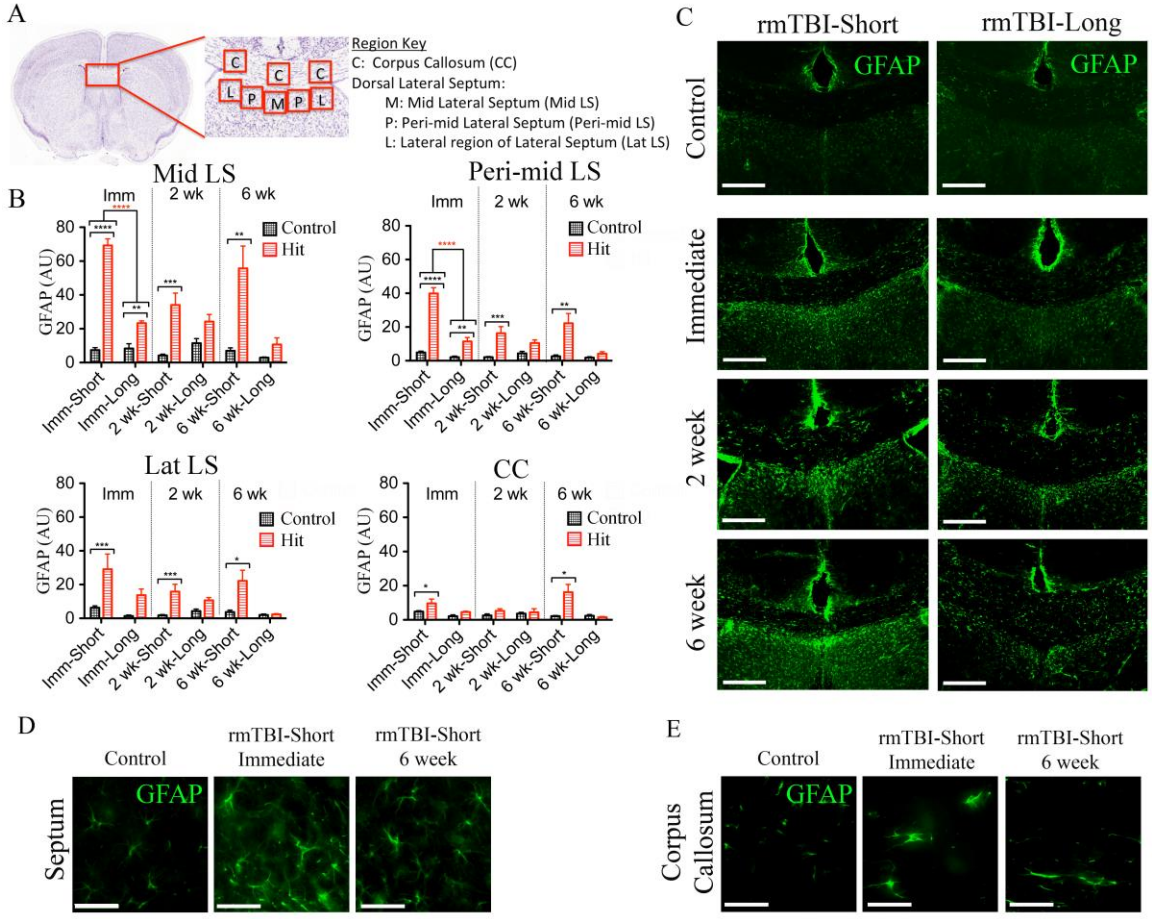

Figure 3: The lateral septum shows immediate and sustained increases in GFAP immunoreactivity following both protocols. (A) Atlas image illustrates regions used for GFAP quantification (200 X 200 μm boxes). (B-C) Graphs of GFAP intensity levels were generated using threshold analysis and are shown with corresponding representative images. 2-way factorial ANOVA (treatment X protocol) performed on each region and post-injury time period shows significant interactions occurring in the mid and peri-mid lateral septal regions at the immediate time point (red *). Post-hoc (t-test) analysis with Bonferonni correction was used to compare rmTBI treatment to respective control groups within each time point and region. All three regions of the dorsal lateral septum show immediate and sustained increases in GFAP in the rmTBI-short protocol (C-left panels). In the rmTBI-long protocol (C-right panels), increased

GFAP is resolved in all septal regions at 2 weeks. The corpus callosum shows a significant increase in GFAP immediately and 6-weeks following the rmTBI-short protocol. (D-E) Representative high magnification images in peri-mid lateral septum and corpus callosum show changes in GFAP expression immediately and 6 weeks following rmTBI-short compared to control. Data are expressed as mean ± SEM (* $p<0.05$, ** $p<0.01$, *** $p<0.001$, **** $p<0.0001$). (Scale bars: 300μm (C), 40μm (D-E)).

Figure 4

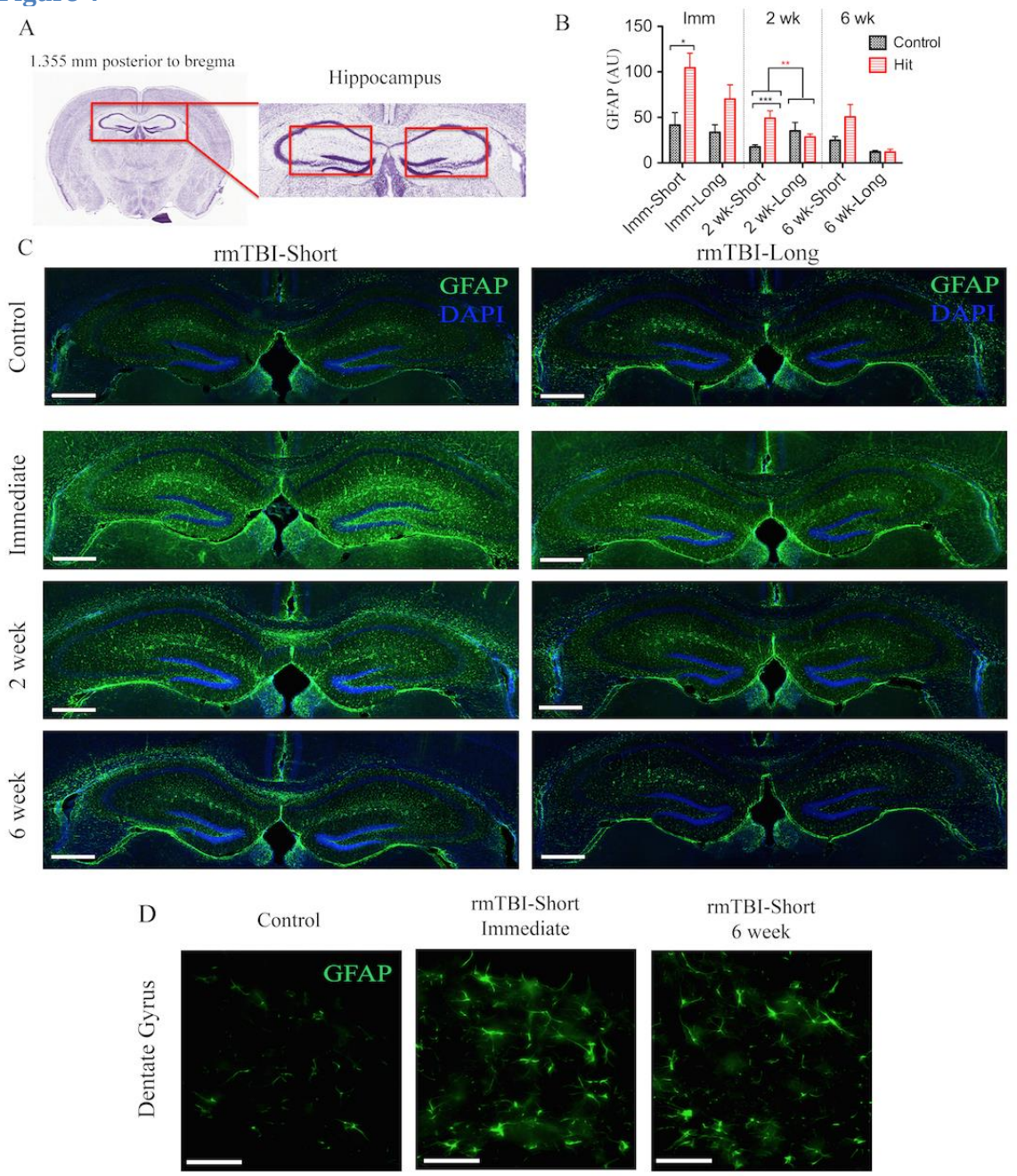

Figure 4: Hippocampus shows significant increases in GFAP immunoreactivity immediately and 2 weeks following rmTBI-short protocol. (A) Boxed region in atlas image is magnified on right to show 1350 X 600μm areas used for GFAP quantification. (B-C) Graph of GFAP quantification using threshold analysis and corresponding representative images shows GFAP expression (green) and DAPI (blue). 2-way factorial ANOVA (treatment X protocol)

showed a significant interaction between treatment and protocol 2 weeks post-injury (red *). Post hoc (t-test) analysis using Bonferonni correction to test for differences between levels within each factor shows significantly increased GFAP in the hippocampus immediately and 2 weeks following the rmTBI-short protocol, with overall GFAP expression levels returning to baseline at 6 weeks. No changes in GFAP expression levels occurred following the rmTBI-long protocol in the hippocampus. (D) Representative high magnification images in dentate gyrus show changes in GFAP expression immediately and 6 weeks following rmTBI-short compared to control. Data are expressed as mean ± SEM (* $p<0.05$, ** $p<0.01$, *** $p<0.001$). (Scale bars: 500μm (C), 50μm (D)).

Figure 5

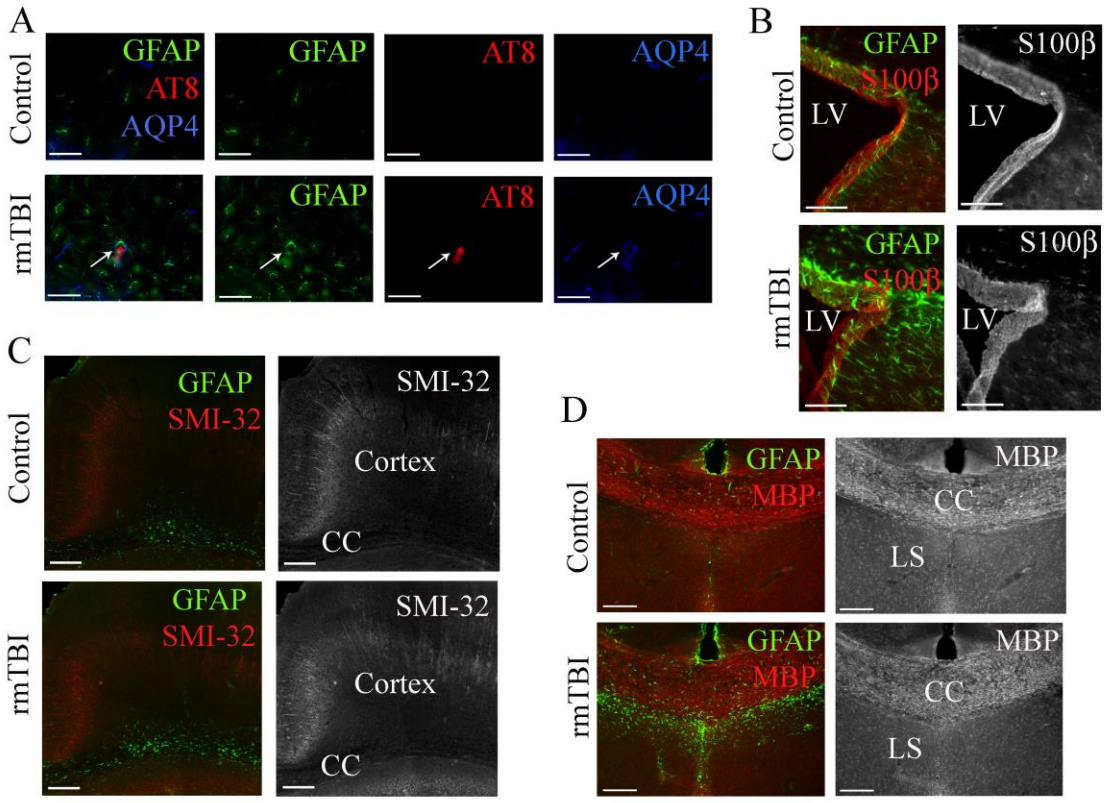

Figure 5. Representative images of null findings. (A) Levels of phosphorylated tau (AT8, white arrow) in the cortex and hippocampus following the rmTBI-short protocol (observed at 6-week time point) were not significantly different from controls. GFAP and AQP4 are present along the perimeter of the AT8 staining, suggesting astrocytic endfeet surround the phosphorylated tau accumulation and/or the accumulation is associated with blood vessels lined by astrocytic endfeet. (B) The ependymal lining of the lateral ventricle remains intact at all time points and in all protocols of rmTBI, as demarked by S100β staining of the ependyma. Elevated GFAP is noted in the dorsal wall of the lateral ventricle immediately following the rmTBI-short protocol. (C-D) No signs of axonal damage (indicated by increased levels of SMI-32) in the cortex or corpus callosum and no observable changes in myelination (MBP) in the corpus

callosum 2-weeks following either rmTBI protocol is observed. Representative images are all from the rmTBI-short protocol and located -1.5mm and 0.5mm relative to Bregma, respectively. (Scale bars: 50μm (A), 100μm (B), 200μm (C), 200μm (D)).

Figure 6

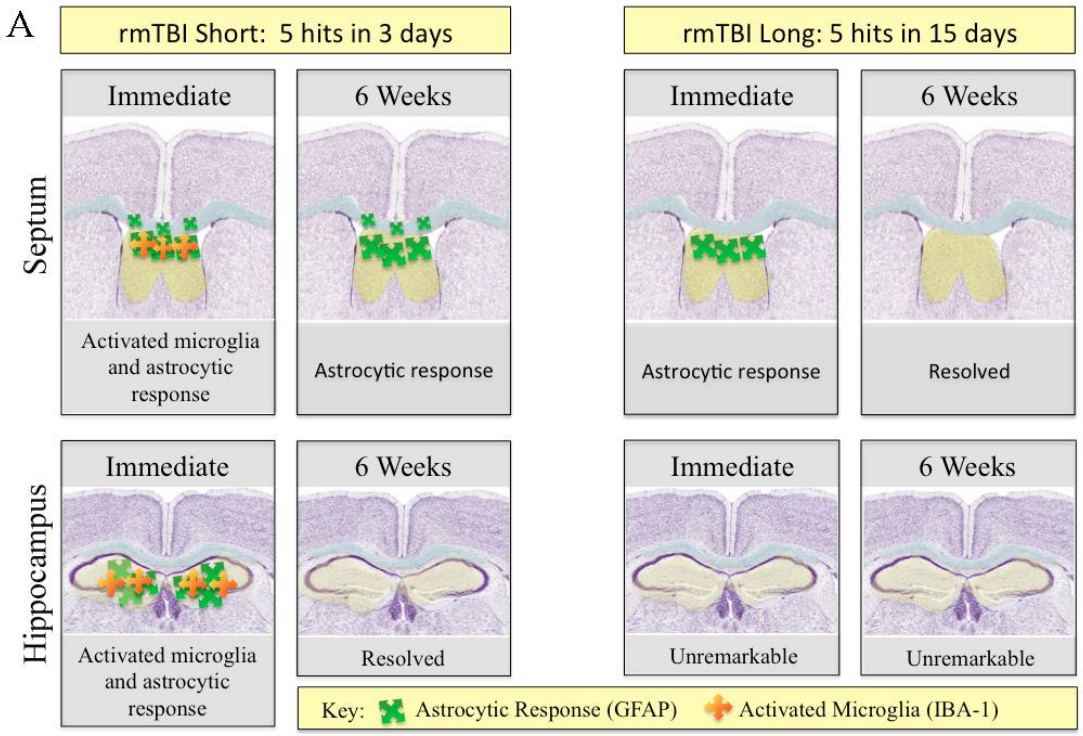

B

Summary of positive and null results (n/c: no change)

Region of Interest	Astrocytic Reaction (GFAP +)	Microglial Activation (IBA-1 +)	Phospho-Tau (AT8 +)	Water Channel Protein Alteration (AQP4+/-)	Reactive Gliosis (S100β+)	Axonal damage SMI-32*	Myelin changes MBP*
Lateral Septum	yes	yes	n/c	n/c	n/c	n/c	n/c
Hippocampus	yes	yes	n/c	n/c	n/c	n/c	n/c
Corpus Callosum	yes	n/c	n/c	n/c	n/c	n/c	n/c
Amygdala	n/c	n/c	n/c	n/c	n/c	n/c	n/c
Cortex	n/c	n/c	n/c	n/c	n/c	n/c	n/c

Ependymal lining of ventricle (S100β)	Intact
Lateral ventricle volume	n/c

* assessed at 2 wk post-injury time point only

Figure 6. Overview of results. (A) Following a rotational model of rmTBI, the astrocytic and microglial response appears to be initially localized to the lateral septum and hippocampus, with a moderate astrocytic response occurring in the corpus callosum. Comparison of the two hit protocols demonstrates the enhanced histological response in select regions when the hits are delivered in rapid succession. (B) Table shows summary of experimental findings including positive and null results.

Table 1

Mid LS Imm					
Source of Variation	**Df**	**F Value**	**P value**	**Signif.**	**Time**
Interaction	1	291.2	< 0.0001	****	imm
Treatment	1	99.98	< 0.0001	****	imm
Protocol	1	108.2	< 0.0001	****	imm
Mid LS 2 wk					
Source of Variation	**Df**	**F Value**	**P value**	**Signif.**	**Time**
Interaction	1	3.224	0.0904	ns	2 wk
Treatment	1	19.97	0.0003	***	2 wk
Protocol	1	0.07205	0.7916	ns	2 wk
Mid LS 6 wk					
Source of Variation	**Df**	**F Value**	**P value**	**Signif.**	**Time**
Interaction	1	3.416	0.0821	ns	6 wk
Treatment	1	6.521	0.0206	*	6 wk
Protocol	1	4.913	0.0406	*	6 wk
Peri Mid LS Imm					
Source of Variation	**Df**	**F Value**	**P value**	**Signif.**	**Time**
Interaction	1	51.53	< 0.0001	****	imm
Treatment	1	154.4	< 0.0001	****	imm
Protocol	1	76.71	< 0.0001	****	imm
Peri Mid LS 2 wk					
Source of Variation	**Df**	**F Value**	**P value**	**Signif.**	**Time**
Interaction	1	3.124	0.0932	ns	2 wk
Treatment	1	17	0.0006	***	2 wk
Protocol	1	0.8093	0.3796	ns	2 wk
Peri Mid LS 6 wk					
Source of Variation	**Df**	**F Value**	**P value**	**Signif.**	**Time**
Interaction	1	3.181	0.0924	ns	6 wk
Treatment	1	5.173	0.0362	*	6 wk
Protocol	1	3.824	0.0672	ns	6 wk
Lat LS Imm					
Source of Variation	**Df**	**F Value**	**P value**	**Signif.**	**Time**
Interaction	1	2.085	0.1708	ns	imm
Treatment	1	23.08	0.0003	***	imm
Protocol	1	7.677	0.015	*	imm
Lat LS 2 wk					
Source of Variation	**Df**	**F Value**	**P value**	**Signif.**	**Time**
Interaction	1	2.645	0.1203	ns	2 wk
Treatment	1	15.39	0.0009	***	2 wk
Protocol	1	0.5063	0.4854	ns	2 wk
Lat LS 6 wk					
Source of Variation	**Df**	**F Value**	**P value**	**Signif.**	**Time**
Interaction	1	2.93	0.1051	ns	6 wk
Treatment	1	3.128	0.0949	ns	6 wk
Protocol	1	4.145	0.0576	ns	6 wk

CC Imm					
Source of Variation	**Df**	**F Value**	**P value**	**Signif.**	**Time**
Interaction	1	1.106	0.3108	ns	imm
Treatment	1	10.8	0.0054	**	imm
Protocol	1	12.34	0.0034	**	imm
CC 2 wk					
Source of Variation	**Df**	**F Value**	**P value**	**Signif.**	**Time**
Interaction	1	0.4421	0.515	ns	2 wk
Treatment	1	1.643	0.2172	ns	2 wk
Protocol	1	0.007682	0.9312	ns	2 wk
CC 6 wk					
Source of Variation	**Df**	**F Value**	**P value**	**Signif.**	**Time**
Interaction	1	3.824	0.0672	ns	6 wk
Treatment	1	2.997	0.1016	ns	6 wk
Protocol	1	3.599	0.0749	ns	6 wk
Hippo Imm					
Source of Variation	**Df**	**F Value**	**P value**	**Signif.**	**Time**
Interaction	1	0.8343	0.3825	ns	imm
Treatment	1	11.75	0.0065	**	imm
Protocol	1	2.103	0.1776	ns	imm
Hippo 2 wk					
Source of Variation	**Df**	**F Value**	**P value**	**Signif.**	**Time**
Interaction	1	10.23	0.0047	**	2 wk
Treatment	1	4.375	0.0501	ns	2 wk
Protocol	1	0.05778	0.8126	ns	2 wk
Hippo 6 wk					
Source of Variation	**Df**	**F Value**	**P value**	**Signif.**	**Time**
Interaction	1	1.482	0.2376	ns	6 wk
Treatment	1	1.444	0.2436	ns	6 wk
Protocol	1	5.047	0.0361	*	6 wk

Table 1. ANOVA Results for GFAP quantification. 2-way full factorial ANOVA (treatment X protocol) for each ROI and post-injury time point revealed treatment (hit, control) as a highly significant factor at the immediate time point in all septal regions (Mid LS F=99.98, Peri Mid LS F=154.4, Lat LS F=23.08) with treatment persisting as a significant factor at 6-wks in the mid

(F=6.52) and peri-mid LS (F=5.17). Treatment was also a significant factor immediately in the corpus callosum (F=10.8) and hippocampus (F=11.75). Protocol was a significant factor at the immediate time point in all septal regions (Mid LS F=108.2, Peri Mid LS F=76.71, Lat LS F=7.677) with and the corpus callosum (F=12.34), and persisted as a significant factor in the mid LS (F=4.913) and hippocampus (F=5.047) at the 6-wk time point. Significant interactions are displayed in **Figures 3 and 4.**

Table 2.

ROI	Protocol	Difference	t value	P value	Sign.
Mid LS	Imm-Short	61.86	20.7	P < 0.0001	****
Mid LS	Imm-Long	15.01	4.452	P < 0.01	**
Mid LS	2 wk Short	29.89	4.801	P < 0.001	***
Mid LS	2 wk Long	12.76	1.763	P > 0.05	ns
Mid LS	6 wk Short	48.68	3.507	P < 0.01	**
Mid LS	6 wk Long	7.803	0.4532	P > 0.05	ns
Peri Mid LS	Imm-Short	35.06	14.78	P < 0.0001	****
Peri Mid LS	Imm-Long	9.383	3.505	P < 0.01	**
Peri Mid LS	2 wk Short	15.36	4.696	P < 0.001	***
Peri Mid LS	2 wk Long	6.141	1.512	P > 0.05	ns
Peri Mid LS	6 wk Short	19.63	3.233	P < 0.01	**
Peri Mid LS	6 wk Long	2.375	0.3154	P > 0.05	ns
Lat LS	Imm-Short	22.87	4.71	P < 0.001	***
Lat LS	Imm-Long	12.3	2.246	P > 0.05	ns
Lat LS	2 wk Short	15.35	4.425	P < 0.001	***
Lat LS	2 wk Long	6.355	1.474	P > 0.05	ns
Lat LS	6 wk Short	18.46	2.773	P < 0.05	*
Lat LS	6 wk Long	0.3025	0.03664	P > 0.05	ns
CC	Imm-Short	4.81	3.27	P < 0.05	*
CC	Imm-Long	2.478	1.493	P > 0.05	ns
CC	2 wk Short	2.697	1.492	P > 0.05	ns
CC	2 wk Long	0.8545	0.4069	P > 0.05	ns
CC	6 wk Short	14.01	2.937	P < 0.05	*
CC	6 wk Long	-0.8525	0.1441	P > 0.05	ns
Hippo	Imm-Short	63.02	3.069	P < 0.05	*
Hippo	Imm-Long	36.5	1.777	P > 0.05	ns
Hippo	2 wk Short	31.44	4.218	P < 0.001	***
Hippo	2 wk Long	-6.581	0.7108	P > 0.05	ns
Hippo	6 wk Short	29.88	2.084	P > 0.05	ns
Hippo	6 wk Long	-0.1975	0.009817	P > 0.05	ns

Table 2. Adjusted t-test values for GFAP Quantification. Listing of t-test values with Bonferonni correction show differences in treatment (hit, control) for each ROI, protocol and time point. Significant P-values are displayed in **Figures 3 and 4**.

Table 3

Average righting times in seconds (Mean ± SEM)						
	Hit 1 (am Day 1)	Hit 2 (pm Day 1)	Hit 3 (am Day 2)	Hit 4 (pm Day 2)	Hit 5 (am Day 3)	Average
rmTBI-short	148 ± 12	181 ± 21	156 ± 15	188 ± 19	151 ± 12	164 ± 7
control-short	37 ± 3	49 ± 4	41 ± 3	42 ± 3	38 ± 3	41 ± 1
	Hit 1 (Day 1)	Hit 2 (Day 4)	Hit 3 (Day 8)	Hit 4 (Day 11)	Hit 5 (Day 15)	Average
rmTBI-long	98 ± 12	66 ± 5	68 ± 6	55 ± 4	63 ± 5	70 ± 3
control-long	26 ± 2	48 ± 6	38 ± 3	26 ± 3	32 ± 3	34 ± 2

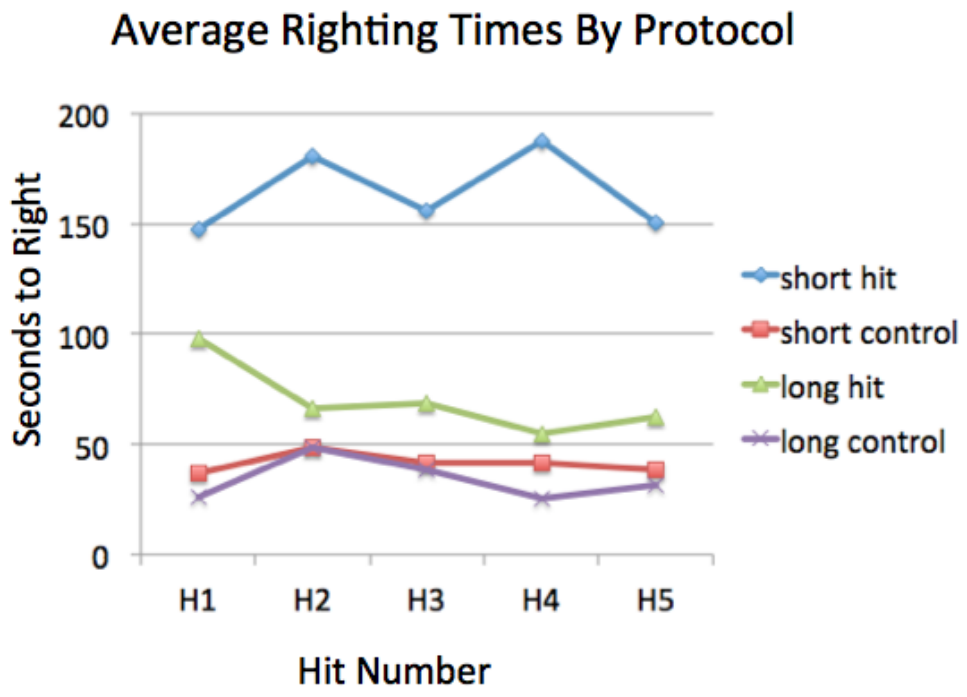

Table 3 with associated Graph. Average righting times following rmTBI and sham treatment (isoflurane only) for both protocols. *(Note: rmTBI data includes righting times from subjects later excluded due to mortality, skull fracture, hemorrhage, etc.).*

Chapter 4: Tissue preparation and three-dimensional imaging of intact biological structures

Introduction

Biological structures within the brain are inherently three-dimensional (3D); however, because of limitations in antibody penetration and light scatter that obscures deep imaging, researchers are often resigned to sectioning through structures and reconstructing the images (Richardson, Lichtman 2015). Sectioning and reconstructing structures can be a lengthy and cumbersome process. For many research applications, it would be ideal to image whole structures rather than just the parts.

Rapidly evolving tissue clearing techniques have recently been developed that render a biological tissue optically clear by removing lipids and/or introducing a medium that has the same refractive index as the cells (Albanese, Chung 2016). Each protocol comes with its own advantages and disadvantages; disadvantages may include tissue shrinkage, expansion, quenching of protein fluorescence, changes in sample characteristic (rendering the tissue stiff, spongy, or fragile), cost and clearing times ranging from days to months (Costantini, Ghobril et al. 2015). Most tissue clearing techniques are designed to either preserve endogenous fluorescent reporter molecules or to be compatible with immunohistochemistry (IHC). Upon evaluating the various tissue clearing protocols, we selected the method for immunolabeling-enabled 3D imaging of solvent-cleared organs termed iDISCO for our initial investigations, which was developed by researchers at Rockefeller University, to optimize IHC with the tissue clearing

process (Renier, Wu et al. 2014). iDISCO permits whole-mount immunolabeling with volume imaging of cleared samples without requiring specialized equipment. Additional studies are also currently underway in our lab to investigate other clearing protocols including CUBIC (Clear, Unobstructed Brain/Body Imaging Cocktails and Computational analysis) (Susaki, Tainaka et al. 2014) and PACT (passive clarity technique), a protocol for passive tissue clearing and immunostaining of intact organs using RIMS (refractive index matching solution), a mounting media for imaging thick tissue (Yang, Treweek et al. 2014, Treweek, Chan et al. 2015). A collaboration with Quorum Technologies Inc. has also been established to test our tissue samples using CLARITY-based techniques (Chung, Wallace et al. 2013). Once a clearing technique is rendered successful in the hands of our lab, it can be applied to a variety of research questions including those related to aging, brain injury and neurodegenerative disease.

Along with tissue clearing, advancements in microscopy are facilitating 3D imaging of intact biological structures deep within the brain. Applications of these techniques will be particularly useful for visualizing structures that span beyond single imaging planes such as investigating below the surface of periventricular gliosis and visualizing septal and hippocampal changes following repeated mild traumatic brain injury (rmTBI). 3D imaging of cleared, immunolabeled tissue can be applied to injury models to investigate the astrocytic and microglial reaction in scar formation within the brain in response to injury.

The goal of the current study is to evaluate tissue preparation and imaging techniques for obtaining high quality 3D images of intact biological structures to enhance future investigations evaluating gliotic changes following brain injury, or in aging or disease. I used the hippocampus and rostral migrating stream (RMS) in my analysis because of the unique cellular organization of

these two regions that includes dense patterning of astrocytes and neuroblasts, which will allow testing of immunolabels we plan to use in future investigations of glial scar formation. By comparing different tissue preparation protocols with 3D optimized whole mount tissue preparation, the study aimed to generate baseline images of successful antibody penetration in thick tissue sections. Results from this study will allow for further comprehensive investigation of changes that occur to cell morphology and tissue structure in injury and disease models.

Methods

Animals

Male and female CD-1 mice (Charles River, Wilmington, MA, USA), age 8-12 wks, were used for all experiments. Animal procedures were approved by the University of Connecticut IACUC and conformed to NIH guidelines.

Tissue clearing and immunostaining with iDISCO protocol

To clear and stain whole tissue sections, we performed the iDISCO protocol as described in Renier et. al., 2014. Briefly, mice were perfused and brains were fixed with paraformaldehyde, then intact brains were dehydrated with methanol, bleached with H2O2, rehydrated, and then placed in blocking solution for 3 days at 37°. Tissue was immunostained with the following antibodies: Goat anti Doublecortin (1:200) (Santa Cruz, TX), Rabbit anti IBA1 (1:500) (Wako Chemicals, VA), Rat anti GFAP (1:250) (Life Technologies, CA). As some of these antibodies were not previously validated with the iDISCO protocol, we first performed antibody validation steps to ensure methanol compatibility, which was successful for all antibodies. Incubation time was 3 days for both primary and secondary antibodies. Following immunostaining, tissue was

dehydrated in tetrahydrofuran (THF) (Sigma), lipid solubilisation was performed using dichloromethane (Sigma) then tissue sections were placed in dibenzyl ether (DBE) (Sigma) for final clearing and to match refraction index to optimize imaging. The specimen was stored in DBE for 1 month then mounted using a 3mm 3D printed chamber containing DBE affixed to a slide using Kwik-sil epoxy (VWR). The chamber was created using a 3D printer (print company: http://www.goactgroup.com/, printing instructions: https://idisco.info/idisco-protocol/) using Visijet M3 Clear resin, which is resistant to DBE.

Whole Mount Immunostaining

Whole mount tissue preparation was performed as previously described (Shook et al, 2014) with the following modifications: Tissue sections were placed in block (10% horse serum, 0.2% Triton) overnight and primary/secondary incubations were set to 3d. This timeframe was based on initial pilot testing of 1-4 days incubation periods, which demonstrated that a minimum of 3 days was required for both primary and secondary antibodies for successful labeling beyond the surface of the tissue. Primary antibodies were used at double their normal concentration: Rat anti-GFAP (1:125), Rabbit anti-IBA-1 (1:250), Guinea Pig anti-Doublecortin (DCX) (1:500) (Millipore, MA), Rabbit anti-AQP4 (1:100) (Sigma-Aldrich, MO). Alexa Fluor dye-conjugated secondary antibodies (Life Technologies) diluted in blocking solution: Donkey anti Rat 488 (1:500), Donkey anti Rabbit 546 (1:500), Donkey anti Guinea Pig 647 (1:100). All specimens were incubated in DAPI at R/T for 25 min prior to final rinses and mounting. Tissue was mounted on slide using a generous amount of Aqua-Poly Mount to ensure even placement of coverslip.

Image Acquisition and Processing

All images were acquired on a Leica TCS SP8 Confocal Microscope. 3D image processing was performed using Leica LAS X 3D Visualization Package. Linear z-stack compensation was required to enhance gain and laser power for imaging beyond a depth of approximately 80 μm.

Results

Modified whole mount processing yields antibody penetration up to 120□m.

In order to pave the way for future studies that plan to use new tissue clearing techniques to facilitate 3D imaging, I first sought out to determine the maximum capacity of antibody penetration for antibodies of interest without the assistance of a tissue clearing method. The two regions of interest selected for these studies were the hippocampus and RMS. These regions are conducive to 3D investigations because both the hippocampus and RMS are comprised of a unique cellular organization of astrocytes and neuroblasts, which can be useful for future studies investigating brain injury and glial scar formation. The hippocampus is of particular interest because we found astrocytes upregulate GFAP in this region following rmTBI (see Chapter 3). As the central focus of my studies is on gliotic changes that occur in aging and injury, the antibodies tested for 3D imaging include GFAP, IBA-1, DCX and AQP4. Astrocytes increase the intermediate filament GFAP in response to mechanical stress and injury (Cullen 2007). IBA-1 is important for identifying changes in neuroimmune activation following injury by allowing visualization of changes in microglial morphology, and DCX is used to label neuroblasts, another primary cell type and distinguishing feature in both of these regions of interest. AQP4 is important in evaluating injury because we found an upregulation of AQP4 in areas of periventricular gliosis in both human and mouse tissue (Chapter 2).

Approximately 500-1000μm thick sections were hand-cut with straight razor from young adult mice, using sagittal sections for the RMS, as this migratory pathway is oriented anterior to posterior within the brain (**Figure 1A**), and using coronal sections for the dentate gyrus of the hippocampus (**Figure 1B**), as this structure is most easily isolated in the frontal plane. After several rounds of testing protocol optimization, I found a 3-day incubation period in primary and secondary antibodies using 0.2% Triton in the blocking solution to assist tissue permeability allowed antibody penetration up to 120μm in depth. Representative 3D images using a hippocampal section display successful antibody penetration for DAPI and GFAP (**Figure 2 A-B**); however, IBA-1 staining appeared slightly globular and did not fully match anticipated microglial morphology. Sample images from an RMS tissue section demonstrate that in addition to GFAP, DCX labeling is also successful up to 100μm in depth, allowing for 3D visualization of migrating chains of neuroblasts and surrounding astrocytes (**Figure 3**). AQP4 also penetrated to the same depth (100μm) in the RMS tissue samples, but IBA-1 staining in the RMS has similar issues to the hippocampal sections (*data not shown*). For all successful immunolabels (GFAP, DAPI and DCX) in both the hippocampus and RMS samples, signal reduction was apparent from 80μm +, which was corrected for by using the Leica TCS SP8 z-compensation tool to enhance gain and laser intensity when acquiring deeper sections of the image.

Initial attempts using iDISCO tissue clearing protocol does not improve 3D imaging

Our next goal was to determine if tissue clearing can enhance 3D imaging to a greater depth beyond the 120μm thickness achieved with the modified whole mount processing using the same antibodies of interest. The iDISCO protocol was selected for the tissue clearing method because it does not require expensive equipment and is optimized for immunostaining (while most other

clearing protocols also work with immunostaining, they are optimized for maintaining endogenous fluorescence). We tested the iDISCO tissue clearing and staining protocol using sections of mouse brain cut similarly to the 500-1000μm thick whole mount sections (**Figure 1**) and also using larger sections up to a half hemisphere sliced coronally at Bregma (**Figure 4A**). All tissue sections were successfully cleared following the 16-day process culminating in incubation in DBE – some tissue shrinkage occurred (**Figure 4B**). Tissue samples were mounted on a slide using a coverslip affixed to the 3D printed imaging chamber containing the refractive index matching solution DBE then imaged on the SP8 confocal microscope. Surprisingly, we found antibody staining limited only to a depth of 65 μm for GFAP and IBA-1 (**Figure 4C),** which was further reduced only days later.

Discussion

In our pilot studies, the modified whole mount method without tissue clearing yielded superior 3D volume imaging compared to tissue prepared with the iDISCO tissue clearing protocol. Our whole mount optimization process successfully produced volume images of the hippocampus and RMS up to a depth of 120μm for GFAP, DCX and DAPI. The 3D images were aided by z-stack compensation to enhance illumination of AB at levels beyond 80μm below the surface. The z-compensation tool is linear, while antibody intensity tends to remain steady then taper off exponentially. Thus, it is important to create multiple set-points when setting up the z-compensation. 3D imaging of the RMS and hippocampus demonstrate distributions of astrocytes, neuroblasts and nuclei in the 3D plane, which can enhance future studies that investigate regional and temporal changes that occur following repeated brain injury. Advantages of the modified whole mount method include no tissue shrinkage, simple and relatively brief (8d) staining and mounting procedures. Disadvantages include limited AB diffusion. Future tests can be

performed to determine if altering the thickness of the tissue section can enhance AB penetration beyond what was observed in the current studies. Trouble shooting strategies for IBA-1, which was not successful using the modified whole mount method, include testing alternative concentrations and using tissue slices of progressive widths.

Results of the iDISCO protocol were inconclusive; tissue clearing appeared successful, however, AB penetration appeared limited to only 65μm, which deteriorated days later. This rapid quenching of fluorescent signal may indicate a problem with the mounting setup, which had small air bubbles trapped inside. The iDISCO protocol requires the tissue to be mounted in the refraction index matching solution DBE, which is highly corrosive thus requiring a specialized mounting chamber. It is possible the air bubbles trapped in the imaging chamber caused the tissue to oxidize, contributing to the antibody deterioration. Our results also revealed prominent tissue shrinkage using the iDISCO protocol, which could affect studies aimed to assess changes in tissue structure. Further studies are required to properly assess the potential depth of staining using the iDISCO protocol.

Regardless of the tissue clearing protocol selected, future studies using thick tissue samples may benefit from using the new method developed at MIT called SWITCH (Murray, Cho et al. 2015), a system-wide control of interaction time and kinetics of chemicals. SWITCH allows for uniform tissue processing by switching reactions on and off. To facilitate even antibody diffusion and labeling, SWITCH uses the detergent sodium dodecyl sulfate (SDS) to inhibit antibody binding during diffusion. A major benefit of SWITCH is that it allows for multiple iterations of antibody staining on the same tissue specimen. This can be extremely useful for performing

comprehensive characterization and analysis of large intact tissue samples. In our rmTBI studies described in Chapter 3, we used two sets of antibody combinations alternating every 50μm section, which still did not allow us to test all of the possible histological changes that might occur following concussive injury. Future rmTBI studies using SWITCH for multiple rounds of immunostaining will enable investigation of gliosis, microglial activation, changes in AQP4 expression, myelin and axonal damage and more within the same tissue section. SWITCH multiplex labeling will be especially important when using thick tissue sections for 3D imaging, because alternating antibody combinations would no longer be an option. SWITCH fixation strategies that work by altering pH to enable even fixation would also useful for future studies using human tissue such as those discussed in Chapter 2.

Conclusion

While the results of our initial testing of the iDISCO protocol were inconclusive, the modified whole mount procedure and resulting 3D images established in this work provide a useful foundation for assessing tissue clearing protocols aimed to optimize 3D imaging of thick tissue samples. 3D visualization and analysis will facilitate investigation of cellular changes that occur in aging, injury and disease that include damage to the ependymal lining, astrocytic and microglial reactions in rmTBI, and changes in cell migration. Future studies utilizing rapidly evolving tissue clearing techniques and multiplexed labeling technology will enhance analyses of intact brain structures such as the hippocampus.

Figures

Figure 1

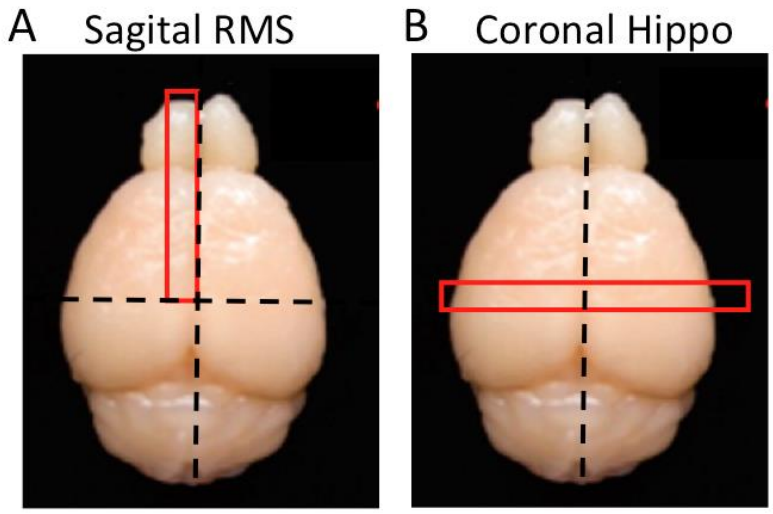

Figure 1. Area of hand-cut dissection of RMS and Hippocampus. Tissue sections (red rectangles) were cut using straight razor hand dissection for the RMS (A) and hippocampus (B) whole mount preparations. Thickness for both sections was approximately 0.5mm.

Figure 2

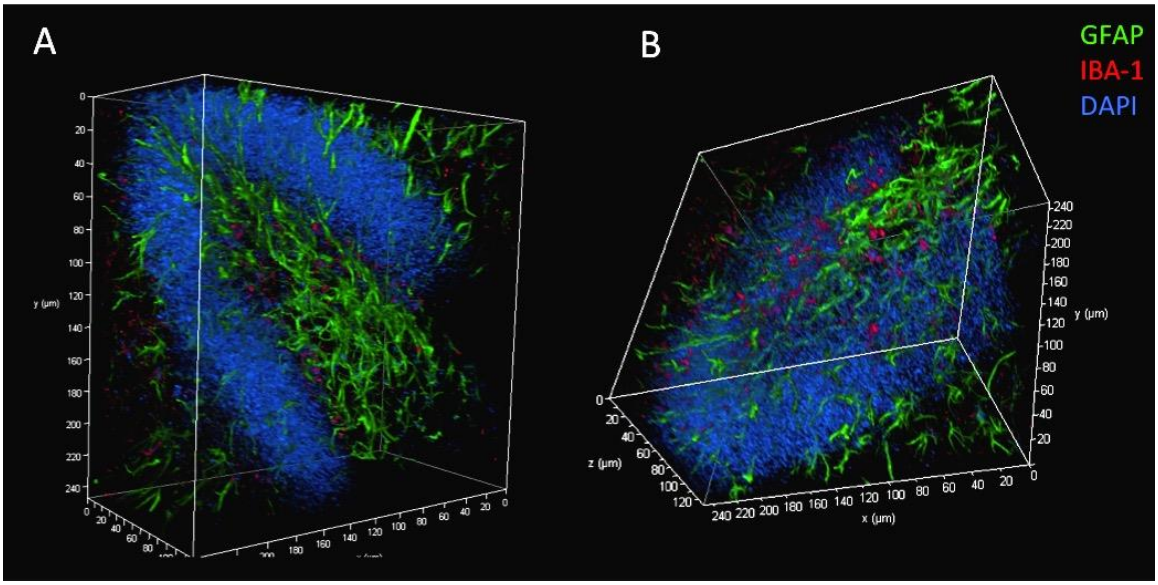

Figure 2. Sample 3D images of hippocampus. Antibody penetration and visualization was successful up to 120µm below the surface for nuclei (DAPI, blue) and astrocytes (GFAP, green), allowing 3D visualization of the dentate gyrus of the hippocampus. Microglial labeling (IBA-1, red) was visible in the sample, but did not appear as robust labeling.

Figure 3

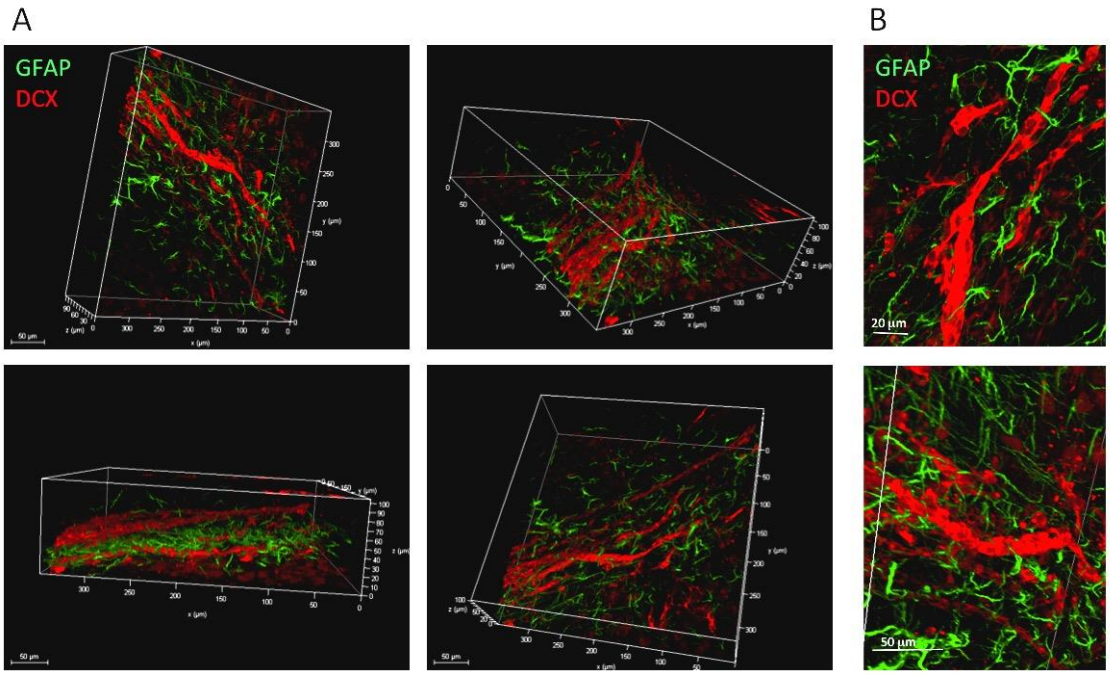

Figure 3. Sample 3D images of the RMS. Astrocyte (GFAP) and neuroblast (DCX) labeling was successful up to 100µm below the surface of the tissue, allowing 3D visualization of migrating neuroblasts and surrounding astrocytes within the RMS.

Figure 4

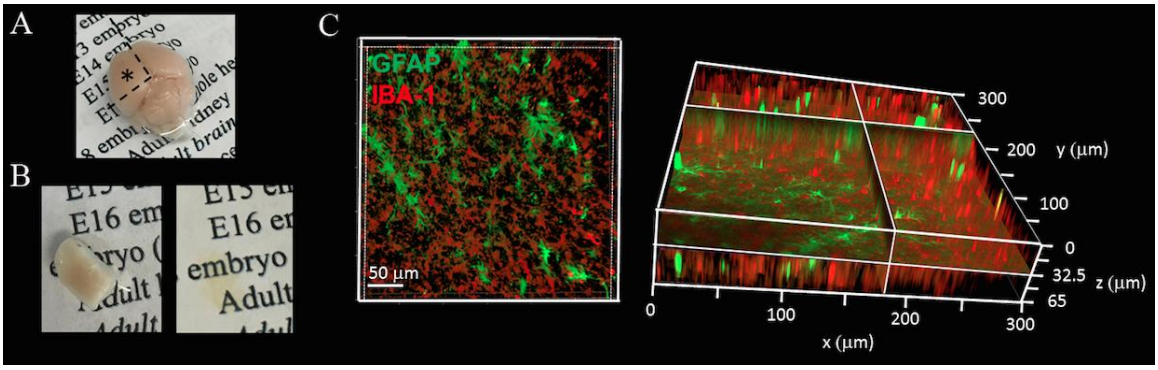

Figure 4. iDISCO Tissue Clearing Protocol and Sample 3D Images. (A) Initial dissection of adult mouse left anterior forebrain (*). (B) Tissue segment from (A) after further dissection of cortical tissue shown before (left) and after (right) iDISCO clearing protocol. (C) Sample 3D (z-stack) images of astrocytes (GFAP, green) and microglia (IBA-1, red) in cleared anterior forebrain tissue. Images were acquired on Confocal Laser Scanning Platform Leica TCS 8 using Leica 3D Visualization Module, which can be further analyzed with Leica Analysis and Quantification Modules to obtain measurements of 3D structures.

Chapter 5: Conclusions

Summary of Chapters 2, 3 and 4

In Chapter 2, I presented our work investigating the link between ventriculomegaly and ependymal gliosis. Age-associated ventriculomegaly is typically attributed to neurodegeneration; however, additional factors might initiate or contribute to progressive ventricular expansion. By directly linking postmortem human MRI sequences with histological features of periventricular tissue, we showed that substantial areas of lateral ventricle surface gliosis were associated with ventriculomegaly. To examine whether loss of ependymal cell coverage resulting in ventricle surface glial scarring can lead directly to ventricle enlargement independent of any other injury or degenerative loss, we modeled in mice the glial scarring found along the lateral ventricle surface in aged humans. Neuraminidase, which cleaves glycosidic linkages of apical adherens junction proteins, was administered intracerebroventricularly to denude areas of ependymal cells. Substantial ependymal cell loss resulted in reactive gliosis rather than stem cell-mediated regenerative repair of the ventricle lining, and the gliotic regions showed morphologic and phenotypic characteristics similar to those found in aged humans. Elevated levels of aquaporin-4, indicative of edema, observed in regions of periventricular gliosis in human tissue were also replicated in our mouse model. 3D modeling together with volume measurements revealed that mice with ventricle surface scarring developed expanded ventricles, independent of neurodegeneration. Through a comprehensive, comparative analysis of the lateral ventricles and associated periventricular tissue in aged human and mouse, followed by modeling of surface gliosis in mice, we have demonstrated a direct link between lateral ventricle surface gliosis and

ventricle enlargement. These studies highlight the importance of maintaining an intact ependymal cell lining throughout aging.

The studies presented in Chapter 3 used a modified weight drop model of rmTBI to perform an extensive regional investigation of histological alterations following repeated concussions. The model generated mild injury replicating the acceleration and rotational forces of mTBI, allowing for repeated applications. We compared two protocols that vary inter-injury interval: rmTBI-short delivered 5 hits in 3 days, rmTBI-long delivered 5 hits in 15 days. Investigation of cellular changes throughout brain regions from 2mm anterior to 2.5mm posterior to Bregma demonstrated immediate microglial activation and increased GFAP intensity following the rmTBI-short protocol in the dorsal lateral septum and hippocampus. 6-weeks following the rmTBI-short protocol, microglial activation was resolved in all regions, while the astrocytic response persisted in the lateral septum. The corpus callosum also had a mild astrocytic response immediately and 6-weeks following the rmTBI-short protocol. Comparison of the two hit protocols demonstrated an enhanced histological response when the hits were delivered in rapid succession. Null findings included no cellular changes in the cortex or amygdala, no p-tau accumulation, no changes in ventricle volume (ependymal lining integrity remains intact), and no findings of diffuse axonal injury or myelin alterations (assessed 2-weeks post injury). In summary, damage in the septal region and hippocampus, both located directly below the corpus callosum and between the lateral ventricles, may be linked to intensified shear force at junctions between gray and white matter. The lateral septum is known to modulate memory and emotions, especially anxiety and fear. Our findings suggest damage to the septo-hippocampal axis from rmTBI may be linked to clinical rmTBI symptomology, including anxiety and memory problems and fenestrated septum pellucidum, which is a notable feature of CTE.

The goal of the studies presented in Chapter 4 was to evaluate tissue preparation and imaging techniques for obtaining high quality 3D images of intact biological structures to enhance future investigations evaluating histological changes in aging, brain trauma or disease. Specifically, the studies developed a modified whole mount processing technique to optimize penetration of immunomarkers useful for evaluating gliotic changes in thick tissue sections, resulting in 3D images up to 120μm thick. These baseline 3D images were then compared against the results obtained using the iDISCO tissue clearing protocol. While my initial attempts of processing tissue using iDISCO did not yield successful results, suggestions for troubleshooting and further studies using the new multiplex processing technique SWITCH are presented to pave the way for future work using 3D visualization. The sample 3D images obtained using the modified whole mount processing that yielded successful antibody penetration of GFAP, DAPI and Doublecortin up to 120μm will provide future researchers with comparisons to ensure the clearing protocol of choice enhances imaging beyond the baseline values provided here.

Together, these studies emphasize the ventricular system and its ependymal lining as important central nervous system features that should be considered in the pursuit of understanding neurophysiological mechanisms underlying changes that occur to the brain in aging, head trauma and neurodegenerative disease.

Discussion of gliotic activation, associated alterations in mechanical properties and ventriculomegaly

Astrocytic and microglial activation

A unifying theme of the studies presented in Chapters 2, 3 and 4 is immunohistochemical analysis of astrocytic and microglial activation in aging and brain injury. The functions of resting astrocytes and microglia include supporting neuronal function and actively promoting a healthy CSN environment. Following injury, astrocytes and microglia become activated, alter morphology and release various cytokines, chemokines, reactive oxygen and nitrogen species as part of the innate inflammatory response (Miller, Chen et al. 2011). These signals help recruit additional astrocytes and microglia to the injury site (Fawcett, Asher 1999). In the cases of severe injury, the astrocytic response can lead to the formation of a "glial scar", as we found along the ependymal lining in aged human tissue (Chapter 2, Shook et al, 2014). While the purpose of forming a glial scar is often to repair or contain injury, it also has the potential to inhibit recovery after injury by impeding regrowth of neuronal processes and neo-vascularization (Kernie, Erwin et al. 2001). Furthermore, in the case of ependymal denudation, gliosis along the ventricular surface alters the CSF-ISF interface, which can have implications in clearance of toxic metabolites, fluid homeostasis and nutrient delivery. In our model of rmTBI, areas of gliosis did not have the characteristics of a glial scar, but the gliotic response was heightened when the subsequent injury was delivered in rapid succession (Chapter 3, Acabchuk et al, 2016). Prior to testing drug treatment strategies aimed to reduce astroglial and microglial activation following brain injury, it is imperative to consider that brain injury causes damage but also stimulates repair; thus, it is essential to distinguish between a helpful and harmful responses when creating drug targets. The astrocytic formations visualized by 3D imaging in Chapter 4

display the normal astrocytic state in two regions of the brain, the astrocyte-dense RMS and the hippocampus. These areas can then be used for comparison to injury or disease states and to evaluate therapeutic interventions.

Consideration of altered mechanical properties

In our studies, astrocytic gliosis played a prominent role in both changes to the ependymal lining in association to ventriculomegaly, and also as a focal response in periventricular structures following rmTBI. While astrocytic gliosis and microglial activation are associated with changes in chemical signaling, they also create changes in physical and mechanical properties of the brain. New imaging methods are being developed that may inform researchers and clinicians regarding how changes in structural integrity of specific brain regions may influence disease progression. Specifically, a new noninvasive method for measuring the mechanical properties of tissue called magnetic resonance elastography (MRE) works by generating vibrations that create minute internal tissue displacements to enable quantification of tissue stiffness (Wang, Ganger et al. 2011). MRE is used to study fibrosis of the liver, and may also prove useful for assessing areas of gliosis in the brain, including the ependymal lining.

Traumatic brain injury has been found to alter the elastic property of the brain under the area of impact. In a controlled cortical impact (CCI) mouse model, MRE was used to demonstrate the biomechanical properties of the brain are altered following injury, causing a reduction in tissue stiffness (Boulet, Kelso et al. 2013). While CCI is a severe injury model that results in massive cell death, results from our rmTBI study demonstrating sustained increases in GFAP in the

lateral septum and hippocampus (Chapter 3, Acabchuk et al, 2016) suggest subtle changes in tissue structure may take place in deeper structures of the brain following repeated concussions.

In addition to gliosis altering the mechanical properties of the brain, microglial activation may also lead to mechanical stress from increased pressure, which activates further cytokine secretion. New hypotheses are being developed that suggest the pathogeneses of Aβ and p-tau accumulation, as well as oncogene activation in cancer, are linked to increased pressure resulting from chronic inflammation (Nogueira, da Veiga Moreira et al. 2015). Inflammation in the ventricular system/CSF pathway is associated with changes in intracranial pressure and subsequent development of hydrocephalus (Del Bigio, Di Curzio 2016). Future studies on aging, brain injury and neurodegenerative disease should take changes in structural and biomechanical forces into consideration.

Ventriculomegaly

CSF flow dynamics and the etiology of ventriculomegaly are more complex processes than previously thought. Traditional assumptions associating ventricle expansion primarily with obstructive hydrocephalus or tissue atrophy can lead to an oversimplified or inaccurate perspective (Rekate 2008). Recent identification of the glymphatic clearance system and brain lymphatic vessels discussed in Chapter 1, along with the results of our studies presented in Chapter 2 emphasize the importance of investigating changes in aging and disease from the perspective of the ventricular system. Results presented in Chapter 2 show damage to the ependymal lining is associated with ventricle expansion in aged humans, and mouse models of ependymal gliosis can lead to ventriculomegaly. While ventriculomegaly is associated with several neurodegenerative diseases including CTE and AD, it is unknown whether this

association is coincidental or causally related (Silverberg, Miller et al. 2010). Our studies assessing ventriculomegaly in an rmTBI mouse model did not reveal alterations in the ependymal lining or ventricle volume following repeated injury; however, this may also be due to a variety of factors (i.e., the disparity of brain volume to ventricle volume ratio between humans and mice, the location of the impact) (Chapter 3, Acabchuk et al, 2016). However, it remains possible that ependymal damage and associated ventriculomegaly contribute to the pathogenesis of CTE following rmTBI. Whether by subtle changes in intraventricular pressure, cilia damage, impaired CSF flow dynamics or other mechanisms, changes to the ventricular system can impair clearance of Aβ and p-tau thus contributing to neurodegenerative decline (Silverberg, Miller et al. 2010, Iliff, Wang et al. 2013, Iliff, Chen et al. 2014). Assessment of ependymal integrity should be a central consideration as researchers revisit previous assumptions of CSF flow dynamics in light of recent discoveries on brain lymphatic vessels, the glymphatic system, and effects of alterations in mechanical stiffness of tissue surrounding the lateral ventricles.

Current rmTBI literature, limitations and future perspective

Comparison of findings from various animal models of mild traumatic brain injury

In order to place the findings of our rmTBI mouse model into context with other recent studies in a concise format, results from notable animal models of brain injury are listed in **Table 1**. An important consideration in generating an animal model of repeated mild injury is to confirm that injury does not cause focal damage in the cortex below the site of injury. Several studies listed in **Table 1** found injury in the cortex. In our studies, no microglial activation or GFAP

upregulation was found below the site of impact, which helps validate the mild nature of the model.

Histological changes commonly noted in rmTBI studies using rodents include astrogliosis and microglial activation. The majority of studies investigate these changes in the hippocampus and in the cortex, but often do not evaluate additional regions of the brain. Our study found a localized histological reaction in the lateral septum, suggesting this region should also be considered as a region of interest in future rmTBI research. Structurally, cellular alterations generated in the septal area may contribute to cavum septum pellucidum in humans, a common feature noted in the pathological stages of CTE (Kiernan, Montenigro et al. 2015). Functionally, the lateral septum may be an important structure of interest in rmTBI research as it is part of the limbic system, and impairments in septal functioning can lead to emotional and memory impairments, two main features of the clinical development of CTE (McKee, Stein et al. 2015).

In order to further the field of rmTBI research, it is essential to be able to compare findings across studies. Currently, this is a difficult endeavor, as each model uses different injury parameters and models are continually being modified, including the development of rodent helmets to minimize skull fractures and hemorrhaging (Leung, Larimore et al. 2014, Petraglia, Plog et al. 2014). So far, all clinical trials of drug interventions for mTBI and TBI have failed to demonstrate clinical efficacy (Marklund and Hillered 2011), but efforts continue to test therapeutic interventions in rmTBI models (Zhang, Teng et al. 2015). Environmental factors including exposure to androgenic-anabolic steroids have been shown to exacerbate microglial activation and axonal injury in a rotational mouse model of repeated head injury (Namjoshi, Cheng et al. 2016). Our studies contained a thorough baseline characterization of a large number

of antibodies across multiple brain regions using three post-injury time points and two different hit protocols, which may contribute to future testing of therapeutic interventions and various environmental exposures.

Only a limited number of animal studies have demonstrated p-tau accumulation following rmTBI. Of the 15 studies listed in **Table 1**, only two studies reported increased p-tau following injury, with one study using a single TBI on AQP4-/- mice (Iliff 2014), and the other using 42 hits on wild-type mice (Petraglia, Plog et al. 2014). Several other studies reported the absence of p-tau following rmTBI (Mouzon, Bachmeier et al. 2014, Bolton, Saatman 2014), including a study that delivered 30 hits to 18m old triple transgenic Alzheimer's (3xTg-AD) mice (Winston, Noël et al. 2016). There are a variety of factors that may contribute to the difficulty in replicating p-tau accumulation in rodent models, which may include differences in brain structure. P-tau accumulations first appear in the depths of the sulci in human CTE, which makes rodent models problematic as rodent brains are lissencephalic. The lack of sulci and gyri means the rodent brain may not endure the same mechanical forces as the human brain following injury, which could impede initiation of p-tau accumulation (Kim, Jeong et al. 2015). Recent advances in understanding p-tau formation suggest p-tau is likely not to be found immediately following rmTBI.

New discoveries highlight limitations of current rmTBI studies as well as potential future contributions

The field of rmTBI research is changing rapidly, as illustrated by a recent discovery from researchers at the Program of Neuroscience at Harvard showing p-tau aggregates are preceded by decreases in the enzyme PIN1, which leads to a conformational change in tau preventing tau

dephosphorylation, known as cis-tau (Kondo, Shahpasand et al. 2015). Antibodies labeling cis-tau show cis-tau formation occurs rapidly following injury, and is upregulated following repeated injury. P-tau aggregates labeled by the AT8 antibody, on the other hand, likely do not occur until 6-12 months following injury in mice, and up to years later in humans according to this new research. Our rmTBI studies used AT8 to test for p-tau formation at time points that extended only until 6 weeks post-injury, which is likely why we had null findings. Given this new discovery, it is highly probable that our model would have demonstrated cis-tau accumulation following injury, and we would expect to find higher levels of cis-tau in the rmTBI-short protocol with hits delivered in rapid succession. As our study was the first to implicate the lateral septum as a region of focal histological response in a mouse model of rmTBI, it would be interesting to investigate the regional distribution of cis-tau accumulation with our protocols in a future study. More promising research is currently underway testing antibodies that prevent cis-tau from forming, in the hopes of suppressing p-tau aggregates and associated neurological, cognitive and behavioral symptoms. These antibodies will be tested in a variety of rmTBI platforms, including weight drop models such as the one employed in our studies. Interestingly, preliminary data presented by Dr. Lu at the TBI Conference in Washington DC (May 2016) found that administering cis-tau antibody intravenously following rmTBI in rodents restores urinary incontinence, balance and memory, the triad of symptoms related to hydrocephalus, in addition to reducing gliosis, microglial activation and p-tau development. Future studies should investigate the link between increases in intraventricular pressure and p-tau progression.

Future perspective on rmTBI research

Future study on concussions will likely unite a variety of techniques and protocols including animal studies, computer-generated modeling and human studies using advanced imaging, serum biomarkers and genetic screening. Data from animal studies will benefit from 3D imaging that will allow visualization and analysis of intact brain structures, and improved immunolabeling allowing greater differentiation of cellular subtypes in response to injury. Together, these advancements will facilitate the development and evaluation of therapeutic interventions. New research advancements will identify vulnerable regions within the brain and link regional injury to clinical outcome. Improved methods for detecting molecular and cellular alterations following concussion will also help to identify heightened risk from additional injury. The results from our studies showing increased histological response following rapidly administered hits and focal damage in the lateral septum, hippocampus, and corpus callosum may contribute to future research testing antibodies preventing p-tau aggregation, the pathognomonic lesion of CTE. By using a holistic view that includes the newly identified brain lymphatic vessels and CSF/ISF clearance routes, studies of repeated brain trauma may link regional histological changes, alterations in fluid barriers (i.e., ependymal lining, the interface of CSF/ISF), and/or changes in structural integrity to the etiology of long term rmTBI symptomology including CTE.

Figures

Table 1

Reported increased P-Tau

Author Year	ROI	Model	Rotation	Cortical injury	Hit # and Inverval	Species	Age	Histological Results
Petraglia 2014	cortex, hippo, amygdala	rubber CCI with helmet; no anesesia			42x 7d; no anesesia	C57/BL/6	3m	GFAP, IBA1 and p-tau (AT8) increased in cortex, hippocampus and amygdala 6m post injury
Illif 2014	cortex	"hit and run" pneumatic-controlled CCI with no anestesia	yes	Yes	1x (not repeated)	C57/BL/6; Aqp4-/-	2-3m	P-tau and IBA-1 increased more in Aqp4−/− compared to WT 28 d post injury suggesting impaired glymphatic function promotes tau pathology after TBI (not mild injury, causes lession)

Reported no change in P-Tau

Author Year	ROI	Model	Rotation	Cortical injury	Hit # and Inverval	Species	Age	Histological Results
Acabchuk 2016	lateral septum, hippo, cc	modified weight drop	yes	no	5x 3d; 5x 15d	CD1	2-3m	GFAP and IBA1 increased in lateral septum, CC and hippocampus following 5x3d but not 5x15d; no changes in p-tau, no ependymal cell loss; no change in ventricle volume
Winston 2016	optic tract	Teflon CCI			30x 30d; 30x 30wk	C57/BL/6; 3xTg-AD	3m, 12m, 18m	30x rmTBI causes increasing white matter damage in optic tract (microglia, silver and flouro Jade-b) in C57; mTBIs did not increase b-amyloid levels or p-tau in 18m old 3xTg-AD mice
Mouzon 2014	cortex, hippo, cc	closed head CCI			1x; 5x 10d	C57/BL/6	9-15m	GFAP and IBA1 increased in CC but not hippocampus 6 and 12m post injury, thinning of CC; no changes in p-tau
Bolton 2014	cortex, hippo, cerebellum, brain stem	silicone CCI skull-exposed			1x; 5x 5d; 5x 10d	C57/BL/6	2-3m	Increased rate of neuronal degeneration (Fluoro- Jade C), GFAP, IBA-1, hemorrhagic lesions using shorter interval (24h vs 48h) in multiple regions (hippocampus, entorhinal cortex, cerebellum and brain stem); No increases in p-tau (PHF-1)

Did not report on P-Tau

Author Year	ROI	Model	Rotation	Cortical injury	Hit # and Inverval	Species	Age	Histological Results
Mannix 2014	cortex, hippo, fibria	modified weight drop (kimwipe)	yes		7x 9d	C57/BL/6	2-3m	GFAP and IBA1 increased in hippocampus and fibria 3m post injury
Luo 2014	cortex, hippo, cc	rubber CCI closed head		Yes	3x 3d	C57/BL/6	2-3m	GFAP increased in ipsilateral cortex (under the impact - not mild), hippocampus (CA3 region), and cc
Aungst 2014	cortex, hippo	fluid percussion with craniotomy		Yes	1x; 3x 6d	S. Dawley rats	2-3m	Sustained micrglial activation in hippocampus and cortex (not mild); reduced NMDA receptor activation in hippocampus
Leung 2014	cortex, hippo	WRAIR Projectile Concussive Impact Model	yes		4x 1hr	S. Dawley rats	adult	Axonal damage in cortex, increased GFAP in hippocampus
Uryu 2002	cortex, hippo, OB	rubber CCI skull-exposed			1x; 2x 2d	APP Tg mice (Tg2576)	9m	Increased amyloid found at longer post-injury time point (16w vs 9w) and repeated hits (2x vs 1x) in APP Tg mice in hippocampus, olfactory bulb, and cortex, but not in striatum, thalamus, cerebellum, brainstem, and spinal cord

Table 1 Continued

Reported changes to ventricle or ependyma								
Author Year	**ROI**	**Model**	**Rota-tion**	**Cortical injury**	**Hit # and Inverval**	**Species**	**Age**	**Histological Results**
Goddeyne 2015	cortex, ventricles	modified weight drop	yes		5x 5d	S. Dawley rats	P20	Hydrocephalus and cortical cell death found in juvenile rat model of rmTBI
Xiong 2014	ependyma, cilia	Lateral fluid perscussion injury (TBI)		Yes	1x (not repeated)	C57/BL/6	1.5m	Ependymal ciliary damage and CSF flow disruption found following TBI, resolved in 4 wks; no ependymal cell loss; no change in ventricle volume

Contains Drug Intervention								
Author Year	**ROI**	**Model**	**Rota-tion**	**Cortical injury**	**Hit # and Inverval**	**Species**	**Age**	**Histological Results and Invervention**
Namjoshi 2016	cc	Closed Head Impact with Rotational Acceleration	yes		2x 2d	C57/BL/6	2m	Androgenic-Anabolic Steroids 8wk exposure prior to rmTBI exacerbated axonal injury (silver stain) and microgliosis in cc
Zhang 2015	cortex, hippo	metal CCI, skull exposed		Yes	1x; 3x 3d	C57/BL/6	2-3m	GFAP and IBA1 increase found in cortex below injury (suggesting not mild) and in hippocampus; reduced with IP injection of drug application 30m after injury (inhibition of monoacylglycerol lipase, an adogenous signaling mediator thought to aid homeostasis after injury)

cc: corpus callosum, CCI: controlled cortical impact

Table 1: Summary of recently published histological findings using rodent models of rmTBI.

Published Work

Acabchuk RL, Briggs D, Angoa-Pérez M, Powers M, Wolferz Jr. R, Soloway M, Stern M, Talbot LR, Kuhn DM, Conover JC, **Repeated Mild Traumatic Brain Injury Causes Focal Response in Lateral Septum and Hippocampus,** In Press, *Concussion*

Acabchuk RL, Sun Y, Wolferz Jr R., Eastman MB., Lennington JB, Shook BA, Conover JC, **3D Modeling of the Lateral Ventricles and Histological Characterization of Periventricular Tissue in Humans and Mouse**. J. Vis. Exp. (99), e52328, doi:10.3791/52328 2015.

Eastman MB, **Acabchuk RL**, Conover JC. Neural Stem Cell Behavior in the Subventricular Zone as a Function of Age. **Neural Stem Cells in Health and Disease.** World Scientific Press. 2015 October.

Shook BA[1], Lennington JB[1]**, Acabchuk RL**[1], Halling M, Sun Y, Peters J, Wu Q, Mahajan A, Fellows DW, Conover JC. **Ventriculomegaly associated with ependymal gliosis and declines in barrier integrity in the aging human and mouse brain**. Aging Cell. 2014 Apr;13(2):340-50. doi: 10.1111/acel.12184. ([1] Co-first authors)

References

References for unpublished work (Chapters 1, 4, 5)

ALBANESE, A. and CHUNG, K., 2016. Whole-brain imaging reaches new heights (and lengths). *eLife,* **5**, pp. e13367.

APOSTOLOVA, L.G., GREEN, A.E., BABAKCHANIAN, S., HWANG, K.S., CHOU, Y.Y., TOGA, A.W. and THOMPSON, P.M., 2012. Hippocampal atrophy and ventricular enlargement in normal aging, mild cognitive impairment (MCI), and Alzheimer Disease. *Alzheimer Disease and Associated Disorders,* **26**(1), pp. 17-27.

AUNGST, S.L., KABADI, S.V., THOMPSON, S.M., STOICA, B.A. and FADEN, A.I., 2014. Repeated mild traumatic brain injury causes chronic neuroinflammation, changes in hippocampal synaptic plasticity, and associated cognitive deficits. *Journal of Cerebral Blood Flow & Metabolism,* **34**(7), pp. 1223-1232.

BARKHOUDARIAN, G., HOVDA, D.A. and GIZA, C.C., 2011. The molecular pathophysiology of concussive brain injury. *Clinics in sports medicine,* **30**(1), pp. 33-48.

BARRIO, J.R., SMALL, G.W., WONG, K.P., HUANG, S.C., LIU, J., MERRILL, D.A., GIZA, C.C., FITZSIMMONS, R.P., OMALU, B., BAILES, J. and KEPE, V., 2015. In vivo characterization of chronic traumatic encephalopathy using [F-18]FDDNP PET brain imaging. *Proceedings of the National Academy of Sciences of the United States of America,* **112**(16), pp. E2039-47.

BOLTON, A.N. and SAATMAN, K.E., 2014. Regional neurodegeneration and gliosis are amplified by mild traumatic brain injury repeated at 24-hour intervals. *Journal of neuropathology and experimental neurology,* **73**(10), pp. 933-947.

BOULET, T., KELSO, M.L. and OTHMAN, S.F., 2013. Long-term in vivo imaging of viscoelastic properties of the mouse brain after controlled cortical impact. *Journal of neurotrauma,* **30**(17), pp. 1512-1520.

BRINKER, T., STOPA, E., MORRISON, J. and KLINGE, P., 2014. A new look at cerebrospinal fluid circulation. *Fluids Barriers CNS,* **11**(10), pp. 10.1186.

CAPILLA-GONZALEZ, V., CEBRIAN-SILLA, A., GUERRERO-CAZARES, H., GARCIA-VERDUGO, J.M. and QUIÑONES-HINOJOSA, A., 2014. Age-related changes in astrocytic and ependymal cells of the subventricular zone. *Glia,* **62**(5), pp. 790-803.

CHOU, Y., LEPORÉ, N., AVEDISSIAN, C., MADSEN, S.K., PARIKSHAK, N., HUA, X., SHAW, L.M., TROJANOWSKI, J.Q., WEINER, M.W. and TOGA, A.W., 2009. Mapping correlations between ventricular expansion and CSF amyloid and tau biomarkers in 240 subjects with Alzheimer's disease, mild cognitive impairment and elderly controls. *NeuroImage,* **46**(2), pp. 394-410.

CHRISMAN, S.P., RIVARA, F.P., SCHIFF, M.A., ZHOU, C. and COMSTOCK, R.D., 2013. Risk factors for concussive symptoms 1 week or longer in high school athletes. *Brain injury,* **27**(1), pp. 1-9.

CHU, W., ZEIDLER, M. and WHITTLE, I.R., 2006. Ventriculomegaly or symptomatic hydrocephalus? Beware of atypical neurological syndromes. *Age and Ageing,* **35**(3), pp. 319.

CHUNG, K., WALLACE, J., KIM, S., KALYANASUNDARAM, S., ANDALMAN, A.S., DAVIDSON, T.J., MIRZABEKOV, J.J., ZALOCUSKY, K.A., MATTIS, J. and DENISIN, A.K., 2013. Structural and molecular interrogation of intact biological systems. *Nature,* **497**(7449), pp. 332-337.

COSTANTINI, I., GHOBRIL, J., DI GIOVANNA, A.P., MASCARO, A.L.A., SILVESTRI, L., MÜLLENBROICH, M.C., ONOFRI, L., CONTI, V., VANZI, F. and SACCONI, L., 2015. A versatile clearing agent for multi-modal brain imaging. *Scientific reports,* **5**.

DEBETTE, S. and MARKUS, H.S., 2010. The clinical importance of white matter hyperintensities on brain magnetic resonance imaging: systematic review and meta-analysis. *BMJ (Clinical research ed.),* **341**, pp. c3666.

DEL BIGIO, M.R., 2010. Ependymal cells: biology and pathology. *Acta Neuropathologica,* **119**(1), pp. 55-73.

DEL BIGIO, M.R., 1995. The ependyma: a protective barrier between brain and cerebrospinal fluid. *Glia,* **14**(1), pp. 1-13.

DEL BIGIO, M.R. and DI CURZIO, D.L., 2016. Nonsurgical therapy for hydrocephalus: a comprehensive and critical review. *Fluids and Barriers of the CNS,* **13**(1), pp. 1.

FAWCETT, J.W. and ASHER, R.A., 1999. The glial scar and central nervous system repair. *Brain research bulletin,* **49**(6), pp. 377-391.

GALGANO, M.A., CANTU, R. and CHIN, L.S., 2016. Chronic Traumatic Encephalopathy: The Impact on Athletes. *Cureus,* **8**(3),.

GATO, A. and DESMOND, M.E., 2009. Why the embryo still matters: CSF and the neuroepithelium as interdependent regulators of embryonic brain growth, morphogenesis and histiogenesis. *Developmental biology,* **327**(2), pp. 263-272.

GIZA, C.C. and HOVDA, D.A., 2001. The neurometabolic cascade of concussion. *Journal of athletic training,* **36**(3), pp. 228.

GODDEYNE, C., NICHOLS, J., WU, C. and ANDERSON, T., 2015. Repetitive mild traumatic brain injury induces ventriculomegaly and cortical thinning in juvenile rats. *Journal of neurophysiology,* **113**(9), pp. 3268-3280.

GRAHAM, R., RIVARA, F.P., FORD, M.A. and SPICER, C.M., 2014. *Sports-Related Concussions in Youth:: Improving the Science, Changing the Culture.* National Academies Press.

GUPTA, S., SOELLINGER, M., GRZYBOWSKI, D.M., BOESIGER, P., BIDDISCOMBE, J., POULIKAKOS, D. and KURTCUOGLU, V., 2010. Cerebrospinal fluid dynamics in the human cranial subarachnoid space: an overlooked mediator of cerebral disease. I. Computational model. *Journal of the Royal Society, Interface / the Royal Society,* **7**(49), pp. 1195-1204.

ILIFF, J.J., CHEN, M.J., PLOG, B.A., ZEPPENFELD, D.M., SOLTERO, M., YANG, L., SINGH, I., DEANE, R. and NEDERGAARD, M., 2014. Impairment of glymphatic pathway function promotes tau pathology after traumatic brain injury. *The Journal of neuroscience : the official journal of the Society for Neuroscience,* **34**(49), pp. 16180-16193.

ILIFF, J.J., WANG, M., ZEPPENFELD, D.M., VENKATARAMAN, A., PLOG, B.A., LIAO, Y., DEANE, R. and NEDERGAARD, M., 2013. Cerebral arterial pulsation drives paravascular CSF-interstitial fluid exchange in the murine brain. *The Journal of neuroscience : the official journal of the Society for Neuroscience,* **33**(46), pp. 18190-18199.

JIMÉNEZ, A.J., DOMÍNGUEZ-PINOS, M., GUERRA, M.M., FERNÁNDEZ-LLEBREZ, P. and PÉREZ-FÍGARES, J., 2014. Structure and function of the ependymal barrier and diseases associated with ependyma disruption. *Tissue barriers,* **2**(1), pp. e28426.

KERNIE, S.G., ERWIN, T.M. and PARADA, L.F., 2001. Brain remodeling due to neuronal and astrocytic proliferation after controlled cortical injury in mice. *Journal of neuroscience research,* **66**(3), pp. 317-326.

KIEFER, M. and UNTERBERG, A., 2012. The differential diagnosis and treatment of normal-pressure hydrocephalus. *Deutsches Arzteblatt international,* **109**(1-2), pp. 15-25; quiz 26.

KIERNAN, P.T., MONTENIGRO, P.H., SOLOMON, T.M. and MCKEE, A.C., 2015. Chronic traumatic encephalopathy: a neurodegenerative consequence of repetitive traumatic brain injury. *Seminars in neurology,* **35**(1), pp. 20-28.

KIM, H., JEONG, E., PARK, D., CZOSNYKA, Z., YOON, B.C., KIM, K., CZOSNYKA, M. and KIM, D., 2015. Finite element analysis of periventricular lucency in hydrocephalus: extravasation or transependymal CSF absorption? *Journal of neurosurgery,* , pp. 1-8.

KONDO, A., SHAHPASAND, K., MANNIX, R., QIU, J., MONCASTER, J., CHEN, C., YAO, Y., LIN, Y., DRIVER, J.A. and SUN, Y., 2015. Antibody against early driver of neurodegeneration cis P-tau blocks brain injury and tauopathy. *Nature,* **523**(7561), pp. 431-436.

KRESS, B.T., ILIFF, J.J., XIA, M., WANG, M., WEI, H.S., ZEPPENFELD, D., XIE, L., KANG, H., XU, Q. and LIEW, J.A., 2014. Impairment of paravascular clearance pathways in the aging brain. *Annals of Neurology,* **76**(6), pp. 845-861.

KUO, C.T., MIRZADEH, Z., SORIANO-NAVARRO, M., RAŠIN, M., WANG, D., SHEN, J., ŠESTAN, N., GARCIA-VERDUGO, J., ALVAREZ-BUYLLA, A. and JAN, L.Y., 2006. Postnatal deletion of Numb/Numblike reveals repair and remodeling capacity in the subventricular neurogenic niche. *Cell,* **127**(6), pp. 1253-1264.

LAUBNER, S., ONDREKA, N., FAILING, K., KRAMER, M. and SCHMIDT, M.J., 2015. Magnetic resonance imaging signs of high intraventricular pressure-comparison of findings in dogs with clinically relevant internal hydrocephalus and asymptomatic dogs with ventriculomegaly. *BMC veterinary research,* **11**(1), pp. 181.

LEUNG, L.Y., LARIMORE, Z., HOLMES, L., CARTAGENA, C., MOUNTNEY, A., DENG-BRYANT, Y., SCHMID, K., SHEAR, D. and TORTELLA, F., 2014. The WRAIR projectile concussive impact model of mild traumatic brain injury: re-design, testing and preclinical validation. *Annals of Biomedical Engineering,* **42**(8), pp. 1618-1630.

LOUVEAU, A., SMIRNOV, I., KEYES, T.J., ECCLES, J.D., ROUHANI, S.J., PESKE, J.D., DERECKI, N.C., CASTLE, D., MANDELL, J.W. and LEE, K.S., 2015. Structural and functional features of central nervous system lymphatic vessels. *Nature,* .

LUO, J., NGUYEN, A., VILLEDA, S., ZHANG, H., DING, Z., LINDSEY, D., BIERI, G., CASTELLANO, J.M., BEAUPRE, G.S. and WYSS-CORAY, T., 2014. Long-term cognitive impairments and pathological alterations in a mouse model of repetitive mild traumatic brain injury. *Frontiers in neurology,* **5**, pp. 12.

MANNIX, R., BERGLASS, J., BERKNER, J., MOLEUS, P., QIU, J., ANDREWS, N., GUNNER, G., BERGLASS, L., JANTZIE, L.L. and ROBINSON, S., 2014. Chronic gliosis and behavioral deficits in mice following repetitive mild traumatic brain injury: Laboratory investigation. *Journal of neurosurgery,* **121**(6), pp. 1342-1350.

MARQUES, F., SOUSA, J.C., SOUSA, N. and PALHA, J.A., 2013. Blood–brain-barriers in aging and in Alzheimer's. *Mol.Neurodegener,* **8**, pp. 38.

MARTLAND, H.S., 1928. Punch drunk. *Journal of the American Medical Association*, **91**(15), pp. 1103-1107.

MATSUMOTO, K., CHIBA, Y., FUJIHARA, R., KUBO, H., SAKAMOTO, H. and UENO, M., 2015. Immunohistochemical analysis of transporters related to clearance of amyloid-β peptides through blood–cerebrospinal fluid barrier in human brain. *Histochemistry and cell biology*, **144**(6), pp. 597-611.

MCCOMB, J.G., 1983. Recent research into the nature of cerebrospinal fluid formation and absorption. *Journal of neurosurgery*, **59**(3), pp. 369-383.

MCCRORY, P., MEEUWISSE, W.H., AUBRY, M., CANTU, R.C., DVORAK, J., ECHEMENDIA, R.J., ENGEBRETSEN, L., JOHNSTON, K., KUTCHER, J.S. and RAFTERY, M., 2013. Consensus statement on concussion in sport: the 4th International Conference on Concussion in Sport, Zurich, November 2012. *Journal of athletic training*, **48**(4), pp. 554-575.

MCKEE, A.C., CAIRNS, N.J., DICKSON, D.W., FOLKERTH, R.D., KEENE, C.D., LITVAN, I., PERL, D.P., STEIN, T.D., VONSATTEL, J. and STEWART, W., 2016. The first NINDS/NIBIB consensus meeting to define neuropathological criteria for the diagnosis of chronic traumatic encephalopathy. *Acta Neuropathologica*, **131**(1), pp. 75-86.

MCKEE, A.C., STEIN, T.D., KIERNAN, P.T. and ALVAREZ, V.E., 2015. The neuropathology of chronic traumatic encephalopathy. *Brain Pathology*, **25**(3), pp. 350-364.

MILLER, G.E., CHEN, E. and PARKER, K.J., 2011. Psychological stress in childhood and susceptibility to the chronic diseases of aging: moving toward a model of behavioral and biological mechanisms. *Psychological bulletin*, **137**(6), pp. 959.

MILLSPAUGH, J., 1937. Dementia pugilistica. *US Naval Med Bull*, **35**, pp. 297-303.

MONKKONEN, K.S., HAKUMAKI, J.M., HIRST, R.A., MIETTINEN, R.A., O'CALLAGHAN, C., MANNISTO, P.T. and LAITINEN, J.T., 2007. Intracerebroventricular antisense knockdown of G alpha i2 results in ciliary stasis and ventricular dilatation in the rat. *BMC neuroscience*, **8**, pp. 26.

MOUZON, B.C., BACHMEIER, C., FERRO, A., OJO, J., CRYNEN, G., ACKER, C.M., DAVIES, P., MULLAN, M., STEWART, W. and CRAWFORD, F., 2014. Chronic neuropathological and neurobehavioral changes in a repetitive mild traumatic brain injury model. *Annals of Neurology*, **75**(2), pp. 241-254.

MURRAY, E., CHO, J.H., GOODWIN, D., KU, T., SWANEY, J., KIM, S., CHOI, H., PARK, Y., PARK, J. and HUBBERT, A., 2015. Simple, Scalable Proteomic Imaging for High-Dimensional Profiling of Intact Systems. *Cell*, **163**(6), pp. 1500-1514.

NAMJOSHI, D.R., CHENG, W.H., CARR, M., MARTENS, K.M., ZAREYAN, S., WILKINSON, A., MCINNES, K.A., CRIPTON, P.A. and WELLINGTON, C.L., 2016. Chronic Exposure to Androgenic-Anabolic Steroids Exacerbates Axonal Injury and Microgliosis in the CHIMERA Mouse Model of Repetitive Concussion. *PloS one,* **11**(1),.

NOGUEIRA, M.L., DA VEIGA MOREIRA, J., BARONZIO, G.F., DUBOIS, B., STEYAERT, J. and SCHWARTZ, L., 2015. Mechanical stress as the common denominator between chronic inflammation, cancer, and Alzheimer's disease. *Frontiers in oncology,* **5**.

OMALU, B.I., DEKOSKY, S.T., MINSTER, R.L., KAMBOH, M.I., HAMILTON, R.L. and WECHT, C.H., 2005. Chronic traumatic encephalopathy in a National Football League player. *Neurosurgery,* **57**(1), pp. 128-134.

PETRAGLIA, A.L., PLOG, B.A., DAYAWANSA, S., CHEN, M., DASHNAW, M.L., CZERNIECKA, K., WALKER, C.T., VITERISE, T., HYRIEN, O. and ILIFF, J.J., 2014. The spectrum of neurobehavioral sequelae after repetitive mild traumatic brain injury: a novel mouse model of chronic traumatic encephalopathy. *Journal of neurotrauma,* **31**(13), pp. 1211-1224.

REAMS, N., ECKNER, J.T., ALMEIDA, A.A., AAGESEN, A.L., GIORDANI, B., PAULSON, H., LORINCZ, M.T. and KUTCHER, J.S., 2016. A Clinical Approach to the Diagnosis of Traumatic Encephalopathy Syndrome: A Review. *JAMA neurology,* .

REKATE, H.L., 2008. The definition and classification of hydrocephalus: a personal recommendation to stimulate debate. *Cerebrospinal Fluid Res,* **5**(2), pp. 2.

REN, Z., ILIFF, J.J., YANG, L., YANG, J., CHEN, X., CHEN, M.J., GIESE, R.N., WANG, B., SHI, X. and NEDERGAARD, M., 2013. 'Hit & Run'model of closed-skull traumatic brain injury (TBI) reveals complex patterns of post-traumatic AQP4 dysregulation. *Journal of Cerebral Blood Flow & Metabolism,* **33**(6), pp. 834-845.

RENIER, N., WU, Z., SIMON, D.J., YANG, J., ARIEL, P. and TESSIER-LAVIGNE, M., 2014. iDISCO: a simple, rapid method to immunolabel large tissue samples for volume imaging. *Cell,* **159**(4), pp. 896-910.

RICHARDSON, D.S. and LICHTMAN, J.W., 2015. Clarifying tissue clearing. *Cell,* **162**(2), pp. 246-257.

RIQUELME, P.A., DRAPEAU, E. and DOETSCH, F., 2008. Brain micro-ecologies: neural stem cell niches in the adult mammalian brain. *Philosophical transactions of the Royal Society of London.Series B, Biological sciences,* **363**(1489), pp. 123-137.

ROALES-BUJÁN, R., PÁEZ, P., GUERRA, M., RODRÍGUEZ, S., VÍO, K., HO-PLAGARO, A., GARCÍA-BONILLA, M., RODRÍGUEZ-PÉREZ, L., DOMÍNGUEZ-PINOS, M. and RODRÍGUEZ, E., 2012. Astrocytes acquire morphological and functional characteristics of

ependymal cells following disruption of ependyma in hydrocephalus. *Acta Neuropathologica,* **124**(4), pp. 531-546.

RYAN, L.M. and WARDEN, D.L., 2003. Post concussion syndrome. *International Review of Psychiatry,* **15**(4), pp. 310-316.

SCHOTT, J.M., FOX, N.C., FROST, C., SCAHILL, R.I., JANSSEN, J.C., CHAN, D., JENKINS, R. and ROSSOR, M.N., 2003. Assessing the onset of structural change in familial Alzheimer's disease. *Annals of Neurology,* **53**(2), pp. 181-188.

SHUKLA, R., VINOD, P. and ABBAS, A., 2010. Normal pressure hydrocephalus: A case report. *Annals of Neurosciences,* **13**(2), pp. 53-55.

SILVERBERG, G.D., MILLER, M.C., MACHAN, J.T., JOHANSON, C.E., CARALOPOULOS, I.N., PASCALE, C.L., HEILE, A. and KLINGE, P.M., 2010. Amyloid and Tau accumulate in the brains of aged hydrocephalic rats. *Brain research,* **1317**, pp. 286-296.

SPASSKY, N., MERKLE, F.T., FLAMES, N., TRAMONTIN, A.D., GARCIA-VERDUGO, J.M. and ALVAREZ-BUYLLA, A., 2005. Adult ependymal cells are postmitotic and are derived from radial glial cells during embryogenesis. *The Journal of neuroscience : the official journal of the Society for Neuroscience,* **25**(1), pp. 10-18.

STEIN, T.D., ALVAREZ, V.E. and MCKEE, A.C., 2014. Chronic traumatic encephalopathy: a spectrum of neuropathological changes following repetitive brain trauma in athletes and military personnel. *Alzheimer's research & therapy,* **6**(1), pp. 1-11.

STEMPER, B.D., SHAH, A.S., BUDDE, M.D., OLSEN, C.M., GLAVASKI-JOKSIMOVIC, A., KURPAD, S.N., MCCREA, M. and PINTAR, F.A., 2016. Behavioral outcomes differ between rotational acceleration and blast mechanisms of mild traumatic brain injury. *Frontiers in neurology,* **7**.

SUSAKI, E.A., TAINAKA, K., PERRIN, D., KISHINO, F., TAWARA, T., WATANABE, T.M., YOKOYAMA, C., ONOE, H., EGUCHI, M. and YAMAGUCHI, S., 2014. Whole-brain imaging with single-cell resolution using chemical cocktails and computational analysis. *Cell,* **157**(3), pp. 726-739.

TOTH, Z., HOLLRIGEL, G.S., GORCS, T. and SOLTESZ, I., 1997. Instantaneous perturbation of dentate interneuronal networks by a pressure wave-transient delivered to the neocortex. *The Journal of neuroscience : the official journal of the Society for Neuroscience,* **17**(21), pp. 8106-8117.

TREWEEK, J.B., CHAN, K.Y., FLYTZANIS, N.C., YANG, B., DEVERMAN, B.E., GREENBAUM, A., LIGNELL, A., XIAO, C., CAI, L. and LADINSKY, M.S., 2015. Whole-body tissue stabilization and selective extractions via tissue-hydrogel hybrids for

high-resolution intact circuit mapping and phenotyping. *Nature protocols,* **10**(11), pp. 1860-1896.

TURNER, R.C., LUCKE-WOLD, B.P., LOGSDON, A.F., ROBSON, M.J., LEE, J.M., BAILES, J.E., DASHNAW, M.L., HUBER, J.D., PETRAGLIA, A.L. and ROSEN, C.L., 2015. Modeling chronic traumatic encephalopathy: the way forward for future discovery. *Frontiers in neurology,* **6**.

UENO, M., CHIBA, Y., MURAKAMI, R., MATSUMOTO, K., KAWAUCHI, M. and FUJIHARA, R., 2016. Blood–brain barrier and blood–cerebrospinal fluid barrier in normal and pathological conditions. *Brain tumor pathology,* **33**(2), pp. 89-96.

URYU, K., LAURER, H., MCINTOSH, T., PRATICO, D., MARTINEZ, D., LEIGHT, S., LEE, V.M. and TROJANOWSKI, J.Q., 2002. Repetitive mild brain trauma accelerates Abeta deposition, lipid peroxidation, and cognitive impairment in a transgenic mouse model of Alzheimer amyloidosis. *The Journal of neuroscience : the official journal of the Society for Neuroscience,* **22**(2), pp. 446-454.

WANG, Y., GANGER, D.R., LEVITSKY, J., STERNICK, L.A., MCCARTHY, R.J., CHEN, Z.E., FASANATI, C.W., BOLSTER, B., SHAH, S., ZUEHLSDORFF, S., OMARY, R.A., EHMAN, R.L. and MILLER, F.H., 2011. Assessment of chronic hepatitis and fibrosis: comparison of MR elastography and diffusion-weighted imaging. *AJR.American journal of roentgenology,* **196**(3), pp. 553-561.

WINSTON, C.N., NOËL, A., NEUSTADTL, A., PARSADANIAN, M., BARTON, D.J., CHELLAPPA, D., WILKINS, T.E., ALIKHANI, A.D., ZAPPLE, D.N. and VILLAPOL, S., 2016. Dendritic Spine Loss and Chronic White Matter Inflammation in a Mouse Model of Highly Repetitive Head Trauma. *The American journal of pathology,* **186**(3), pp. 552-567.

XIE, L., KANG, H., XU, Q., CHEN, M.J., LIAO, Y., THIYAGARAJAN, M., O'DONNELL, J., CHRISTENSEN, D.J., NICHOLSON, C., ILIFF, J.J., TAKANO, T., DEANE, R. and NEDERGAARD, M., 2013. Sleep drives metabolite clearance from the adult brain. *Science (New York, N.Y.),* **342**(6156), pp. 373-377.

XIONG, G., ELKIND, J.A., KUNDU, S., SMITH, C.J., ANTUNES, M.B., TAMASHIRO, E., KOFONOW, J.M., MITALA, C.M., COLE, J. and STEIN, S.C., 2014. Traumatic brain injury-induced ependymal ciliary loss decreases cerebral spinal fluid flow. *Journal of neurotrauma,* **31**(16), pp. 1396-1404.

YANG, B., TREWEEK, J.B., KULKARNI, R.P., DEVERMAN, B.E., CHEN, C., LUBECK, E., SHAH, S., CAI, L. and GRADINARU, V., 2014. Single-cell phenotyping within transparent intact tissue through whole-body clearing. *Cell,* **158**(4), pp. 945-958.

ZHANG, J., TENG, Z., SONG, Y., HU, M. and CHEN, C., 2015. Inhibition of monoacylglycerol lipase prevents chronic traumatic encephalopathy-like neuropathology in

a mouse model of repetitive mild closed head injury. *Journal of Cerebral Blood Flow & Metabolism*, **35**(3), pp. 443-453.

ZIMMER, E.R., LEUZY, A., GAUTHIER, S. and ROSA-NETO, P., 2014. Developments in tau PET imaging. *The Canadian Journal of Neurological Sciences*, **41**(05), pp. 547-553.

References for published work

Chapter 2

Bergmann O, Liebl J, Bernard S, Alkass K, Yeung MS, Steier P, Kutschera W, Johnson L, Landen M, Druid H, Spalding KL , Frisen J (2012). The age of olfactory bulb neurons in humans. *Neuron*. 74, 634-639.

Blanpain C, Horsley V , Fuchs E (2007). Epithelial stem cells: turning over new leaves. *Cell*. 128, 445-458.

Bouab M, Paliouras GN, Aumont A, Forest-Berard K , Fernandes KJ (2011). Aging of the subventricular zone neural stem cell niche: evidence for quiescence-associated changes between early and mid-adulthood. *Neuroscience*. 173, 135-149.

Conover JC, Doetsch F, Garcia-Verdugo JM, Gale NW, Yancopoulos GD , Alvarez-Buylla A (2000). Disruption of Eph/ephrin signaling affects migration and proliferation in the adult subventricular zone. *Nat Neurosci*. 3, 1091-1097.

Conover JC , Shook BA (2011). Aging of the subventricular zone neural stem cell niche. *Aging and Disease*. 2, 49-63.

Cserr HF (1971). Physiology of the choroid plexus. *Physiol Rev*. 51, 273-311.

Curtis MA, Kam M, Nannmark U, Anderson MF, Axell MZ, Wikkelso C, Holtas S, van Roon-Mom WM, Bjork-Eriksson T, Nordborg C, Frisen J, Dragunow M, Faull RL , Eriksson PS (2007). Human neuroblasts migrate to the olfactory bulb via a lateral ventricular extension. *Science*. 315, 1243-1249.

Del Bigio MR (2010). Ependymal cells: biology and pathology. *Acta Neuropathol*. 119, 55-73.

Del Carmen Gomez-Roldan M, Perez-Martin M, Capilla-Gonzalez V, Cifuentes M, Perez J, Garcia-Verdugo JM , Fernandez-Llebrez P (2008). Neuroblast proliferation on the surface of the adult rat striatal wall after focal ependymal loss by intracerebroventricular injection of neuraminidase. *The Journal of Comparative Neurology*. 507, 1571-1587.

Doetsch F , Alvarez-Buylla A (1996). Network of tangential pathways for neuronal migration in adult mammalian brain. *Proceedings of the National Academy of Sciences of the United States of America*. 93, 14895-14900.

Doetsch F, Garcia-Verdugo JM , Alvarez-Buylla A (1997). Cellular composition and three-dimensional organization of the subventricular germinal zone in the adult mammalian brain. *The Journal of neuroscience : the official journal of the Society for Neuroscience*. 17, 5046-5061.

Enwere E, Shingo T, Gregg C, Fujikawa H, Ohta S , Weiss S (2004). Aging results in reduced epidermal growth factor receptor signaling, diminished olfactory neurogenesis, and deficits in fine olfactory discrimination. *J Neurosci*. 24, 8354-8365.

Fazekas F, Kleinert R, Offenbacher H, Schmidt R, Kleinert G, Payer F, Radner H , Lechner H (1993). Pathologic correlates of incidental MRI white matter signal hyperintensities. *Neurology*. 43, 1683-1689.

Figarella-Branger D, Lepidi H, Poncet C, Gambarelli D, Bianco N, Rougon G , Pellissier JF (1995). Differential expression of cell adhesion molecules (CAM), neural CAM and epithelial cadherin in ependymomas and choroid plexus tumors. *Acta Neuropathol (Berl)*. 89, 248-257.

Fuchs E, Tumbar T , Guasch G (2004). Socializing with the neighbors: stem cells and their niche. *Cell*. 116, 769-778.

Haj-Yasein NN, Vindedal GF, Eilert-Olsen M, Gundersen GA, Skare O, Laake P, Klungland A, Thoren AE, Burkhardt JM, Ottersen OP , Nagelhus EA (2011). Glial-conditional deletion of aquaporin-4 (Aqp4) reduces blood-brain water uptake and confers barrier function on perivascular astrocyte endfeet. *Proceedings of the National Academy of Sciences of the United States of America*. 108, 17815-17820.

Iliff JJ, Wang M, Liao Y, Plogg BA, Peng W, Gundersen GA, Benveniste H, Vates GE, Deane R, Goldman SA, Nagelhus EA , Nedergaard M (2012). A Paravascular Pathway Facilitates CSF Flow Through the Brain Parenchyma and the Clearance of Interstitial Solutes, Including Amyloid beta. *Science translational medicine*. 4, 147ra111.

Jimenez AJ, Garcia-Verdugo JM, Gonzalez CA, Batiz LF, Rodriguez-Perez LM, Paez P, Soriano-Navarro M, Roales-Bujan R, Rivera P, Rodriguez S, Rodriguez EM , Perez-Figares JM (2009). Disruption of the neurogenic niche in the subventricular zone of postnatal hydrocephalic hyh mice. *Journal of neuropathology and experimental neurology*. 68, 1006-1020.

Jin K, Sun Y, Xie L, Batteur S, Mao XO, Smelick C, Logvinova A , Greenberg DA (2003). Neurogenesis and aging: FGF-2 and HB-EGF restore neurogenesis in hippocampus and subventricular zone of aged mice. *Aging Cell*. 2, 175-183.

Johanson C, Stopa E, McMillan P, Roth D, Funk J , Krinke G (2011). The distributional nexus of choroid plexus to cerebrospinal fluid, ependyma and brain: toxicologic/pathologic phenomena, periventricular destabilization, and lesion spread. *Toxicol Pathol*. 39, 186-212.

Kuchler S, Graff MN, Gobaille S, Vincendon G, Roche AC, Delaunoy JP, Monsigny M , Zanetta JP (1994). Mannose dependent tightening of the rat ependymal cell barrier. In vivo and in vitro study using neoglycoproteins. *Neurochem Int*. 24, 43-55.

Leys D, Soetaert G, Petit H, Fauquette A, Pruvo JP , Steinling M (1990). Periventricular and white matter magnetic resonance imaging hyperintensities do not differ between Alzheimer's disease and normal aging. *Arch Neurol*. 47, 524-527.

Luo J, Daniels SB, Lennington JB, Notti RQ , Conover JC (2006). The aging neurogenic subventricular zone. *Aging Cell*. 5, 139-152.

Luo J, Shook BA, Daniels SB , Conover JC (2008). Subventricular zone-mediated ependyma repair in the adult mammalian brain. *J Neurosci*. 28, 3804-3813.

Marcus DS, Fotenos AF, Csernansky JG, Morris JC , Buckner RL (2010). Open access series of imaging studies: longitudinal MRI data in nondemented and demented older adults. *J Cogn Neurosci*. 22, 2677-2684.

Marcus DS, Wang TH, Parker J, Csernansky JG, Morris JC , Buckner RL (2007). Open Access Series of Imaging Studies (OASIS): cross-sectional MRI data in young, middle aged, nondemented, and demented older adults. *J Cogn Neurosci*. 19, 1498-1507.

Maslov AY, Barone TA, Plunkett RJ , Pruitt SC (2004). Neural stem cell detection, characterization, and age-related changes in the subventricular zone of mice. *J Neurosci*. 24, 1726-1733.

Mirzadeh Z, Merkle FT, Soriano-Navarro M, Garcia-Verdugo JM , Alvarez-Buylla A (2008). Neural stem cells confer unique pinwheel architecture to the ventricular surface in neurogenic regions of the adult brain. *Cell Stem Cell*. 3, 265-278.

Palha JA, Santos NC, Marques F, Sousa J, Bessa J, Miguelote R, Sousa N , Belmonte-de-Abreu P (2012). Do genes and environment meet to regulate cerebrospinal fluid dynamics? Relevance for schizophrenia. *Front Cell Neurosci*. 6, 31.

Papadopoulos MC , Verkman AS (2007). Aquaporin-4 and brain edema. *Pediatr Nephrol*. 22, 778-784.

Quinones-Hinojosa A, Sanai N, Soriano-Navarro M, Gonzalez-Perez O, Mirzadeh Z, Gil-Perotin S, Romero-Rodriguez R, Berger MS, Garcia-Verdugo JM , Alvarez-Buylla A (2006). Cellular composition and cytoarchitecture of the adult human subventricular zone: a niche of neural stem cells. *J Comp Neurol*. 494, 415-434.

Resnick SM, Pham DL, Kraut MA, Zonderman AB , Davatzikos C (2003). Longitudinal magnetic resonance imaging studies of older adults: a shrinking brain. *The Journal of neuroscience : the official journal of the Society for Neuroscience*. 23, 3295-3301.

Roales-Bujan R, Paez P, Guerra M, Rodriguez S, Vio K, Ho-Plagaro A, Garcia-Bonilla M, Rodriguez-Perez LM, Dominguez-Pinos MD, Rodriguez EM, Perez-Figares JM , Jimenez AJ (2012). Astrocytes acquire morphological and functional characteristics of ependymal cells following disruption of ependyma in hydrocephalus. *Acta neuropathologica*. 124, 531-546.

Rodriguez EM, Guerra MM, Vio K, Gonzalez C, Ortloff A, Batiz LF, Rodriguez S, Jara MC, Munoz RI, Ortega E, Jaque J, Guerra F, Sival DA, den Dunnen WF, Jimenez AJ, Dominguez-Pinos MD, Perez-Figares JM, McAllister JP , Johanson C (2012). A cell junction pathology of neural stem cells leads to abnormal neurogenesis and hydrocephalus. *Biol Res*. 45, 231-242.

Rutishauser U , Jessell TM (1988). Cell adhesion molecules in vertebrate neural development. *Physiol Rev*. 68, 819-857.

Sanai N, Berger MS, Garcia-Verdugo JM , Alvarez-Buylla A (2007). Comment on "Human neuroblasts migrate to the olfactory bulb via a lateral ventricular extension". *Science*. 318, 393; author reply 393.

Sanai N, Nguyen T, Ihrie RA, Mirzadeh Z, Tsai HH, Wong M, Gupta N, Berger MS, Huang E, Garcia-Verdugo JM, Rowitch DH , Alvarez-Buylla A (2011). Corridors of migrating neurons in the human brain and their decline during infancy. *Nature*. 478, 382-386.

Sanai N, Tramontin AD, Quinones-Hinojosa A, Barbaro NM, Gupta N, Kunwar S, Lawton MT, McDermott MW, Parsa AT, Manuel-Garcia Verdugo J, Berger MS , Alvarez-Buylla A (2004). Unique astrocyte ribbon in adult human brain contains neural stem cells but lacks chain migration. *Nature*. 427, 740-744.

Scahill RI, Schott JM, Stevens JM, Rossor MN , Fox NC (2002). Mapping the evolution of regional atrophy in Alzheimer's disease: unbiased analysis of fluid-registered serial MRI. *Proc Natl Acad Sci U S A*. 99, 4703-4707.

Sener RN (2002). Callosal changes in obstructive hydrocephalus: observations with FLAIR imaging, and diffusion MRI. *Comput Med Imaging Graph*. 26, 333-337.

Shen Q, Wang Y, Kokovay E, Lin G, Chuang SM, Goderie SK, Roysam B , Temple S (2008). Adult SVZ stem cells lie in a vascular niche: a quantitative analysis of niche cell-cell interactions. *Cell Stem Cell*. 3, 289-300.

Shook BA, Manz DH, Peters JJ, Kang S , Conover JC (2012). Spatiotemporal changes to the subventricular zone stem cell pool through aging. *The Journal of neuroscience : the official journal of the Society for Neuroscience*. 32, 6947-6956.

Sival DA, Guerra M, den Dunnen WF, Batiz LF, Alvial G, Castaneyra-Perdomo A , Rodriguez EM (2011). Neuroependymal denudation is in progress in full-term human foetal spina bifida aperta. *Brain Pathol*. 21, 163-179.

Snippert HJ, van der Flier LG, Sato T, van Es JH, van den Born M, Kroon-Veenboer C, Barker N, Klein AM, van Rheenen J, Simons BD , Clevers H (2010). Intestinal crypt homeostasis results from neutral competition between symmetrically dividing Lgr5 stem cells. *Cell*. 143, 134-144.

Sofroniew MV (2009). Molecular dissection of reactive astrogliosis and glial scar formation. *Trends Neurosci*. 32, 638-647.

Tavazoie M, Van der Veken L, Silva-Vargas V, Louissaint M, Colonna L, Zaidi B, Garcia-Verdugo JM , Doetsch F (2008). A specialized vascular niche for adult neural stem cells. *Cell Stem Cell*. 3, 279-288.

Tropepe V, Craig CG, Morshead CM , van der Kooy D (1997). Transforming growth factor-alpha null and senescent mice show decreased neural progenitor cell proliferation in the forebrain subependyma. *J Neurosci*. 17, 7850-7859.

Verkman AS (2008). Mammalian aquaporins: diverse physiological roles and potential clinical significance. *Expert Rev Mol Med*. 10, e13.

Wang C, Liu F, Liu YY, Zhao CH, You Y, Wang L, Zhang J, Wei B, Ma T, Zhang Q, Zhang Y, Chen R, Song H , Yang Z (2011). Identification and characterization of neuroblasts in the subventricular zone and rostral migratory stream of the adult human brain. *Cell Res*. 21, 1534-1550.

Zador Z, Stiver S, Wang V , Manley GT (2009). Role of aquaporin-4 in cerebral edema and stroke. *Handb Exp Pharmacol*, 159-170.

Chapter 3

1. *Faul M, Xu L, Wald MM, Coronado VG*. Centers for Disease Control and Prevention. Traumatic brain injury in the United States. GA, USA.www.cdc.gov/traumaticbraininjury/pdf/blue_book.pdf.
2. *Guskiewicz KM, McCrea M, Marshall SW* et al. Cumulative effects associated with recurrent concussion in collegiate football players: the NCAA Concussion Study. *JAMA* 290(19),2549–2555 (2003).
3. *Karlin AM*. Concussion in the pediatric and adolescent population: "different population, different concerns". *PM R* 3(10), S369–S379 (2011).
4. *Buzzini SRR, Guskiewicz KM*. Sport-related concussion in the young athlete. *Curr. Opin. Pediatr.*18(4), 376–382 (2006).
5. *Guskiewicz KM, Marshall SW, Bailes J* et al. Association between recurrent concussion and late-life cognitive impairment in retired professional football players. *Neurosurgery* 57(4), 719–726(2005).
6. *Meehan WP, Bachur RG*. Sport-related concussion. *Pediatrics* 123(1), 114–123 (2009).
7. *Toledo E, Lebel A, Becerra L* et al. The young brain and concussion: imaging as a biomarker for diagnosis and prognosis. *Neurosci. Biobehav. Rev.* 36(6), 1510–1531 (2012).
8. *Cavanaugh JT, Guskiewicz KM, Stergiou N*. A nonlinear dynamic approach for evaluating

postural control. *Sport. Med.* 35(11), 935–950 (2005).

9. *Mulligan I, Boland M, Payette J*. Prevalence of neurocognitive and balance deficits in collegiate aged football players without clinically diagnosed concussion. *J. Orthop. Sports Phys. Ther.*42(7), 625–632 (2012).
10. *McCrory P, Meeuwisse WH, Aubry M* et al. Consensus statement on concussion in sport: the 4th International Conference on Concussion in Sport held in Zurich, November 2012. *Br. J. Sports Med.* 47(5), 250–258 (2013).
11. *Harmon KG, Drezner JA, Gammons M* et al. American Medical Society for Sports Medicine position statement: concussion in sport. *Br. J. Sports Med.* 47(1), 15–26 (2013).
12. *Borich MR, Cheung KL, Jones P* et al. Concussion: current concepts in diagnosis and management. *J. Neurol. Phys. Ther.* 37(3), 133–139 (2013).
13. *Singman EL*. Automating the assessment of visual dysfunction after traumatic brain injury.*Med. Instrum.* 1(3), 6 (2013).
14. *Slobounov S, Gay M, Johnson B, Zhang K*. Concussion in athletics: ongoing clinical and brain imaging research controversies. *Brain Imaging Behav.* 6(2), 224–243 (2012).
15. *Zhang K, Johnson B, Pennell D, Ray W, Sebastianelli W, Slobounov S*. Are functional deficits in concussed individuals consistent with white matter structural alterations: combined FMRI & DTI study. *Exp. Brain Res.* 204(1), 57–70 (2010).
16. *Johnson VE, Stewart W, Smith DH*. Axonal pathology in traumatic brain injury. *Exp. Neurol.*246, 35–43 (2013).
17. *Mayer AR, Ling J, Mannell MV* et al. A prospective diffusion tensor imaging study in mild traumatic brain injury. *Neurology* 74(8), 643–650 (2010).
18. *Slobounov SM, Gay M, Zhang K* et al. Alteration of brain functional network at rest and in response to YMCA physical stress test in concussed athletes: RsFMRI study. *Neuroimage* 55(4),1716–1727 (2011).
19. *Black AM, Cat C, Sergio LE, Macpherson AK*. The epidemiology of concussions: number and nature of concussions and time to recovery among female and male canadian varsity athletes 2008 to 2011. *Clin. J. Sport Med.* doi:10.1097/JSM.0000000000000308 (2016) (Epub ahead of print).
20. *Gorbet DJ, Sergio LE*. The behavioural consequences of dissociating the spatial directions of eye and arm movements. *Brain Res.* 1284, 77–88 (2009).
21. *Gorbet DJ, Sergio LE*. Don't watch where you're going: the neural correlates of decoupling eye and arm movements. *Behav. Brain Res.* 298, 229–240 (2016).
22. *Brown J, Dalecki M, Hughes C, Macpherson AK, Sergio LE*. cognitive–motor integration deficits in young adult athletes following concussion. *BMC Sports Sci. Med. Rehabil.* 7(1), 1 (2015).
23. *Hawkins KM, Sergio LE*. Visuomotor impairments in older adults at increased Alzheimer's disease risk. *J. Alzheimers Dis.* 42(2), 607–621 (2014).
24. *Salek Y, Anderson ND, Sergio L*. Mild cognitive impairment is associated with impaired visual-motor planning when visual stimuli and actions are incongruent. *Eur. Neurol.* 66(5), 283–293(2011).
25. *Granek J, Pisella L, Stemberger J, Vighetto A, Rossetti Y, Sergio LE*. Decoupled visually-guided reaching in optic ataxia: differences in motor control between canonical and non-

canonical orientations in space. *PLoS ONE* 8(12), 1–18 (2013).

26. *Hawkins KM, Goyal AI, Sergio LE*. Diffusion tensor imaging correlates of cognitive-motor decline in normal aging and increased Alzheimer's disease risk. *J. Alzheimers Dis.* 44(3), 867–878(2015).
27. *Jantzen KJ, Anderson B, Steinberg FL, Kelso JA.* A prospective functional MR imaging study of mild traumatic brain injury in college football players. *Am. J. Neuroradiol.* 25(5), 738–745(2004).
28. *Sayegh PF, Hawkins KM, Neagu B, Crawford JD, Hoffman KL, Sergio LE*. Decoupling the actions of the eyes from the hand alters beta and gamma synchrony within SPL. *J. Neurophysiol.*111(11), 2210–2221 (2014).
29. *Tremblay S, Henry LC, Bedetti C* et al. Diffuse white matter tract abnormalities in clinically normal ageing retired athletes with a history of sports-related concussions. *Brain* 137(11),2997–3011 (2014).
30. *Gorbet DJ, Staines WR, Sergio LE*. Brain mechanisms for preparing increasingly complex sensory to motor transformations. *Neuroimage* 23(3), 1100–1111 (2004).
31. *Hawkins KM, Sayegh P, Yan X, Crawford JD, Sergio LE*. Neural activity in superior parietal cortex during rule-based visual-motor transformations. *J. Cogn. Neurosci.* 25(3), 436–454(2013).
32. *Sayegh PF, Hawkins KM, Hoffman KL, Sergio LE*. Differences in spectral profiles between rostral and caudal premotor cortex when hand-eye actions are decoupled. *J. Neurophysiol.* 110(4),952–963 (2013).
33. *Johnson EW, Kegel NE, Collins MW*. Neuropsychological assessment of sport-related concussion. *Clin. Sports Med.* 30(1), 73–88 (2011).
34. *Talavage TM, Nauman E, Breedlove EL* et al. Functionally-detected cognitive impairment in high school football players without clinically-diagnosed concussion. *J. Neurotrauma* 31, 327–338(2010).
35. *Kissick J, Johnston KM*. Return to play after concussion: principles and practice. *Clin. J. Sport Med.* 15(6), 426–431 (2005).
36. *Messier J, Kalaska JF*. Differential effect of task conditions on errors of direction and extent of reaching movements. *Exp. Brain Res.* 115(3), 469–478 (1997).
37. *Tippett WJ, Krajewski A, Sergio LE*. Visuomotor integration is compromised in Alzheimer's disease patients reaching for remembered targets. *Eur. Neurol.* 58(1), 1–11 (2007).
38. *Tippett WJ, Sergio LE, Black SE*. Compromised visually guided motor control in individuals with Alzheimer's disease: can reliable distinctions be observed? *J. Clin. Neurosci.* 19(5), 655–660(2012).
39. *Tippett WJ, Sergio LE*. Visuomotor integration is impaired in early stage Alzheimer's disease.*Brain Res.* 1102(1), 92–102 (2006).
40. *Lenroot RK, Giedd JN*. Sex differences in the adolescent brain. *Brain Cogn.* 72(1), 46–55(2010).
41. *Gail A, Klaes C, Westendorff S*. Implementation of spatial transformation rules for goal-directed reaching via gain modulation in monkey parietal and premotor cortex. *J. Neurosci.* 29(30),9490–9499 (2009).
42. *Gorbet DJ, Sergio LE*. Preliminary sex differences in human cortical BOLD fMRI activity

during the preparation of increasingly complex visually guided movements. *Eur. J. Neurosci.* 25(4),1228–1239 (2007).

43. *Werner C, Engelhard K*. Pathophysiology of traumatic brain injury. *Br. J. Anaesth.* 99(1), 4–9(2007).
44. *Bartnik BL, Hovda DA, Lee PWN*. Glucose metabolism after traumatic brain injury: estimation of pyruvate carboxylase and pyruvate dehydrogenase flux by mass isotopomer analysis. *J. Neurotrauma* 24(1), 181–194 (2007).
45. *Bergsneider M, Hovda DA, Lee SM* et al. Dissociation of cerebral glucose metabolism and level of consciousness during the period of metabolic depression following human traumatic brain injury. *J. Neurotrauma* 17(5), 389–401 (2000).
46. *Giza CC, Hovda DA*. The neurometabolic cascade of concussion. *J. Athl. Train.* 36(3), 228–235(2001).
47. *Verweij BH, Muizelaar JP, Vinas FC, Peterson PL, Xiong Y, Lee CP*. O-15-212-mitochondrial dysfunction after experimental and human brain injury and its possible reversal with a selective N-type calcium channel antagonist (SNX-111). *Clin. Neurol. Neurosurg.* 99, S102 (1997).
48. *D'Ambrosio R, Maris DO, Grady MS, Winn HR, Janigro D*. Selective loss of hippocampal long-term potentiation, but not depression, following fluid percussion injury. *Brain Res.* 786(1),64–79 (1998).
49. *Sick TJ, Pérez-Pinzón MA, Feng Z-Z*. Impaired expression of long-term potentiation in hippocampal slices 4 and 48 h following mild fluid-percussion brain injury *in vivo*. *Brain Res.*785(2), 287–292 (1998).
50. *McKee AC, Cantu RC, Nowinski CJ* et al. Chronic traumatic encephalopathy in athletes: progressive tauopathy after repetitive head injury. *J. Neuropathol. Exp. Neurol.* 68(7), 709–735(2009).
51. *De Beaumont L, Tremblay S, Henry LC, Poirier J, Lassonde M, Theoret H*. Motor system alterations in retired former athletes: the role of aging and concussion history. *BMC Neurol.* 13,109 (2013).
52. *McAllister TW, Sparling MB, Flashman LA, Guerin SJ, Mamourian AC, Saykin AJ*. Differential working memory load effects after mild traumatic brain injury. *Neuroimage* 14(5), 1004–1012(2001).
53. *Chen J-K, Johnston KM, Frey S, Petrides M, Worsley K, Ptito A*. Functional abnormalities in symptomatic concussed athletes: an fMRI study. *Neuroimage* 22(1), 68–82 (2004).
54. *Tremblay S, De Beaumont L, Henry LC* et al. Sports concussions and aging: a neuroimaging investigation. *Cereb. Cortex* 23(5), 1159–1166 (2013).
55. *Virji-Babul N, Borich MR, Makan N* et al. Diffusion tensor imaging of sports-related concussion in adolescents. *Pediatr. Neurol.* 48(1), 24–29 (2013).
56. *Chamard E, Lassonde M, Henry L* et al. Neurometabolic and microstructural alterations following a sports-related concussion in female athletes. *Brain Inj.* 27(9), 1038–1046 (2013).
57. *Granek J, Sergio LE*. Evidence for distinct brain networks in the control of rule-based motor behavior. *J. Neurophysiol.* 114(2), 1298–1309 (2015).
58. *Giedd JN, Rapoport JL*. Structural MRI of pediatric brain development: what have we learned and where are we going? *Neuron* 67(5), 728–734 (2010).

59. *Slobounov S, Sebastianelli W, Simon R*. Neurophysiological and behavioral concomitants of mild brain injury in collegiate athletes. *Clin. Neurophysiol.* 113(2), 185–193 (2002).
60. *Thompson PM, Sowell ER, Gogtay N* et al. Structural MRI and brain development. *Int. Rev. Neurobiol.* 67, 285–323 (2005).
61. *Plamondon R, Alimi AM*. Speed/accuracy trade-offs in target-directed movements. *Behav. Brain Sci.* 20(2), 249–279 (1997).
62. *Bogacz R, Wagenmakers EJ, Forstmann BU, Nieuwenhuis S*. The neural basis of the speed-accuracy tradeoff. *Trends Neurosci.* 33(1), 10–16 (2010).
63. *Battistone M, Woltz D, Clark E*. Processing speed deficits associated with traumatic brain injury: processing inefficiency or cautiousness? *Appl. Neuropsychol.* 15(1), 69–78 (2008).